



# **Low-Cost Digital Ultrasound Beamformer Design using Field Programmable Gate Arrays**

**By**

**Basem Ahmed Hassan**

Systems and biomedical Engineering Department  
Faculty of Engineering, Cairo University

A thesis submitted to the  
Faculty of Engineering, Cairo University  
In Partial Fulfillment of the  
Requirements for the degree of  
Master of Science

In

**SYSTEMS AND BIOMEDICAL ENGINEERING**

FACULTY OF ENGINEERING, CAIRO UNIVERSITY  
GIZA, EGYPT  
2012

# **Low-Cost Digital Ultrasound Beamformer Design using Field Programmable Gate Arrays**

**By**

**Basem Ahmed Hassan**

Systems and biomedical Engineering Department  
Faculty of Engineering, Cairo University

A thesis submitted to the  
Faculty of Engineering, Cairo University  
In Partial Fulfillment of the  
Requirements for the degree of  
Master of Science  
In  
**SYSTEMS AND BIOMEDICAL ENGINEERING**

Under the supervision of

Prof. Dr. Yasser Mostafa Kadah

Systems and biomedical Engineering Department  
Faculty of Engineering, Cairo University

FACULTY OF ENGINEERING, CAIRO UNIVERSITY  
GIZA, EGYPT  
OCTOBER 2012

# **Low-Cost Digital Ultrasound Beamformer Design using Field Programmable Gate Arrays**

**By**

**Basem Ahmed Hassan**

Systems and biomedical Engineering Department  
Faculty of Engineering, Cairo University

A thesis submitted to the  
Faculty of Engineering, Cairo University  
In Partial Fulfillment of the  
Requirements for the degree of  
Master of Science

In

**SYSTEMS AND BIOMEDICAL ENGINEERING**

Approved by the Examining Committee:

---

**Prof. Dr. Yasser Mostafa Kadah, Thesis Main Advisor**

---

**Prof. Dr. Magdy Fekry, Member**

---

**Prof. Dr. Mohammed Ibrahim El Adway, Member**

FACULTY OF ENGINEERING, CAIRO UNIVERSITY  
GIZA, EGYPT  
OCTOBER 2012

### Abstract

Real-time ultrasonic imaging systems have been available for more than sixty years and are becoming an important tool in the practice of modern medicine. During this time much has occurred to the basic architecture and functions of these clinical systems and their beamformers, which are, in many ways, the most important components of these systems. Throughout most of the 30 years of real time imaging, analog beamformers have been the mainstay of all ultrasonic instruments. But at the present time the industry is undergoing a major shift toward digital beamformation with the introduction of several commercial systems. Our thesis describes a novel extendable Beamforming architecture design in both of the system-level Hardware and Firmware design level. In the Hardware design, we were targeting the compactable application as well as the extendable applications where the power, level of integration and the feasibility of the replication are critical. The three main components that have the greatest influence on the hardware design and system performance of the signal-processing board are the Analog to Digital Converters (ADCs), the Beamformer transmitter and the FPGA. We could utilize the TI AFE5801 as the analog front end of the beamforming by using its eight ADC in one IC as well as using the LM96570 the ultrasound transmitter as an integrated solution for sending a Full control ultrasound signal over selecting beam directions for eight channels. This led to a dramatic decrease of the size, cost and the power making from the proposed design an ideal solution for the low-cost ultrasound imaging devices. On the other hand due to the firmware design we utilized the next-generation high level synthesis tool VIVADO HLS tool the new IP and system-centric design environment to accelerate the design productivity with up to 4 X productivity gain. Using this tool led us to achieve the optimum degree of FPGA parallelism. The technical challenges in digital beamformation will be reviewed, we will have a look at our digital beamformers simulation and its performance compared in terms of beam width, side lobe levels and signal-to-noise ratio. Finally, the future work of our digital beamformer in the context of advanced features and the missing will be discussed.

## **ACKNOWLEDGMENTS**

---

## **ACKNOWLEDGMENTS**

Firstly I would like to thank God for giving me health and patience in completing this thesis. Over the two years that I spent on research, for my thesis, many people have helped me to reach my objective of completing it. I take this opportunity to thank them all. The time spent on my graduate work has not only been, learning exercise academically but also an enriching one personally. First of all I would like to thank my thesis advisor, Dr. Yasser Mostafa Kadah for his remarkable patience. I would like to thank my kind and humble friends; I would like to mention how much I appreciate every professor at Cairo University that I have had the pleasure to know. The Noacknowledgement would be complete without mentioning the support, acceptance, and love of my family, my Father, my Mother, My Brothers, Sisters, my wife and my Child.

## **Table of Contents**

<b>ACKNOWLEDGMENT .....</b>	<b>IV</b>
<b>TABLE OF CONTENETS.....</b>	<b>V</b>
<b>LIST OF TABLES .....</b>	<b>IX</b>
<b>LIST OF FIGURES .....</b>	<b>XV</b>
<b>NOMENCLATURE.....</b>	<b>XVI</b>
<b>ABSTRACT.....</b>	<b>III</b>
<b>CHAPTER 1: THESIS OVERVIEW.....</b>	<b>1</b>
1.1. Introduction .....	1
1.2. Thesis Overview , problem definition.....	2
1.2.1. Ultrasound system basic functionality.....	2
1.2.2. Thesis problem definition.....	4
1.2.3. Thesis motivation.....	4
1.3. Thesis objective.....	5
1.4. Thesis Contribution.....	6
1.4.1. Hardware Design Contribution.....	6
1.4.2. Firmware Design Contribution.....	6
1.5. Thesis organization .....	7
<b>CHAPTER 2: BACKGROUND AND LITERATURE REVIEW .....</b>	<b>8</b>
2.1. Introduction .....	8
2.1. Wave-motion.....	8
2.2. Wave Propagation .....	9
2.3. Aperture Theory and Far Field Directivity Functions.....	11
2.4. Beamwidth and sidelobe.....	12
2.5. Wave focusing and steering .....	15
2.6. Receive focusing (Beamforming).....	17
2.7. Grating lobes .....	18
2.8. Image formation .....	19
2.9. 2D Imaging Transducers .....	20
2.9.1. Linear array.....	20
2.9.2. Phased array.....	20
2.10. Summery .....	20

<b>CHAPTER 3: BEAMFORMER THEORY OF OPERATION.....</b>	<b>22</b>
3.1. Analog beamforming.....	22
3.2. Digital beamforming .....	24
3.2.1. Classes of the Digital Beamforming.....	24
3.2.2. Digital Beamformer basics. ....	24
3.2.2.1. Frequency spectrum .....	26
3.2.2.2. Sample rate and Quantization.....	27
3.2.2.3. Signal to noise ratio (SNR). ....	27
3.2.2.4. SNR and bit depth. ....	28
3.2.3. Physical Limitations. ....	28
3.2.4. Ultrasound digital beamforming implementations .....	29
3.2.5. Digital beamforming Development. ....	31
3.2.5.1. Digital beamforming Earlier Development.....	31
3.2.5.2. Digital beamforming existing technology comparison. ....	34
3.3. Summary. ....	36
<b>CHAPTER 4: DIGITAL BEAMFORMER HARDWARE DESIGN.....</b>	<b>37</b>
4.1. Introduction .....	37
4.2. Hardware design requirement .....	37
4.3. Hardware design architecture .....	37
4.4. Component selection .....	38
4.5. Digital Beamformer Hardware Design. ....	40
4.5.1. Overview.....	41
4.5.2. Power system.....	42
4.5.3. FPGA. 43	
4.5.4. DDR2 memory.....	44
4.5.5. Flash memory (Configuration memory).....	45
4.5.6. Beamformer transmitter.....	45
4.5.7. Beamformer receiver .....	46
4.6. Cost analysis.....	48
4.7. Summery. ....	49
<b>CHAPTER 5: DIGITAL BEAMFORMER FIRMWARE DESIGN.....</b>	<b>50</b>
5.1. Introduction .....	50
5.2. Introduction .....	50
5.3. Background .....	50
5.3.1. FPGA .....	50

## Table of Contents

---

5.3.2. Verilog HDL .....	51
5.3.3. FPGA Synthesizing Process. ....	51
5.3.4. Re-programmability.....	52
5.3.5. XILINX Embedded Development KIT (EDK). ....	53
5.3.5.1. MicroBlaze Software Processor. ....	53
5.3.5.2. Beamformer Embedded Development Kit (EDK) Platform. ....	54
5.3.5.3. HW & SW Co-Design.....	55
5.3.6. Vivado High Level Synthesize (HLS).....	57
5.3.6.1. Overview. ....	57
5.3.6.2. High-Level Synthesis Architecture. ....	57
5.4. HDL Modules description.....	58
5.4.1. Interfacing Cores. ....	58
5.4.1.1. Uwire Core. ....	58
5.4.1.2. Deserialization with Buffering IP Core.....	60
5.4.1.3. Signal channel interface. ....	61
5.4.1.4. Deserializing timing. ....	62
5.4.1.5. Deserializing Data Buffer.....	63
5.4.1.6. MAC.....	65
5.4.1.7. DDR Memory.....	65
5.4.2. Engine Cores.....	66
5.4.2.1. Beamformer Transmitter IP Core.....	67
5.4.2.1.1. Beamformer Transmitter New IC.....	67
5.4.2.1.2. Digital Beamformer transmitter algorithm. ....	68
5.4.2.2. Beamformer Receiver DAS Core.....	68
5.4.2.2.1. DAS core module. ....	69
5.4.2.2.1.1. Manager Module. ....	71
5.4.2.2.1.2. Interpolation. ....	71
5.4.2.2.1.3. Apodization. ....	74
5.4.2.2.1.4. Delaying.....	75
5.4.2.2.1.5. Summation. ....	76
5.5. Challenges and Limitations.....	77
5.6. Summery. ....	77
<b>CHAPTER 6: Ultrasound digital beamformer implementation .....</b>	<b>79</b>
6.1 Introduction .....	79
6.2 System Parameters .....	79
6.3 DAS implementation.....	81
6.3.1 DAS Image Formation.....	81
6.3.2 DAS Initialization Module .....	81
6.3.3 DAS Setup Module.....	82
6.3.4 DAS Running Module .....	83

## Table of Contents

---

6.3.4.1	Summing Data.....	85
6.3.4.2	Interpolation Filter.....	85
6.3.4.3	Combining Data .....	85
6.4	DAS Simulation and Results.....	86
6.4.1	Testing Phantoms.....	86
6.4.2	Testing Configuration.....	87
6.4.3	Testing Results.....	88
6.5	HDL Design performance .....	93
6.5.1	HDL Clock performance .....	93
6.5.2	Device resource utilization and clock performance tradeoff .....	94
6.5.3	Digital Beamformer Utilization.....	94
6.5.3.1	Default RTL Synthesizing.....	94
6.5.3.2	Performance Optimization .....	95
6.5.4	FPGA VS DSP Performance .....	96
6.6	HDL verification and Test Benches .....	96
6.7	Software Simulation and Result Verification. ....	98
6.7.1	Testing Environment. ....	98
6.7.2	Testing Vectors and reference. ....	98
6.7.3	VIVADO HLS Simulation and Verification. ....	99
6.8	Implementation summary and Discussion .....	106
	<b>CHAPTER 7: DISCUSSION .....</b>	<b>107</b>
7.1.	Discussion .....	107
7.2	Delay and Sum Algorithm Limitation.....	109
7.2.1	Synthetic Aperture Imaging Architecture.....	110
	<b>CHAPTER 8: CONCLUSION AND FUTURE WORK .....</b>	<b>111</b>
8.1.	Review of work completed .....	111
8.2	Future development ideas.....	111
8.2.1	Short-Term Future Development.....	112
8.2.2	Long-Term Future Development.....	112
8.2.2.1	Proposed Design of the SAR.....	112
8.3	Conclusion.....	114
	<b>Appendix A, DBF H/W Schematics.....</b>	<b>115</b>
	<b>Appendix B, XILINX Platform Studio .....</b>	<b>123</b>

**Table of Contents**

---

**Appendix C, VIVADO HLS..... 130**

**Appendix D, DBF Frequency –domain methods ..... 137**

**References ..... 138**

## List of Figures

Figure 1.1 - obstetrical ultrasound images demonstrating both 2D (left) and 3D (right down) reconstructions .....	1
Figure 1.2- portable ultrasound system block diagram .....	3
Figure 1.3 - Graphical representation of all of the components involved in the complete beamformer system.....	5
Figure 2.1 -showing Compression and the rarefaction of the longitudinal waves.....	9
Figure 2.2 -Reflection and transmission at a discontinuity .....	10
Figure 2.3-Linear apertures of length L meters lying along the X-axis. Also shown is a field point with spherical coordinates (r, $\theta$ , y) .....	12
Figure 2.4- Rectangular, triangular and hanning amplitude windows.....	13
Figure 2.5-polar of the magnitude of the normalized horizontal far-field beam pattern of the rectangular amplitude window for (a) $L/\lambda=4$ , (b) $L/\lambda=2$ . .....	14
Figure 2.6- polar of the magnitude of the normalized horizontal far-field beam pattern of the triangular amplitude window for (a) $L/\lambda=4$ , (b) $L/\lambda=2$ . .....	14
Figure 2.7- polar of the magnitude of the normalized horizontal far-field beam pattern of the hanning amplitude window.....	15
Figure 2.8 - Generalized sketch of a geometrically focused ultrasound path. The solid lines show an approximate path of constant relative strength. ....	15
Figure 2.9 - Timed electrical excitations create radial wave-fronts expanding from each element wave.....	16
Figure 2.10 - Non-symmetric excitation patterns direct an ultrasound beam off of the transducer axis (A), and combined with focusing produce a steered focused beam (B) ...	16
Figure 2.11 - Receive focus beamforming a) geometric transducer b) array without delays c) array with delays applied to compensate for signal arrival time differences.....	17
Figure 2.12 - Approximation of path difference for wave incident upon transducer elements as related to the element spacing .....	18

## List of Figures

---

Figure 2.13- Shows Different ultrasound imaging modes .....	19
Figure 2.14 - Array transducer types a) Linear Array b) Phased Array .....	20
Figure 3.1 - Analog beamformer types .....	23
Figure 3.2 – Shows basic geometry for beamformer calculations.....	25
Figure 3.3-Shows 15 MHZ Transducer pulse.....	26
Figure 3.4– Theoretical radiation patterns showing .....	27
Figure 3.5- Shows frequency spectrum ultrasound with signal level 1.0V signal noise ratio SNR. ....	28
Figure 3.6 -SNR VS bit depth.....	28
Figure 3.7- System operation of earliest attempt at digitally controlling delays .....	31
Figure 3.8a Principle OP digital delay line.....	32
Figure 3.8b- Phased array ultrasound system with digital delays.....	32
Figure 3.9- Block diagram of the ultrasonic imaging instrument when the analog circuitry is replaced by digital circuitry .....	33
Figure 3.10 - Fully digital beamformed using baseband interpolation .....	34
Figure 4.1 - Pictorial representation of beamformer system PCB Connections .....	38
Figure 4.2- The Digilent Atlys Spartan 6 FPGA Development Kit.....	40
Figure 4.3- Digital Beamformer system architecture.....	41
Figure 4.4- Digital beamformer power section .....	42
Figure 4.5 – Diagram showing major FPGA I/O bus connections per bank .....	43
Figure 4.6- DDR memory section.....	45
Figure 4.7- Flash Memory section .....	45
Figure 4.8- Digital beamformer transmitter IC .....	46

## List of Figures

---

Figure 4.9- Digital beamformer transmitter interface with FPGA. ....	46
Figure 4.10-Digital beamformer receiver IC architecture .....	47
Figure 4.11- Digital Beamformer receiver interfacing with FPGA.....	47
Figure 4.12 - System cost per beamformer channel compared as the size of the system is increased.....	48
Figure 5.1.-shows the interconnection between CLBs .....	51
Figure 5.2.Shows the FPGA Design Flow .....	52
Figure 5.3.Shows the arrangement of the SPI FLASH.....	53
Figure5.4 The figure shows a functional block diagram of the MicroBlaze core. ....	54
Figure 5.5 - Basic Embedded Design Process Flow .....	55
Figure 5.6 – Shows the BF XPS platform.....	55
Figure 5.7 – EDK Co-design diagram .....	56
Figure 5.8 showing the block diagram of VIVADO HLS .....	58
Figure 5.9- The top level block diagram for the Uwire IP Core.....	59
Figure 5.10-Interface between MicroBlaze AXI BUS and Uwire IP .....	60
Figure 5.11- High-speed bit clock, LCLK, is six times the ADCLK sampling clock .....	60
Figure 5.12- a one-channel receiver module.....	61
Figure 5.13-A 12-bit parallel word with a jumbled data bit order.....	62
Figure 5.14-Show the even bits clocked with CLK0.....	63
Figure 5.15- Show the even bits clocked with CLK180.....	63
Figure 5.16- self-addressing Part of the memory.....	64
Figure 5.17- 16-deep FIFO can be constructed using four bits .....	64
Figure 5.18-Show the top level block diagram of the XPS Ethernet Lite MAC .....	65

**List of Figures**

---

Figure 5.19-show the DDR memory controller block diagram .....66

Figure 5.20- a complete transmitter beamformer Module.....67

Figure 5.21- US beamformer Tx IP core architecture. ....68

Figure 5.22 Internal architecture of the US beamformer receiver.....69

Figure 5.23- Basic methods of time domain beamforming for passive.....70

Figure5.24 Signal-to-Noise ratio using Lagrange filters. ....72

Figure 5.25-showing generation of the filter coefficient. ....73

Figure 5.26- showing hanning window for generating our FIR filter coefficient. ....74

Figure 5.27- shows the coordinate system used to determine the time delay.....75

Figure 5.28- Adder module functional diagram. ....77

Figure 6.1-Shows the simple flow chart for the beamforming initialization module. ....82

Figure 6.2-Beamformer setting up flow.....83

Figure 6.3- Beamformer running flow.....84

Figure- 6.4 Images produced with single transmit and receive focus displayed over a 40 dB range.....88

Figure 6.5- Comparison of 6-dB beamwidth versus focal range for a wire object obtained using configuration A. ....89

Figure 6.6 -Comparison of 6-dB beamwidth versus depth for a wire object imaged using configuration A. ....89

Figure 6.7 -Surface plots of images of a six wire phantom obtained from (a) configuration B. (b) configuration C and (c) configuration D. ....90

Figure 6.8- Simulated lateral beamwidth versus range for (a) configuration B (b) configuration C and (c) configuration D.....92

Figure 6.9 -Frequency spectrum beam plot of Images of a wire phantom .....92

Figure 6.10- design viewer. ....94

## List of Figures

---

Figure 6.11-showing the default synthesizing result. ....	95
Figure 6.12 -design viewer after the performance optimization.....	95
Figure 6.13- showing Project Performance Optimization. ....	95
Figure 6.14- Edge and phase detect (+) diagram for beamformer receiver .....	97
Figure 6.15- Edge and phase detect (-) diagram for beamformer receiver .....	97
Figure 6.16- Code composer studio view.. .....	98
Figure 6.17- TI Testing & validation folder. ....	98
Figure 6.18-many test cases references for beamformer validation method. ....	99
Figure 6.19 -Content of the input folder. ....	99
Figure 6.20 -Testing welcome message.....	100
Figure 6.21 -Initializing the beamforming stage.....	100
Figure 6.22 -Configuring the beamformer with the general parameters. ....	101
Figure 6.23 -Allocating memory for different component of the beamforming. ....	101
Figure 6.24 -Loading interpolation filter coefficient. ....	102
Figure 6.25 -Configuring the apodization gain for each of scanning line. ....	102
Figure 6.26 -Configuring the delay values for each scan line. ....	103
Figure 6.27 -Reading the raw scan line vector from TI input folder. ....	103
Figure 6.28- Running the beamformer operation on the selected scanning line. ....	104
Figure 6.29 -Writing the result output vector into file for comparing.....	104
Figure 6.30 -Beamformer logging view.....	105
Figure 6.31 -All the beamformer where successfully output the exact as the Ref .....	105
Figure 6.32 -Comparing the reference with the result for single test case vector. ....	105

## List of Figures

---

Figure 7.1 -MSAF system with a five element active .....	110
Figure 8.1 - Overview of the beamformer is architecture.....	113
Figure A.1-show the power supply section of the ultrasound Beamformer... ..	115
Figure A.2- FPGA Banks section comprising the 4 banks of the SPARTAN 6.....	116
Figure A.3-show the power banks section .....	117
Figure A.4- show programming the FPGA using JTAG and the SPI flash.....	118
Figure A.5- Digital beamformer operation for buffering and rest of DAS Operation.....	119
Figure A.6-show 2 LM96570 ultrasound transmitters .....	120
Figure A.7-show2 ICs are acting the whole Beamformer receiver... ..	121
Figure A.8-Transmitter (High voltage side) and the receivers (Low voltage side) .....	122
Figure B.1- XPS Project Window.....	123
Figure B.2- Project Information Area, Project Tab. ....	124
Figure B.3- Project Files Displayed in the Project Explorer Tab. ....	127
Figure B.4- Modified Version of hello-world, c File.....	127
Figure B.5-Slave and master configuration. ....	129
Figure B.6- Show module interface register. ....	129
Figure B.7- Shows user module interfacing with other modules.....	129
Figure C.1- control and datapath behavior in HLS.....	132
Figure C.2 options in the synthesizing.....	133
Figure C.3 showing 3 sequence sub-functions in non-pipeline behavior. ....	134
Figure C.4 showing 3 sequence sub-functions in pipelining behavior. ....	135

## **List of Tables**

Table 4.1 - Cost summary for 64 channel systems.....	48
Table 6.1- Beamformer receiver configuration Parameters default values .....	79
Table 6.2- Beam width and side lobe level Vs. Focal range: (a) without apodization, (b) rectangular apodization and (c) hanning apodization[21]. .....	89
Table 6.3 - Resolution of a wire target away from the focus of LOO mm for (a) without apodization, (b) rectangular apodization and (c) hanning apodization[21]. .....	90
Table 6.4- The percentage narrowing of the lateral resolution of system C and D referenced to system B[21] .....	94.
Table 6.5 -Shows performance comparison between FSP & FPGA .....	96

**LIST OF ABBREVIATIONS**

3D	: Three Dimensions
A/D	: Analog to Digital
AFE	: Analog Front End
Amp	: Amplifier
ASIC	: Application Specific Integrated IC
AXI	: Advanced extensible Interface
BF	: Beamformer
CW	: Continuous Wave
D/A	: Digital to Analog
DAS	: Delay and Sum
DBF	: Digital Beamformation
DDR	: Double Data Rate
DSP	: Digital Signal Processor
EDK	: Embedded Development Kit
FFT	: Fast Fourier Transform
FIR	: Finite Impulse Response
FPGA	: Field Programmable Gate Array
I/O	: Input / Output
IIR	: Infinite Impulse Response
IC	: Integrated Circuit
LCD	: Liquid Crystal Displays
LMB	: Local Memory Bus
LVDS	: Low Voltage Differential Signal
OEM	: Original Equipment Manufacturer
PGA	: Programmable Gain Amplifier
PLB	: Peripheral Local Bus
PW	: Pulse Wave

## List of ABBREVIATIONS

---

RISC : Reduced Instruction Set

RxBF : Receiver of the Beamformer

SoC : System on Chip

SNR : Signal to noise ratio

T/R : Transmit/Receive

TGC : Time Gain Control

VCA : Variable Controlled Amplifier

VHDL : Very High Speed Hardware Description Language

# Chapter 1

## Thesis Overview

### 1.1 Introduction

Ultrasound imaging is regularly used in cardiology, obstetrics, gynecology, abdominal imaging, etc. Its popularity arises from the fact that it provides high-resolution images without the use of ionizing radiation [1]. It is also mostly non-invasive, although an invasive technique like intra-vascular imaging is also possible. Non-diagnostic use of ultrasound is finding increased use in clinical applications, (e.g., in guiding interventional procedures). Medical ultrasound has gained popularity in the clinical practice as a quick, compact, and affordable diagnostic tool. It has the advantage over computed tomography and magnetic resonance imaging methods in that the preparation for a scan is minimal, and no health hazards are involved. Basically Beamforming is the front processing of the ultrasound (Sometimes called scanners), before it was based on the analog processing and it had the disadvantage of the analog world. On the other hand by utilizing the digitalization of the modern digital beamformer and making it signal processing based technique used in sensor arrays for directional signal transmission or reception [2]. This is achieved by combining elements in the array in such a way that signals at particular angle experience constructive interference and while others experience destructive interference. Beamforming can be used at both the transmitter and receiver side to achieve spatial selectivity.



Figure 1.1 - obstetrical ultrasound images demonstrating both 2D (left) and 3D (right down) reconstructions. [2-3]

Beamforming can be used for both radio and sound waves. It has found numerous applications in radar; sonar, seismology, wireless communications, radio astronomy, speech, acoustics, and biomedicine see Figure 1.1 showing an example of ultrasound image.

### 1.2 Thesis Overview, Problem definition

Recently, portable and lightweight ultrasound scanners have been developed, which greatly expand the range of situations and sites for which medical Ultrasound can be used. The evolution of ultrasound scanners is directly influenced by developments in analog and digital electronics. The number of functions and image quality increases, and the implementation price for any given function decreases with time. One powerful approach for increasing the flexibility and compactness of an ultrasound scanner is to move processing functions from analog to digital electronics. Ultrasound systems are signal processing intensive. With various imaging modalities and different processing requirements in each modality, digital signal processors (DSP) are finding increasing use in such systems. The advent of low power system-on-chip (SOC) with DSP and RISC processors is allowing Original Equipment Manufacturer (OEMs) to provide portable and low cost systems without compromising the image quality necessary for clinical applications; in medicine found its first widespread acceptance in obstetrics [6], [7], where concerns about fetal safety and cost made it the only real option. This thesis introduces digital Beamformer design and the signal processing aspects of the ultrasound system using FPGA with taking TI digital beamformer DSP implementation as reference design and performance as well.

#### 1.2.1 Ultrasound System Basic Functionality

Figure 1.2 shows the basic functionality of an ultrasound system. It demonstrates how transducers focus sound waves along scan lines in the region of interest. The term ultrasound refers to frequencies that are greater than 20 kHz, which is commonly accepted to be the upper frequency limit the human ear can hear. Typically, ultrasound systems operate in the 2 MHz to 20 MHz frequency range, although some systems are approaching 40 MHz for harmonic imaging. In principle, the ultrasound system focuses sound waves along a given scan line so that the waves constructively add together at the desired focal point. As the sound waves propagate towards the focal point, they reflect off on any object they encounter along their propagation path. Once all of the reflected waves have been measured with the transducers, new sound waves are transmitted towards a new focal point along the given scan line. Once all

of the sound waves along the given scan line have been measured, the ultrasound system focuses along a new scan line until all of the scan lines in the desired region of interest have been measured. To focus the sound waves towards a particular focal point, a set of transducer elements are energized with a set of time-delayed pulses to produce a set of sound waves that propagate through the region of interest, which is typically the desired organ and the surrounding tissue. This process of using multiple sound waves to steer and focus a beam of sound is commonly referred to as beamforming [5].

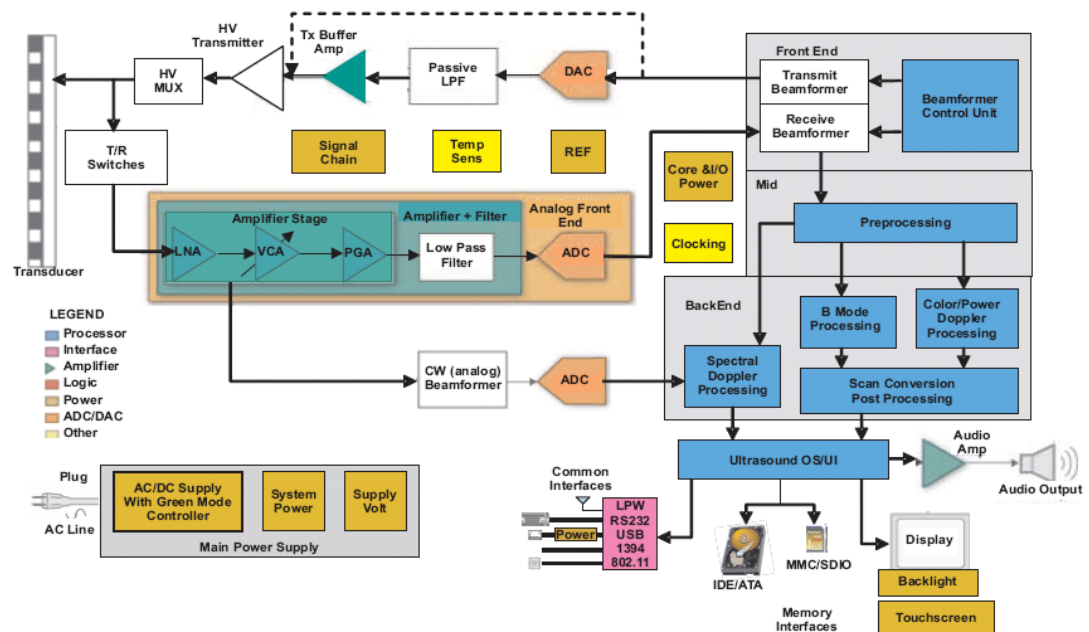


Figure 1.2 -portable ultrasound system block diagram [5]

Once the transducers have generated their respective sound waves, they become sensors that detect any reflected sound waves that are created when the transmitted sound waves encounter a change in tissue density within the region of interest. By properly time delaying the pulses to each active transducer, the resulting time-delayed sound waves meet at the desired focal point that resides at a pre-computed depth along a known scan line. The amplitude of the reflected sound waves forms the basis for the ultrasound image at this focal point location. Envelope detection is used to detect the peaks in the received signal and then log compression is used to reduce the dynamic range of the received signals for efficient display. Once all of the amplitudes for all of the focal points have been detected, they can be displayed for analysis by the doctor or technician. Since the coordinate system, in which the ultrasound system usually operates, does not match the display coordinate systems, a

coordinate transformation, called scan conversion, needs to be performed before being displayed on a CRT monitor [5].

### **1.2.2 Thesis Problem definition**

Beamforming in commercial equipment may have variations and employ different techniques. A distinction that is important in the industry is whether a beamformer is analog, hybrid or digital. An analog beamformer uses analog delay elements for focusing. A hybrid beamformer may introduce analog mixers for fine delay and/or basebanding. A digital beamformer will have analog-to-digital converters immediately following the TGC amplifiers, where all focusing delays are implemented digitally. The earliest phased array beamformers were developed in the late 1960's for imaging of the brain [9] and improved in the early 1970's for echocardiography [10, 11, and 12]. These early systems involved relatively simple implementations of beamformer functions [9, 10]. For focusing lumped L-C delay lines were used as delay elements. Real-time sector scanning, where the beams are steered in particular directions, required rapid switching among a great number of delay configurations, which required a complex control system and produced undesirable switching noise in the analog delay lines. For dynamic focusing and steering, L-C delay lines as delay elements were extremely bulky, since the delay patterns for focal points through the depth along the radial direction are different for each element and for each steering direction, requiring very complex switching circuitry. Also due to inherent artifacts such as insertion loss, impedance mismatching and switching transients the L-C lines were replaced by electronic delays. Gradually, digital beamformation evolved from beamformers with electronic delays to complete digital beamformation systems (DBF). Underlying all these changes, are known mathematical relationships. Digital beamformation has witnessed significant advances and changes recently. It has evolved from simple delay and add architecture to complex synthetic array beamforming with many features like phase aberration correction etc., while techniques like frequency-domain beamforming, have not received wide acceptance.

### **1.2.3 Thesis motivation**

The general motivation to move towards low-power and low cost ultrasound digital beamformer based on FPGA is new modern integrated solutions. These complete receiver/transmitter ICs helped us in designing an ideal research platform that can accommodate all the needs for a wide variety of transducers in a single unit. to digital

beamformation. Our proposed design is willing to achieve multifunction use in a flexible format of following features:

- The resolution of ultrasonic images is greatly enhanced using digital control of weight vector to achieve beamwidth control.
- It enables more precise and rapid changing of the receiver delay times, so that the focal point may track the returning echoes along any steering direction.
- A sufficiently high dynamic range of the echo information can be stored. Frame rate can be increased by simultaneously forming multiple beams.
- Reducing the cost of the ultrasound imaging devices because of getting rid of the extra number of discrete components.
- Reducing the power consumption of the ultrasound scanner.
- Achieve the desired portability of the device by allowing us to integrate a complete 16 -channel ultrasound Beamformer using a single, standard (FPGA) chip.

### 1.3. Thesis Objective

The goal of the thesis has been the development of a versatile ultrasound Beamforming (Front End) platform. In order to create the complete system design we

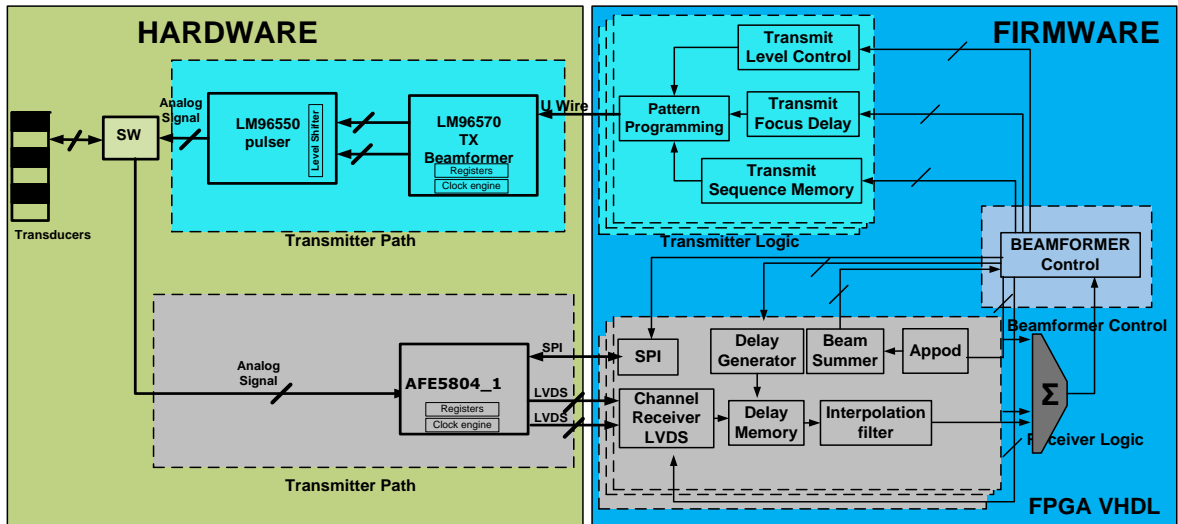


Figure 1.3 - Graphical representation of all of the components involved in the complete beamformer system. Hardware and firmware processing stage divisions are shown.

need to go through development in a number of areas. Existing beamformer hardware is usually designed for real-time 2D image formation often using serial processing with minimum cost by our proposed design. We introduced and define the main idea of our work in this thesis, by defining the complex system of the ultrasound system. A complete map of the system is shown in Figure 1.3. In principle there are two main sections the Hardware and

Firmware design. The Hardware design includes two HW paths separated by HV SW; the first path is the transmitter path which comprises two ICs, the transmitter beamformer and the pulser ICs. In the Firmware design, there are two three main components, the control unit (MicroBlaze software processor), transmitter logic and the receiver logic all both Transmitter and receiver core IP is written by VHDL and synthesized and optimized by VIVADO .

### 1.4. Thesis Contribution

The proposed design selected to implement a beamformer has a great effect on the speed, accuracy, and cost of the entire system. In general, our contribution in the system design can be divided into two fields as follows:

#### 1.4.1. Hardware Design Contribution

The Hardware design has a significant influence on the Digital beam former designs by many of aspects which are:

- **We replaced the low-cost Spartan 6 FPGA by Virtex 6 while maintaining the desired performance, causing a dramatically decreasing in the cost of the proposed board.**
- **We utilized a software processor (MicroBlaze) usage instead of external CPU IC, resulting in a decrease of the board logic (removing interfaces between CPU and FPGA), power consumption, size as well as the cost by removing CPU IC.**
- **Using Xilinx EDK tools enabled us to use Xilinx IP library like MAC, DDR and SPI interfaces causing a reduction in the design cost.**
- **We Integrated the LM96570 as the BF Transmitter; this enabled us to remove the pattern control logic from the FPGA in order to decrease more logic inside the FPGA.**
- **We Used a Complete BF Receiver Analog Front End IC, which integrates full 8 ADC channel with AGC in one compact IC. As a result of that we could achieve a dramatically reduction in the power consumption, the board size and the cost.**
- **Designing our owned IP cores for the special interfaces like the Uwire interface, Deserialized interface with buffering and timing control IP; These IPs will enable us for establishing a framework for future work.**
- **Creating the whole hardware schematic for the digital beamformer system and we are ready for the manufacturing in the Future**

#### 1.4.2. Firmware Design contribution

The Firmware design has a significant influence on the Digital beam former designs by many of aspects which are:

- **Using a well-defined US development KIT from TI, it includes a reach library of test vector from which we could verify our development against its reference vectors.**
- **We designed a digital beamformer framework referenced from the TI US development kit running in VIVADO HLS IDE.**
- **We succeeded in utilizing the VIVADO HLS in developing our receiver digital beamformer to produce it in a ready-made IP core working in EDK.**
- **We succeeded in the optimization phase of the IP core. We decreased the complete design of the beamformer from latency of 400,000 cycle (11 nsec) to 41,000cycles (nine nsec) against 100,000 cycles (one nsec) of the TI C64X DSP for 64 channel operation. This means we could achieve (1/3) of the DSP processing for the 64 channel processing (almost the same processing time for our target at 16 channel beamforming processing).**

### 1.5. Thesis Organization

The organization of thesis chapters from chapter one to seven is based on describing and defining the subjects. Specifying the layout of thesis chapters and the thesis motivation is described in chapter one. It is also introducing a thesis overall view with describing of the ultrasound system basic functionality. Chapter two gives background and literature review for the digital beamforming. This chapter describes the ultrasound wave characteristics, physical limitations and different types of beamforming. Chapter three describes the theory of operation which the ultrasound Beamformer operation is based on. It also discusses the differences between analog and digital beamforming as well as listing for the different existing technologies of the digital beamforming; furthermore, there is a discussion for the main digital beamformer signal processing parameters. Chapter Four describes the Hardware design by listing the Hardware design requirement and the Hardware design architecture also it discusses the idea behind the component's selections. Chapter Five introduces the design of the firmware beamformer from high level view; it describes the main architecture of the FPGA, and also it describes the different modules in the system transmitter, Receiver and MicroBlaze as the control unit of the system. Chapter Six describes in details the implementation of the firmware from low level design view of the digital Beamformer, and also it describes in details each module functionality as well as the considerations should be taken while its implementation. Chapter Seven is describing what is missing in the design and what is planning to continue to design in the future.

## **Chapter 2**

### **Physics of the Ultrasound**

#### **2.1 Introduction**

Ultrasound imaging was conceived of and developed out of sonar shortly after World War 2. It was during this period that the first 2D ultrasound images of soft tissues were shown by Wild and Reid [8], [9]. Since those early days, ultrasound technology has steadily improved; with the development of arrays in the 70's [10], the first digital techniques in the 80's, and advanced integration in the 90's. All conventional diagnostic ultrasound equipment depends on the ability of ultrasound waves to reflect from tissue interfaces. By measuring the time taken for echoes to return to the receiver, the location of the echo producing interface can be specified. Other imaging parameters include the amplitudes and the frequency spectra of the echoes. A full appreciation of the role of diagnostic ultrasound, its limitations and biological effects can only be gained by considering the physics of the propagation of sound waves in biological tissue. The propagation of sound waves is due to the elastic properties of the medium supporting the wave phenomenon. For most cases the propagation of ultrasound in tissue is a longitudinal compression wave i.e. a wave in which particle displacement is in the direction of wave motion. Exceptions do occur, for instance the propagation of sound in bone has a large transverse component due to the finite shear modulus of bone. The great virtue of ultrasound is the relatively non-hazardous non-invasive imaging of soft-tissue. Our concern will be largely with diagnostic ultrasound frequencies over the range 1-15 MHz.

#### **2.2 Wave-motion**

Acoustic waves are mechanical waves i.e. acoustic energy is transferred between two points in the medium while leaving the intervening medium essentially unchanged after transfer. Mechanical waves are of two fundamental types:

- Longitudinal: the oscillating particles of the medium are displaced parallel to the direction of motion (direction of energy transfer).
- Transverse: the oscillating particles of the medium are displaced in a direction perpendicular to the motion of the wave.

When the elasticity of the medium causes neighboring particles to display a similar oscillation, a wave is set up, and the oscillation appears to move through the medium with

some velocity of propagation. A single oscillation may set up a pulse or a series of oscillations can set up a wave train.

### 2.3 Wave propagation

Ultrasound transducers make use of longitudinal acoustic waves which the oscillations occur in the longitudinal direction or the direction of wave propagation. Since compressional and dilatational forces are active in these waves, they are also called pressure or compressional waves. Compression waves can be generated in liquids, as well as solids because the energy travels through the atomic structure by a series of compressions and expansion (rarefaction) movements as shown in Figure 2.1.

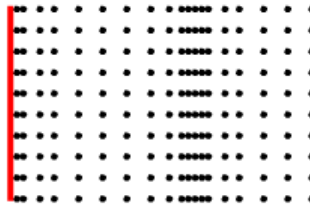


Figure 2.1 -showing Compression and the rarefaction of the longitudinal waves [10].

The speed with which the acoustic wave can travel is determined by the properties of the region in which it is traveling. The properties of primary influence to the wave are the density and bulk modulus [11]. The speed is related to these variables as in Equation 2.1:

$$c = \sqrt{k/\rho} \quad , \quad (2.1)$$

Where  $\rho$  is material density (in Kg/m<sup>3</sup>), and  $K$  is the adiabatic bulk modulus (in GPA). As this equation shows, waves travel faster in a stiffer medium than in a compressible one; and similarly travel faster in lower density materials than in higher. This second statement may seem counterintuitive, however it is important to realize that changes in bulk modulus tend to dominate over density changes, so while steel is 3 times as dense as water, it is nearly 50 times less compressible[12]. Transmission and reflection are similarly based upon the material properties of the media under consideration. In order to simplify our understanding of these Matching qualities, we use the concept of acoustic impedance. The characteristic acoustic impedance of a medium is defined as in Equation 2.2. Transmission and reflection is similarly based upon the material properties of the media under consideration. In order to simplify our understanding of these matching qualities, we use the concept of acoustic impedance. The characteristic acoustic impedance of a medium is defined as in Equation 2.2:

$$Z_a = \rho * c \quad , \quad (2.2)$$

Characteristic acoustic impedance, like its electrical counterpart, is a measure of the opposition of the medium to the propagation of a sound wave. When two mediums have a similar acoustic impedance they can be said to be “well matched” and sound waves will transfer between them with very little reflection. For normal incident waves, this impedance measure behaves similarly to its electrical counterpart, and reflection and transmission coefficients for waves traveling from material 1 to material 2 can be calculated as the following in equation 2.3 and 2.4 [18]:

$$R = \left[ \frac{Z_{a1} - Z_{a2}}{Z_{a1} + Z_{a2}} \right]^2 , \quad (2.3)$$

$$T = \frac{4 Z_{a1} Z_{a2}}{[Z_{a1} + Z_{a2}]^2} , \quad (2.4)$$

Where  $Z_a$  the acoustic impedance of the materials, R is the percent of reflected acoustic energy and T is the percent transmitted wave energy. We can also make use of an acoustic version of Snell’s Law to predict angle shifts in wave propagation caused by the interface Also the transmission of sound waves across an interface between two media is most directly described via this notion of sub- and supersonic wave crests. If a plane wave is incident onto the interface, the point of reflection in medium 1 generates a disturbance in medium 2 (Fig. 2.2) [17]:

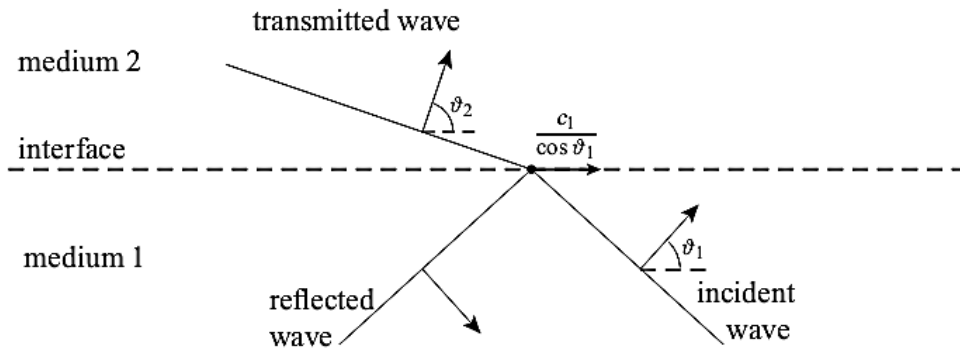


Figure 2.2 -Reflection and transmission at a discontinuity [17].

With sound speed  $c_1$  in medium 1 and direction of incidence  $(\cos \theta_1, \sin \theta_1)$  the disturbance velocity, measured along the interface, (the phase speed) is  $c_1 / \cos \theta_1$ . Depending on  $\theta_1$  and the ratio of soundspeeds  $c_1/c_2$  this disturbance moves with respect to medium 2 either supersonically, resulting into transmission of the wave, or subsonically, resulting into so-called total reflection (the transmitted wave is exponentially small). In case of transmission the phase

speeds of the incident and transmitted wave has to match (the trace-velocity matching principle, [17])

$$\frac{\sin \theta_i}{\sin \theta_t} = \frac{C_{.1}}{C_{.2}} \quad , \quad (2.5)$$

What these equations suggest is that a wide range of intuition we have gained from the field of optics, translates directly into the field of ultrasound.

## 2.4 Aperture Theory and Far Field Directivity Functions.

"Aperture" in acoustics is used to refer to either a single electroacoustic transducer or an array of electroacoustic transducers. The complex Aperture function, that is, the magnitude and phase of the sound distribution within the aperture, determines the Fresnel and Fraunhofer diffraction patterns of the aperture, which in turn determines the beam profile of a transducer element. The basic equations that are derived from complex aperture theory are used to describe the performance of a single transducer and an array of transducers. The derivations below are not presented in their entirety [19]. These basic equations are used in the simulations carried out in this thesis. The far-field and the near-field criterion are given by the following two equations [19]:

$$r > \pi R^2 \lambda > 1.356R \quad , \quad [19] \quad (2.6)$$

$$1.356R < r < \pi R^2 / \lambda \quad , [19] \quad (2.7)$$

Where,

$$r = \sqrt{x^2 + y^2 + z^2} . \quad (2.8)$$

is the magnitude of the position vector to a field point and R is the maximum range. The far field directivity function of a general volume aperture is given by[19],

$$D(f, s) = F_{r_a} \{A(f, r_a)\} = \int_{-\infty}^{\infty} A(f, r_a) \exp(+j2\pi s \cdot r_a) dr_a, \quad (2.9)$$

Where

$$r_a = (X_a, Y_a, Z_a), \quad (2.10)$$

$$s = (f_x, f_y, f_z), \quad (2.11)$$

Are the spatial frequencies

$$dr_a = dx_a dy_a dz_a. \quad (2.12)$$

$$A(f, r_a) = a(f, r_a) \exp[+j\theta(f, r_a)] , \quad (2.11)$$

Where  $a(f, r_a)$  is the amplitude and  $\theta(f, r_a)$  is the phase of the response at spatial location  $r_a$  of the aperture, both of them are real functions (The amplitude function is also called the amplitude window)

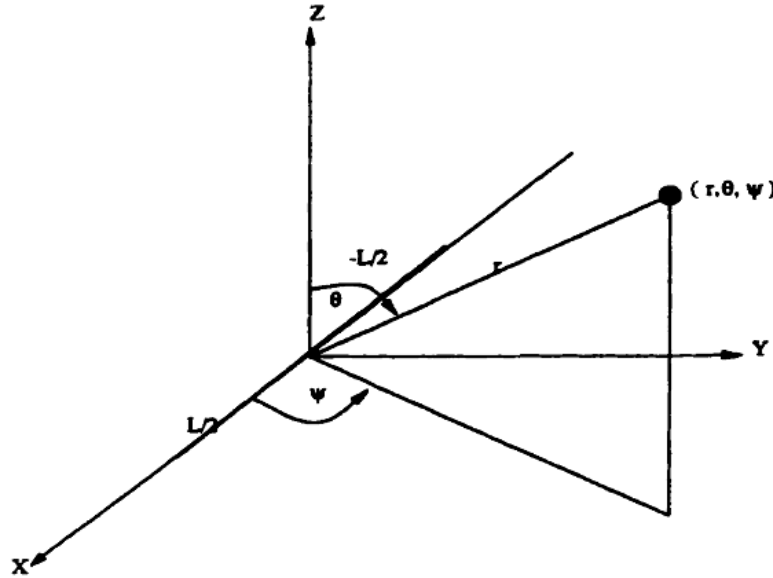


Figure 2.3 Linear apertures of length L meters lying along the X-axis. Also shown is a field point with spherical coordinates  $(r, \theta$  and  $\psi)$  [19].

## 2.5 Beamwidth and sidelobe

To determine the far-field beam pattern, beamwidth, and the relationship between beamwidth and sidelobe levels of far-field beam patterns, the elements are windowed i.e. each element are given a 'weight', thus controlling the transducer response. This is called apodization and is implemented with help of amplitude windows which are discussed next. In general as in the rectangular amplitude window it is defined by[20]:

$$\mathit{rect}(x/l) = \begin{cases} 1, & |x| \leq l/2 \\ 0, & |x| > l/2 \end{cases} \quad (2.13)$$

The amplitude of the complex frequency response of the transducer is constant along the length L of the transducer, regardless of the magnitude of frequency f with zero phases (Figure 2.4).

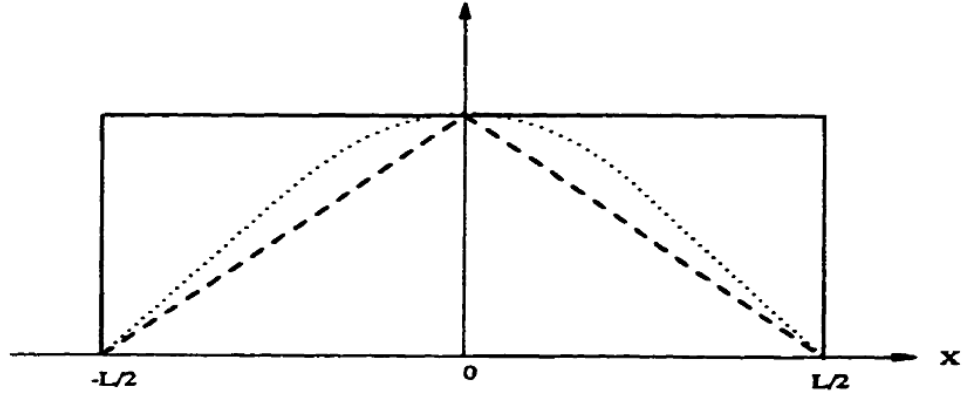


Figure 2.4-Rectangular (solid), triangular (dash) and hanning (dot) amplitude windows[20].

Or

$$D\left(\frac{\sin \theta}{\lambda}\right) = F_{x_4}\{\cos^2(\pi x/L) \text{rect}(\pi x/L)\} = \quad (2.14)$$

$$0.5 \sin c\left(\frac{\sin \theta}{\lambda} L\right) + 0.5 F_{x_4}\{\cos(2\pi x_4/L) \text{rect}(x_4/L)\}.[20]$$

This is the un-normalized far-field beam pattern of the hanning amplitude window. Referring to Eq. (2.9), the normalization factor is giving by[20]

$$D_{\text{MAX}} = D(f, 0) = L/\pi . \quad (2.15)$$

The normalized far-field directivity functions as defined as following[21];

$$D_N\left(\frac{\sin \theta}{\lambda}\right) = \frac{D\left(\frac{\sin \theta}{\lambda}\right)}{D_{\text{max}}} . \quad (2.16)$$

By substituting the previous Equations into Eq. (2.16) results in the normalized far-field beam pattern of the hanning amplitude window (see figure 2.4);

$$D_N\left(\frac{\sin \theta}{\lambda}\right) = \frac{\cos\left(2\pi\left(\frac{\sin \theta}{\lambda}\right)L\right)}{1 - \left(2\left(\frac{\sin \theta}{\lambda}\right)L\right)^2} , \quad (2.17)$$

Looking at the plot for the normalized far-field beam pattern of the various amplitude windows discussed above (figure 2.4), one sees that the first sidelobe level of the hanning amplitude windows are approximately -23dB, while the sidelobe levels for the rectangular amplitude windows are approximately -13 and -27 dB, respectively, this can be attributed to the way the windows approaches zero at the end point  $x=\pm L/2$ . The triangular window approaches zero in a comparatively smooth fashion i.e. with a smaller slope than the other two amplitude windows and hence has lower sidelobe levels. A reduction in sidelobe levels results

in a wider main lobe; see figures (2.5), (2.6) and (2.7) show the polar of normalization far-field beam pattern for amplitude windows discussed, as given by Equations (2.16), (2.17) and the plots, the main lobe width is dependent on the aperture length and wavelength. The beam width directly proportional to the wavelength  $\lambda$  and inversely proportional to the length  $L$  of the aperture. The figures shows the beam patterns for two different ratios of  $L/\lambda$ [21].

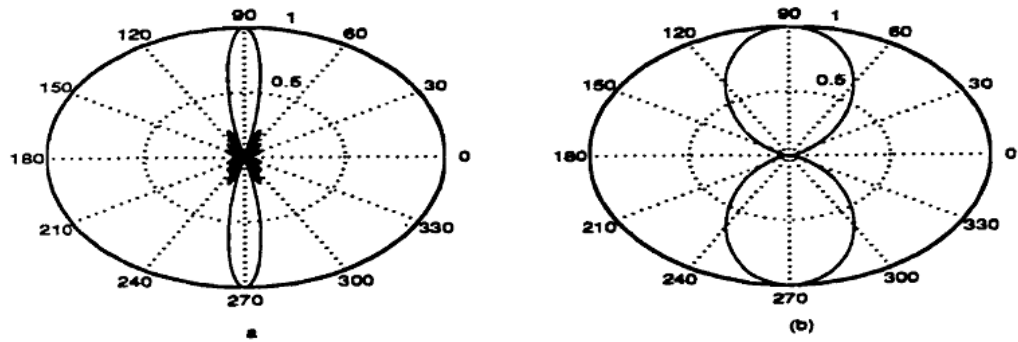


Figure 2.5-polar of the magnitude of the normalized horizontal far-field beam pattern of the rectangular amplitude window for (a)  $L/\lambda=4$ , (b)  $L/\lambda=2$ [21].

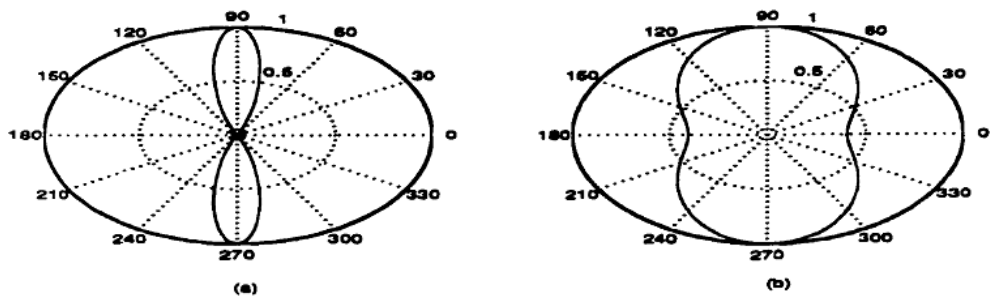


Figure 2.6-polar of the magnitude of the normalized horizontal far-field beam pattern of the triangular amplitude window for (a)  $L/\lambda=4$ , (b)  $L/\lambda=2$ [21].

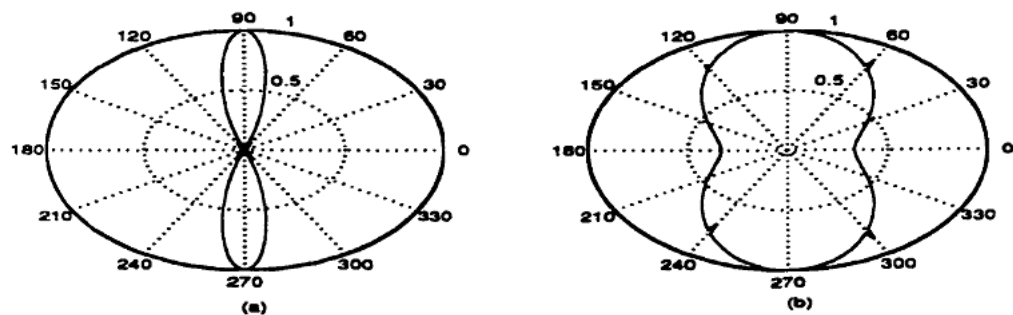
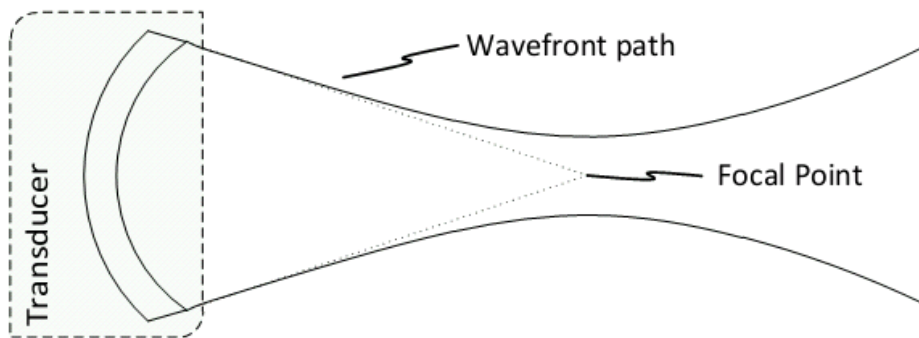


Figure 2.7- polar of the magnitude of the normalized horizontal far-field beam pattern of the hanning amplitude window for (a)  $L/\lambda=4$ ,  $L/\lambda=2$ [21].

## 2.6 Wave focusing and steering

A travelling plane wave will tend to spread from the edges as it travels using a process of diffraction. This phenomenon is described by the Huygens-Fresnel principle, which describes each point on a wave front as a source for an expanding radial wave. As the wave expands, its energy is spread across a greater region. The further the wave has traveled, the greater the reduction in wave amplitude, and the greater the reduction in amplitude of any reflections from the wave. In order to create a high amplitude wave-front (to improve the echo strength) the energy from the wave can be focused. Focusing the wave controls the travel path of the acoustic energy so that its signal strength is maximized within a desired region as shown in Figure 2.3.



**Figure 2.8-Generalized sketch of a geometrically focused ultrasound path. The Solid lines show an approximate path of constant relative strength [4].**

A transducer is any object that transforms energy from one type to another. In ultrasound we are usually interested in transforming electrical energy into acoustic energy, and the reverse. The transducer shown in Figure 2.1 is geometrically focused, which means that the focal point is determined by the curvature of the transducer. The same effect could also be achieved by using an acoustic lens. In either case, the focal point cannot be easily changed, and for this reason geometrically-focused transducers have limited use in a clinical setting. In order to be able to control the focus, a new type of transducer needs to be considered, and a new way of exciting it. An array transducer divides the transducer surface into sub regions, each of which can be controlled separately through separate electrical connections. The subdivided regions of an array are referred to as elements. When each element in an array is excited at different times, the diffraction of the individual wave fronts generated from each element can be planned in order to create a focused pulse as shown in Figure 2.4.

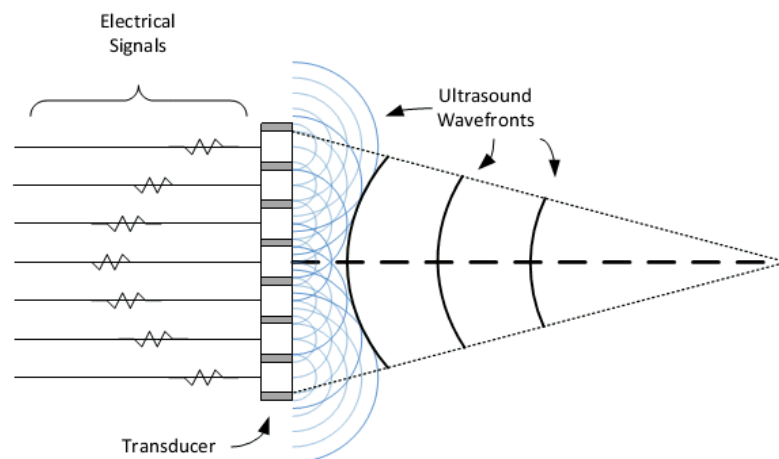


**Figure 2.9 – Timed electrical excitations create radial wave-fronts expanding from each element that constructively interferes in order to create a combined focused wave [4].**

Since it is the timing of the electrical excitation that creates the converging acoustic wave fronts, by adjusting the pattern of delays applied, the focal region can be adjusted. This process is called transmit focusing.

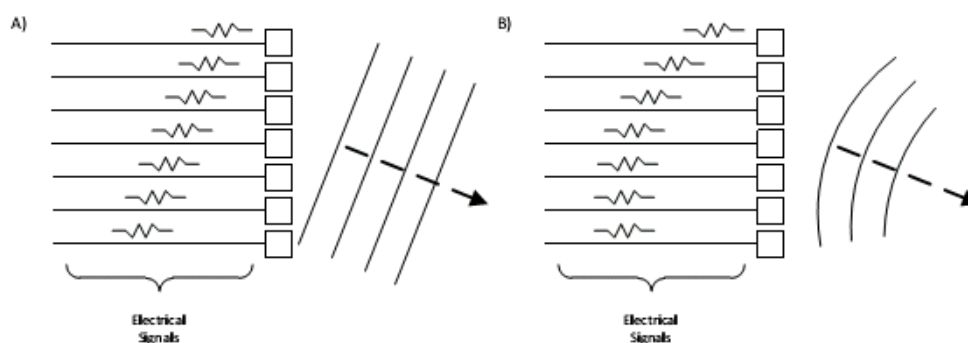


**Figure 2.10 – Non-symmetric excitation patterns direct an ultrasound beam off of the transducer axis (A), and combined with focusing produce steered focused beam (B)[3]**

Array transducers also make it possible to steer the beam off the transducer axis. Beam steering (illustrated in Figure 2.5a) is accomplished by skewing the transmit delay pattern so that it is no longer symmetric about the central axis of the transducer. The resulting ultrasound wave front is angled or steered away from the axis. Transducer arrays that employ beam steering as well as beam focusing are referred to as phased arrays. It should be noted that there are practical limits to the possible steering angles that the transducer can achieve. Typically steering angles are kept within the front  $90^\circ$  arc, beyond which, steering becomes difficult due to the limited directivity of the array elements. Transmit focusing and beam steering can also be combined so that the beam is focused along a steered path as shown in Figure 2.5b.

## 2.7 Receive focusing (beamforming)

All ultrasound transducers are reversible. An electrical pulse applied to a transducer will generate a sound wave; similarly, a sound wave incident upon a transducer will generate an electrical signal. This is how the echoes created in the medium are received. After a sound pulse is transmitted, the transducer begins to listen for reflections. When the reflections arrive back at the transducer they are converted into electrical signals, and the amplitude of the signals is proportional to the pressure of the sound wave that created them. In this case, the fundamental frequency of the transducer acts as a carrier signal, with its amplitude indicating the reflection size. The echo signal is extracted by taking the envelope of the received signal. In a geometrically focused transducer, signals from the focal region will arrive at the same time at the transducer surface, and thus create a large electrical signal. In an array, however, the signals will all arrive at different times at each element. These situations are shown in Figure 2.6(a) and (b).

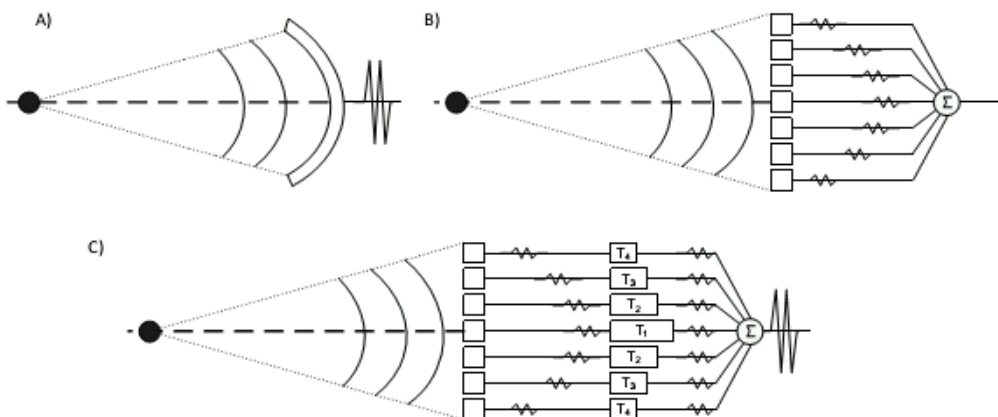


**Figure 2.11 - Receive focus beamforming a) geometric transducer b) array without delays c) Array with delays applied to compensate for signal arrival time differences [4].**

The differences in signal arrival time at each element need to be compensated for by delaying the electrical signals after they are received. If the same transmit delays are applied to the received signals, then waves originating from the focal region will constructively interfere, increasing their amplitude. Signals from outside of this region will not be aligned, and will tend to destructively interfere, reducing their impact on the final output. This process will create the same amplitude of signal as occurs due to a geometric focus. This is demonstrated in Figure 2.6c. The process of delaying the received signals in order to create focus is called beamforming. Beamforming is the inverse operation of transmit focusing, so all of the details discussed previously applying to transmit focusing, also apply to receive focusing. In addition, since beamforming delays are applied as the signals are received, it is

possible to change the delays during reception. Since there is a different fixed delay for signals from different depths, we can sweep our receive focal point as the signals are collected to keep an entire line of received data in focus during a single transmit [13]. This process of changing the receive delays while the signal is being received is called dynamic receive focus beamforming.

## 2.8 Grating Lobes

Constructive interference is relied upon to create a focused beam from an array transducer, both during transmit and receive. However, if the spacing of array elements is not fine enough, undesired constructive interference can occur in the imaging field. The result of this interference is referred to as grating lobes, and occurs when the path difference between two adjacent elements is an integer multiple of the pulse wavelength. The path difference is a function of the element spacing, and can be approximated as shown in Figure 2.7.

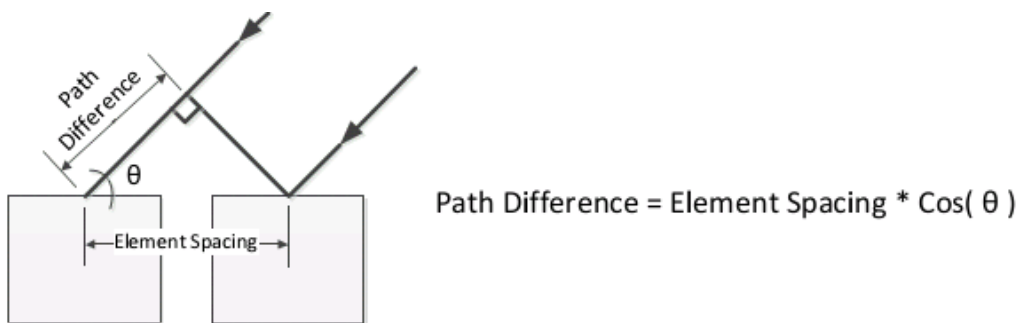


**Figure 2.12 - Approximation of path difference for wave incident upon transducer elements as related to the element spacing [5].**

Any energy coming from a grating lobe is indistinguishable from energy from the actual focal region. This can cause artifacts such as ghosting in the ultrasound image. When elements are spaced with a one wavelength separation, grating lobes will occur only along the plane of the transducer. However, steering the beam off axis will shift the grating lobes into the imaging region. Reducing the spacing further to half a wavelength is required to completely eliminate their effect.

## 2.9 Image formation

The ultrasound diagnostic system can display the various imaging modes by receiving and processing the various signals reflected. Among the imaging modes, B-mode (brightness mode) is a representative ultrasound image display mode, which is expressed with reflection intensities of tissues depending on acoustic impedance differences between the tissues. Also,

the ultrasound diagnostic system has C-mode (color blood flow) and D-mode (Doppler spectrum) as the major imaging modes, which display the mean velocity of blood flow using the Doppler effect of ultrasound by moving targets. In case of a tumor in B-mode image, it is difficult to observe a tissue having the reflection intensity not larger than those of neighboring tissues.

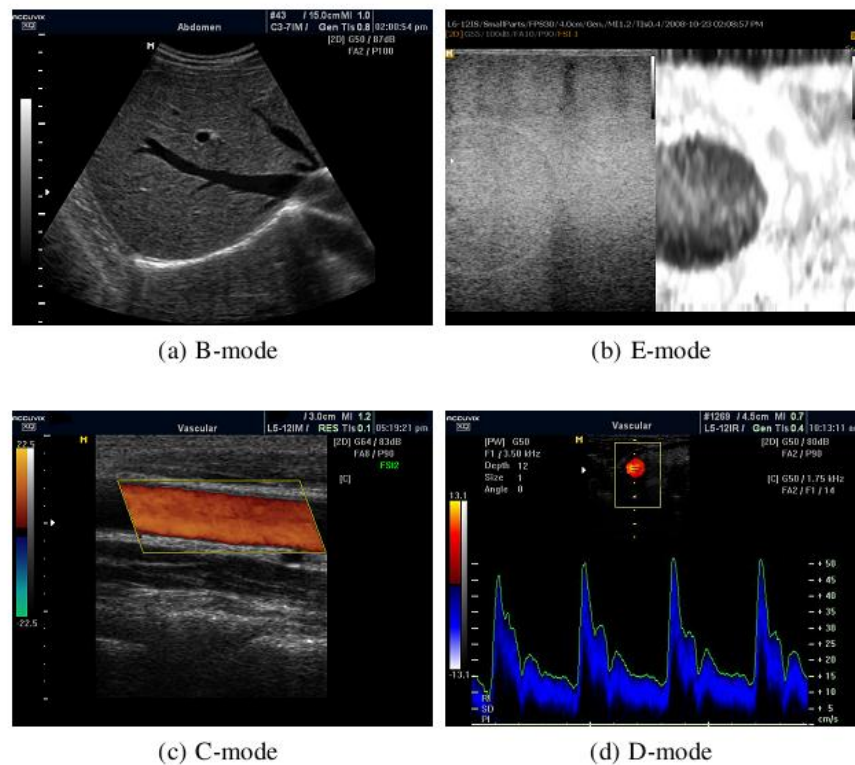


**Figure 2.13- Shows Different ultrasound imaging modes [10].**

So, there exists an optional E-mode (elastography), which can show the mechanical characteristics of the tissues such as tumor or cancer, and many investigations on the ultrasound elastography are in progress. This paper describes the basic principles of B-mode imaging process as a representative ultrasound image, present the issues of ultrasound medical imaging, and proposes the mathematical solution on the issues, specially, the application of elastography[62].

### 2.10 2D Imaging Transducers

Transducers can be made in a variety of structural arrangements. There are several broad categories of transducer arrangement that are typically used for 2D imaging; they are linear arrays, phased arrays, and annular arrays.

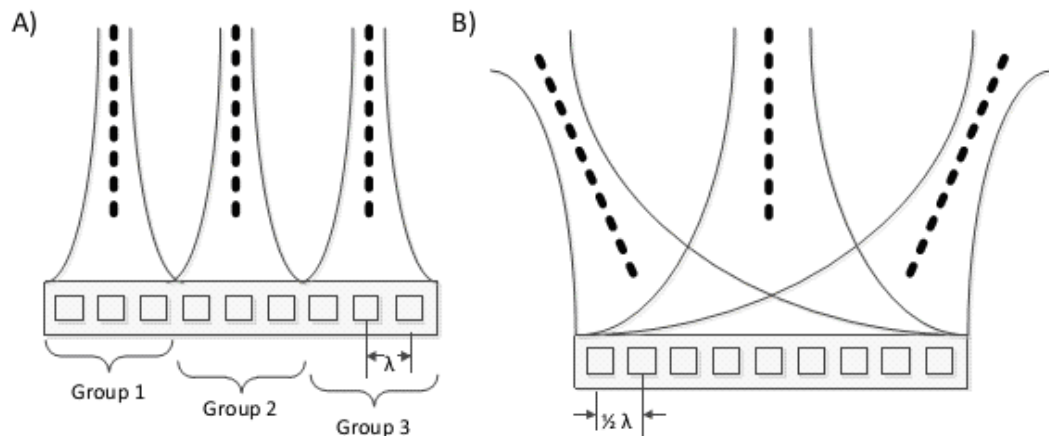


Figure 2.14 - Array transducer types a) Linear Array b) Phased Array [5].

### 2.10.1 Linear Array

A linear array consists of a long strip of elements spaced with full wavelength separation. Elements are then used in groups. Each sub group of elements is dedicated to producing a single transmission line. Because of the full wavelength separation, beams are not steered off of their axis to avoid grating lobes. If a fan beam is desired, the elements may be physically arranged along a curve. A linear array transmission scheme is demonstrated in Figure 2.12a.

### 2.10.2 Phased Array

A phased array is shown in Figure 2.12b. This transducer uses a strip of rectangular transducer elements in order to produce a beam. The strip elements are spaced at half a wavelength separation (or less). This spacing allows for off-axis beam steering without inducing grating lobes into the field, which is how this array is primarily used [16]. The image is made up of image lines that spread from the array over a range of angles, forming the familiar arc sector shape. Each line in the image is usually a separate transmission focused along an image line.

## 2.11 Summery

In this chapter, we described the ultrasound wave characteristics; we discussed the equations of the wave propagation, characteristic acoustic impedance, reflection and refraction of the ultrasound waves. .On the other hand we discussed the effect of the apodization gain valued on both of the beamwidth and the sidelobe and we described the effect of the three apodization types the rectangular windows, the triangular windows and the hanning

apodization. Furthermore, we studied the wave focusing and steering and how can we use the waves of delays to steer and focus the ultrasound beam to certain focal point and the vice versa. We discussed how we can use the same delay shape for retrieving these waves after being reflected from the body of concern (beamforming). Moreover we discussed the different ultrasound imaging modes B, E, C and D. Finally we discussed both types of the 2D Transducers which are Linear Array and Phased array transducers.

## **Chapter 3**

### **Digital Beamforming theory of operation**

The ultrasound beamformer re-aligns the received signals in order to produce B-scan lines. The method used to realign the signals, and the accuracy with which it can be performed, affects the quality of images obtained from the system. The primary method of realigning the signals is called the Delay and Sum method (DAS). This simply refers to the process of delaying the signal from each channel, and summing them together. There are many different electronic implementations that have been developed in order to realize a DAS beamformer. In this section we, will review the common types of beamformers, and contrast the strengths and weaknesses of each design.

#### **3.1. Analog Beamforming**

The earliest beamformers introduced delays through the addition of fixed electrical delay lines in the receive path. The major advantage of analog (continuous time) delays is that the signals ideally are not affected by traveling through the delay lines. These analog delays could be implemented simply as long transmission lines, where the transmission line length would determine the signal propagation delay. This works well at high-frequencies ( $> 50$  MHz) but at lower frequencies the required transmission lines are prohibitively long. Instead delays were often composed of lumped inductor capacitor (LC) circuits. This simple fixed delay structure would not allow for the delay to be varied. In order to improve the performance and versatility of the analog beamformer, the fixed delay line was replaced by a tapped delay line (TDL) [26], [27]. A TDL breaks the single long analog delay into small delay sections. By using an analog multiplexer (MUX), the signal can be brought out after different numbers of TDL segments. Digital logic can control the MUX selection, and the output from each can be added to provide the beamformed output. Figure 3.1a shows the structure of a tapped-delay line analog beamformer. In order to accurately beamform the signals using a TDL beamformer, then spacing of delay taps (and therefore the number of taps required) must be equal to the smallest delay step tolerable.

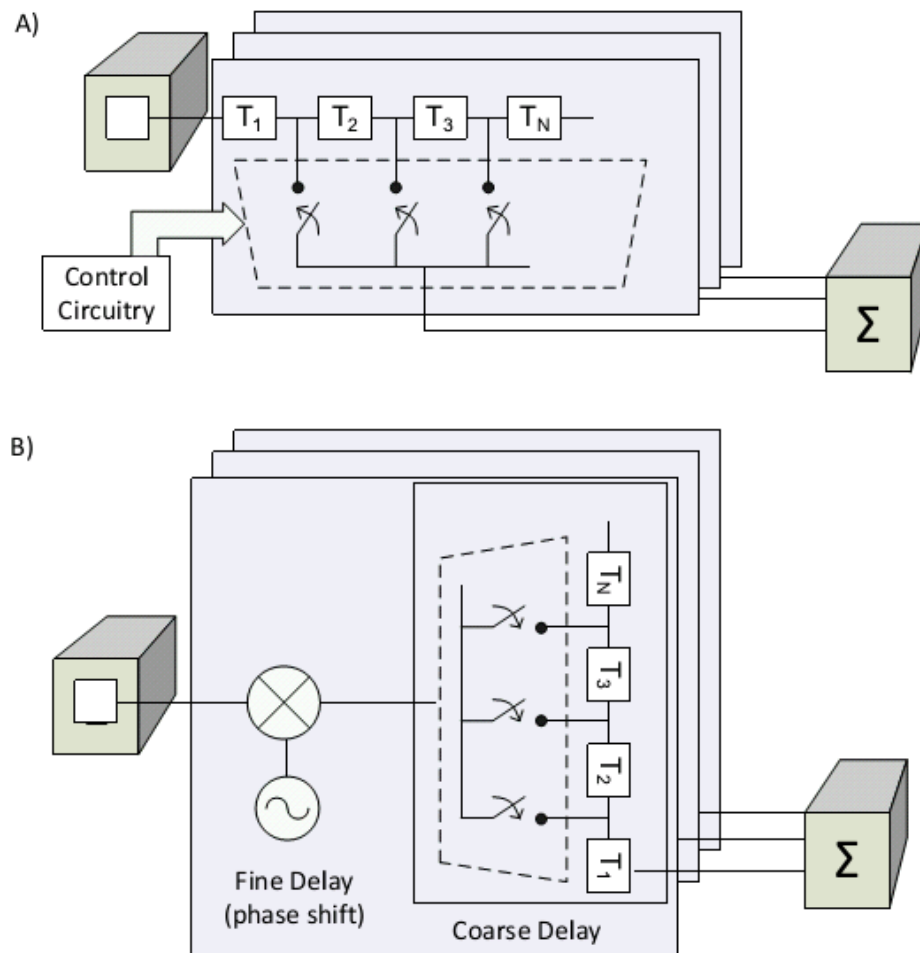


**Figure 3.1 - Analog beamformer types, A) a delay line beamformer uses selectable fixed taps to vary the delay on each signal B) a coarse/fine delay beamformer uses fixed taps for Coarse adjustment along with a phase shift for fine adjustment[26].**

This requires a huge amount of hardware, even for small array sizes. Furthermore, the engineering challenge to create each TDL with perfect matching to both the analog MUX tap, as well as following element, was significant. The Coarse/fine Analog Beamformer was designed to address these issues. One design is shown in Figure 3.1b. This implementation has been used in both commercial and recent research projects [28]. The coarse/fine beamformer divides the delays into a fine delay that can be controlled with precision and a coarse delay made up of larger TDL sections as discussed previously. The fine delay is most commonly provided by a phase shift, rather than a true delay. This approximation works well enough for small delays, and can be varied with great precision through a phase shift mixer. The TDL can be implemented in a number of ways such as: LC delay lines (as discussed previously), serial-analog memories [29], Analog shift registers, or surface acoustic wave delay lines [30].

## **3.2. Digital beamforming**

Most modern systems convert the analog signals received from the transducer into a digital form before beamforming. After conversion, beamforming can then be handled using digital logic.

### **3.2.1. Classes of the Digital Beamforming**

Existing digital beamforming techniques can be categorized into two classes, namely time domain beamforming or frequency domain beamforming. These classes relate to the domain that the echoed image data is processed or operated on. Time domain beamforming is associated with conventional methods, whereby signals are shifted or translated in time, and is more easily visualized by humans. Frequency domain beamforming often requires the translation of sampled data, after A/D conversion, to its frequency domain equivalent and an operation such as a phase-shift is performed within the frequency domain, equating to a time delay in the time domain. The extra processing required for translation is generally balanced with a more efficient or cost effective way of frequency domain implementation. Mucci presented a brilliant paper describing and comparing, from a hardware perspective, the available efficient digital beamforming algorithms from both time and frequency domains and the advantages and disadvantages of each [31]. Although the paper is almost twenty years old, the content and issues outlined are still more than relevant for today's imaging systems. Emphasis was placed on non-adaptive conventional procedures but references were still made to more intelligent methods that utilized adaptive techniques such as phase aberration correction. Please see appendix D for more details about frequency domain.

### **3.2.2. Digital Beamformer basics**

The functions of a beamformer include the following [21] :

- **Generate transmit timing and possible apodization (the term apodization will be used as a synonym for weighting, tapering and shading) during transmit .**
- **Supply the time delays and signal processing during receive .**
- **Supply apodization and summing of delayed echoes .**
- **Possible additional signal processing related activities.**

The goal of all of these functions is to create a narrow, uniform beam with low side lobes over as long a depth as possible. During both transmit and receive operations. Appropriate

delays are supplied to accomplish the focusing and steering needed. Figure 3.2 demonstrates the geometry that is usually used.

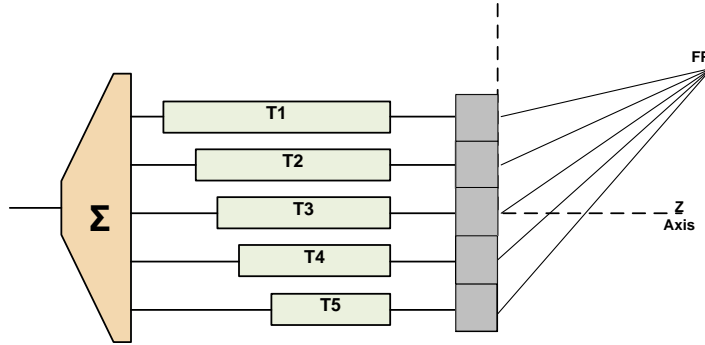


Figure 3.2 – Shows basic geometry for beamformer calculations

Figure 3.2 also illustrates the reception process. Wavefronts are shown emanating from a point source labeled as FP. These signals are received by the array elements, amplified and passed on to the delay lines. The delay lines are shown as rectangular boxes whose length corresponds to the desired delay. Finally, the echoes are passed on to the apodization/summer stage, which takes the contributions from each element, multiplies them with a weighting function, and adds up the results. The transmit operation is essentially the inverse of receive focusing; time delays from a common synchronization signal are generated by some means, often down counters, and the array elements are fired accordingly. It is assumed the array elements act as point sources and generate the required wavefronts. The general expression for the received echo  $r(t)$  [33]:

$$r(t) = \sum_{i=1}^N A_{ri} \sum_{j=1}^N A_{xj} s \left( t - \tau_{ri} - \tau_{xj} + \frac{2R_{fp}(t)}{c} \right). \quad (3.1)$$

In this expression, the transmitted waveshape is  $s(t)$ . The A's refer to whatever weighting function that might be applied to each of the channels during transmitting and receiving operations. In the simplest case these would be equal to one for uniform aperture weighting.  $2R_{fp}(t)$  is the distance of the source point (FP) from the center of the transducer array and  $c$  is the velocity of the wavefront in meters per second.. Similarly,  $\tau$  is refer to transmitting and receive delays applied during transmit and receive beamformation operations.  $i$  and  $j$  are indices of the receive and transmit elements, respectively, and subscripts  $r$  and  $x$  refer to receive and transmit operations. These four parameters,  $A_{xj}, A_{ri}, \tau_{ri}$  and  $\tau_x$ , will form the basis of the discussion on beamformer evolution; changes in their values and in the methods by which their role has been implemented has defined the different generation of instruments. Quality of beamformation is strongly influenced by them. Finally, in Equation 3.1,  $N$  is the

number of transmit and receive elements and will assumed to be constant. N is also an important factor in establishing the performance level and the cost of an ultrasound system. Referring to Figure 3.2, the expression for determining the values for the transmitting and the receiving delays given a desired focal point is [33]:

$$\tau_i = \frac{1}{c} \left[ \sqrt{(X_i - X_{fp})^2 + Z_{fp}^2} - R_{fp} \right], \quad (3.2)$$

where c is the speed of sound, r, is the transmit or receive delay,  $X_{fp}$ , and  $z_{fp}$ , are the coordinates of the point at which we wish to focus, and RB is the distance from the origin or the phase center to that focal point. We will give a brief demonstration about the signal-processing parameters of the ultrasound signal; accordingly, we can determine the proper design requirements. In general, our transducer pulse signal (for 15 MHZ) will appear in the time domain as oscillation pulse within certain period of time and will reach zero amplitude after this time as shown in figure 3.3.

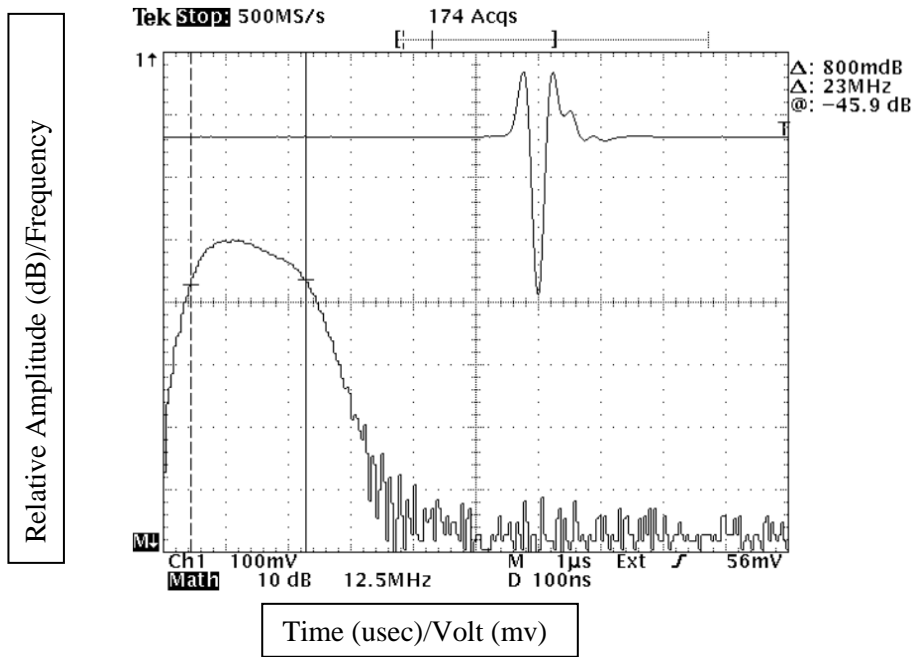


Figure 3.3- Shows 15 MHZ Transducer pulse [14].

In general, the ultrasound signal transmitted signal is determined by different parameters determine its shape and its proper strength to reach the required body depth.

### 3.2.2.1. Frequency Spectrum

The transducer signal characterized by its frequency spectrum, by having a look on the ultrasound pulse in figure 3.2, we find out that the entire transmitted ultrasound signal is

below the 20 MHz, as well as we can notice the harmonics after 23 MHz thus according to the Nyquist theory, we should sample at least of 40 MHz.

### 3.2.2.2. Sample Rate and Quantization

The main challenge when dealing with digitized data is the effect of quantization on the quality of the resulting image [3]. When the signal is sampled, it is quantized in both time and amplitude. This essentially rounds the precision of the sampled signal. The effect of this rounding can be quite significant, when the full range of signals is considered. For time quantization, choosing the closest sample time causes the constructive and destructive interference to imperfectly align, reducing the output signals amplitude. The effect of amplitude quantization is similar. Figure 3.11 shows example radiation patterns simulated with different time and amplitude quantization levels. A secondary lobe level of around -60dB is desirable to achieve “clinical quality” images.

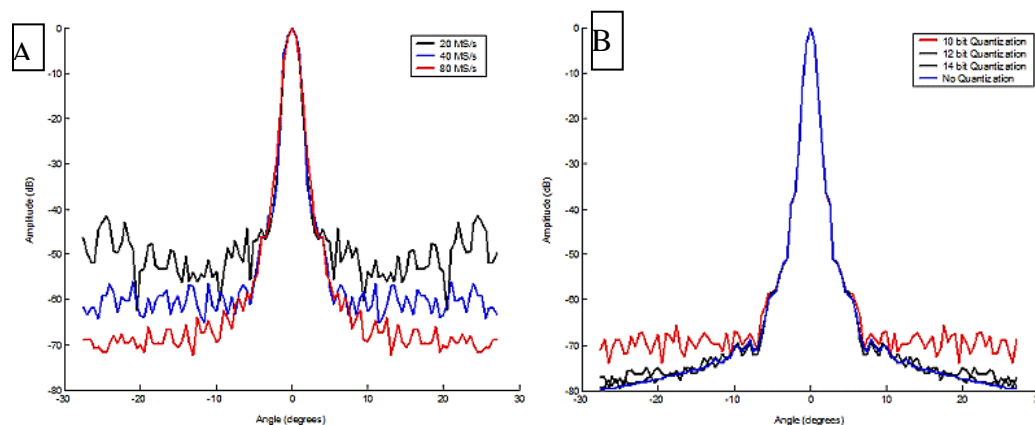
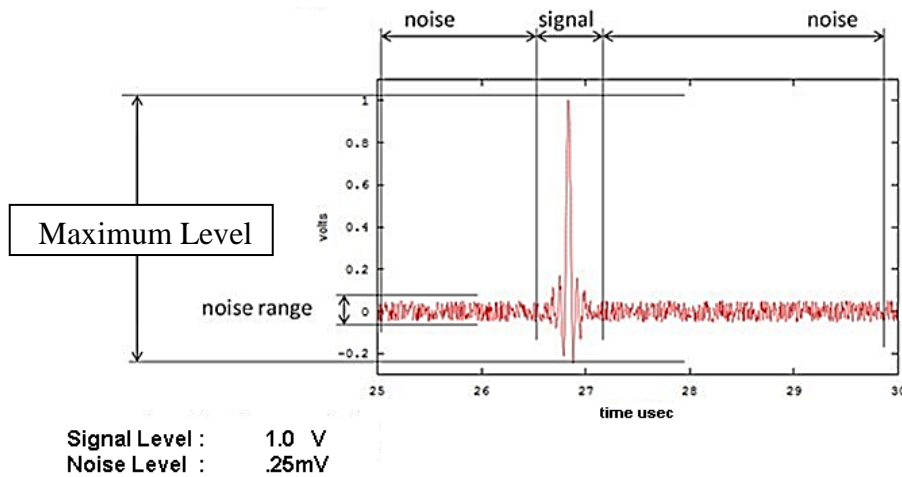


**Figure 3.4– Theoretical radiation patterns showing A) the reduction in secondary lobe level with slower sampling rate time quantization B) the reduction in secondary lobe level with decreasing amplitude quantization bit depth [3].**

### 3.2.2.3. Signal to noise ratio (SNR)

SNR is the ratio of the measured signal to the range noise level. Our ultrasound signal received signal is about 1.0V and the noise range is about 25mv so our SNR equal 72 db.



$$SNR = 20 \cdot \log(\text{signal}/\text{noise}) = 20 \cdot \log(4000) = 72 \text{ DB}$$

Figure 3.5. Shows frequency spectrum ultrasound with signal level 1.0V signal noise ratio SNR.

### 3.2.2.4. SNR and bit depth

SNR is represented in dB, but for digital system we need bits representation  
Bit depth is the number of bits used to represent that number, Relation between bit depth and dB is:

$$\text{BitDepth} \geq 10^{\left(\frac{SNR}{20}\right)} \quad (3.1).$$

Bit	7	6	5	4	3	2	1	0
Means	+/-	64	32	16	8	4	2	1
Value	0	0	1	1	1	0	1	0

$+( 0 \cdot 64 + 1 \cdot 32 + 1 \cdot 16 + 1 \cdot 8 + 0 \cdot 4 + 1 \cdot 2 + 0 \cdot 1 ) = 58$

bits	range	dB
1	2	6
2	4	12
3	8	18
4	16	24
5	32	30
6	64	36
7	128	42
8	256	48
9	512	54
10	1024	60
11	2048	66
12	4096	72
13	8192	78
14	16384	84
15	32768	90
16	65536	96

1 bit = 2x value

$$20 \cdot \log_{10}(2) \approx 6 \text{ dB}$$

$72 \text{ dB} \xrightarrow{\text{implies}} 10^{(72/20)} = 3981 \approx 12 \text{ bits}$

$$\text{BitDepth} \geq 10^{(SNR/20)}$$

Figure 3.6 SNR VS bit depth

### 3.2.3. Physical limitations

The speed with which an ultrasound pulse travels in a medium is a characteristic of the medium material. The attenuation that a wave experiences is a combination of absorption and scattering, is related to frequency and temperature, as well as material properties. The

attenuation in water is approximately  $0.7 \text{ dB}/(\text{cm} * \text{MHz})$ [12]. This effectively places limits on the possible imaging depth achievable for a given transducer/beamformer arrangement. For example, if the maximum system gain available is +50dB, and the ADC quantizes with 12 bits of precision (giving  $\sim 70\text{dB}$  of SNR range), this gives a complete system range of approximately 120dB for a single element transducer. So we can determine that the signal from a 5MHz transducer would be too small to be detected at 17.1cm of depth ( $120 / (5\text{MHz} * 2 * 0.7)$ ). Having determined the maximum depth possible, we can then use this to determine the maximum round trip time of flight (speed of sound in the medium is approximately the same as water (1510 m/s) .

Using this speed we can estimate the time required for a signal to penetrate to its maximum depth and return. Continuing the above example, it would require approximately 0.22ms ( $0.171\text{m} * 2 / 1510\text{m/s}$ ) to complete the trip. By taking the reciprocal of this time-of-flight, we can determine another key limiting factor for any ultrasound system: the maximum number of pulses that can be completed per second. Again to continue our example, this system could achieve 4415 pulses per second. At real time frame rates (25FPS), this allows for 176 pulses per frame. This number is not particularly limiting for 2D imaging, unless an unusually large number of scan lines or

### **3.2.4. Ultrasound digital beamforming implementations**

The specific hardware selected to implement a beamformer has a great effect on the speed, accuracy, and cost of the entire system. In general, the type of digital logic hardware can be used to broadly categorize how beamformers approach the task. These groups are: micro-processor based, software based, and Field Programmable Gate Array (FPGA) or Application Specific Integrated Circuit (ASIC) based. The first delayed calculation beamformers to be used were micro-processor based beamformers. In these systems, the digitized data is recorded into a RAM buffer. Once recorded, a microprocessor (or similarly, a Digital Signal Processor) is used to select the desired samples and sum them together to produce an output image. Microprocessor technology has steadily improved over the past few decades, increasing in speed while decreasing in price. Even with these gains, microprocessors are inherently a serial processing device, meaning that each operation must be performed sequentially with at most a single possible operation per clock cycle. By its very nature this means that each additional channel adds a multiplier to the amount of time required for processing the data, and the total time required to beamform a single line is proportional to the

number of array elements. While microprocessor based systems have been made to handle real-time 3D volumes of data, the required hardware was both large and expensive [36].

Another implementation of a digital beamformer that has become possible only very recently is a software beamformer. In this beamformer, the delay and sum operations are performed in software on a PC. Hardware is only used to digitize the signals. This moves the bulk of the work of the beamforming process into a low cost, but high performance general purpose processor. The major benefit of software beamformer based systems is the ease with which they can be constructed. By making use of existing sampling cards and drivers, very little additional hardware is required to complete the system. Further, since all data is available on a PC environment, the difficulties of development of new experimental processing techniques is greatly eased. Unfortunately, these systems are bandwidth limited, even using modern PCIe buses. An average PCIe (2.0, x8) bus in a current generation system can support a theoretical maximum 4GB/s transfer rate, with implemented versions achieving far less. This speed is sufficient for 40 channels of high-speed ADC data (65Ms/s, 12bit), with marketed versions falling far short of the theoretical transfer rate. Because of these limitations, it is not currently possible to conduct high-speed, high-channel beamforming using these systems. Beyond this, the sampling hardware is sufficiently expensive itself to offset the cost of the savings by using PC beamforming with larger systems. This option remains viable for fast development with low speed, and arrays with a small number of elements.

Either an FPGA or ASIC device is capable of implementing a hardware based beamforming method. An FPGA is a hardware chip that is comprised of reconfigurable logic circuits. The physical hardware connections within the device can be reconfigured so that its digital logic functions are arranged to perform nearly any logical operation desired. By contrast an ASIC is designed at a silicon level to perform the desired series of operations, and manufactured to only include the necessary logic for its original design. ASICs are significantly more expensive to both design and develop, but can produce cost savings when produced in large batches.

ASICs are mainly used by larger companies. In both devices the approach to beamforming is the same. The beamforming operations are performed using digital logic gates, in each device. By its nature, digital logic is parallel, and pipelined for high throughput. For ultrasound beamformers, this results in extremely high-speed performance. Also, since each channel is processed in parallel, additional channels require more hardware to process, but the processing time remains almost the same. The main limitation of ASIC and FPGA

designs is their complexity to produce. They require a significant amount of support circuitry, and can take a long time to develop and debug.

### 3.2.5. Digital beamforming Development

The idea of building a platform for research is not new. There has been a need in the ultrasound community for this type of application for a number of years [37].

Up until very recently, there have been no options available. Over the past few years, however a few companies have started to produce flexible beamformers to fulfill this role. This section will trace the development of digital beamformation. We will start from the very early designs and work our way towards the present.

#### 3.2.5.1 Digital beamforming Earlier Development

The earliest works on use of digital control for delays appeared in 1975 [38]. A technique was developed for use of charge coupled devices (CCD) to provide programmable time variable analog signal delay for scanning a linear ultrasonic phased array. This technique had dynamic focusing depths of 2 to 40 cm. The element delays were controlled by a 8080 microprocessor. Figure 3.6 shows the system operation of the earliest attempt at digitally controlling delays.

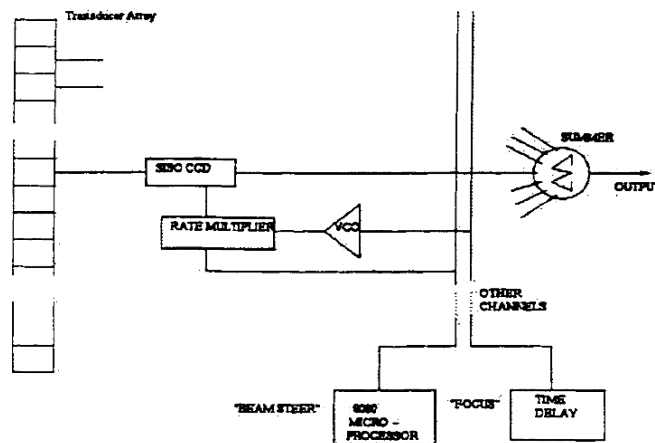


Figure -3.7 Simplified system operation of earliest attempt at digitally controlling delays [38]

Even though digital control was used to control delays, the concurrent use of analog delay lines created major problems in imaging like image artifacts. This led to the development of electronic delay lines and new techniques for dynamically varying the electronic delay lines. For the first time, the concept of sampled data systems was used to implement circuits for electronic delay lines [38]. The underlying principle behind these delay schemes involved

buffering the sampled data in a memory with independent read-write ports. The stored samples are read out after an appropriate number of clock cycles to generate an on-line, pipeline delay (Figure 3.7a).

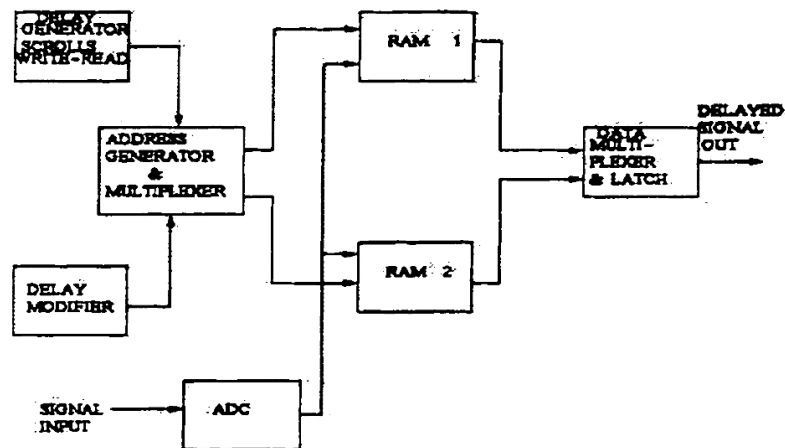


Figure -3.8a Principle OP digital delay line [32]

Another variation of implementing a delay line was also described [32, 39]. A FIFO (first in first out) device in conjunction with a RAM memory was used. The FIFO eliminates the addressing circuitry needed for RAM implementation. The delays thus implemented are long with high precision broad bandwidth and minimum phase distortion. Furthermore, the development and refinement of IC electronic components made these schemes attractive. Figure 3.7b shows the general architecture of digital beamformer implemented.

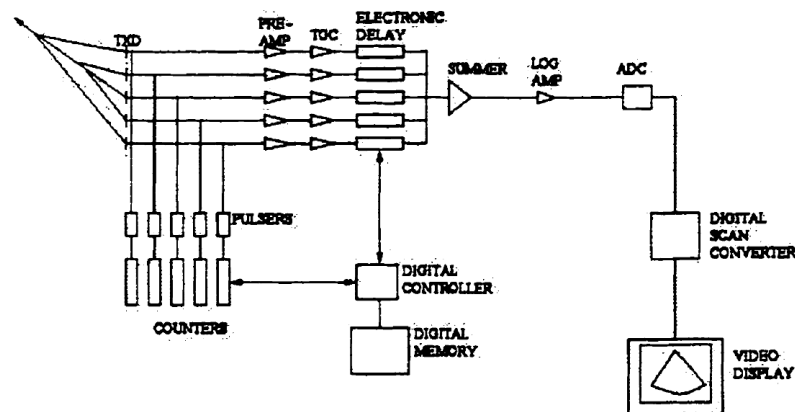


Figure 3.8b- Phased array ultrasound system with digital delays[39]

Figure 3.8 is a block diagram of earliest digital system constructed where all analog circuitry is replaced by digital circuitry [39]. In this 16-channel system, the microprocessor controller fixed the times at which each transmitter sends an electrical pulse to its transducer element, to steer the acoustic signal in the desired direction. The echo signals after amplification are digitized and fed to a digital delay circuit consisting of FIFO memory element.

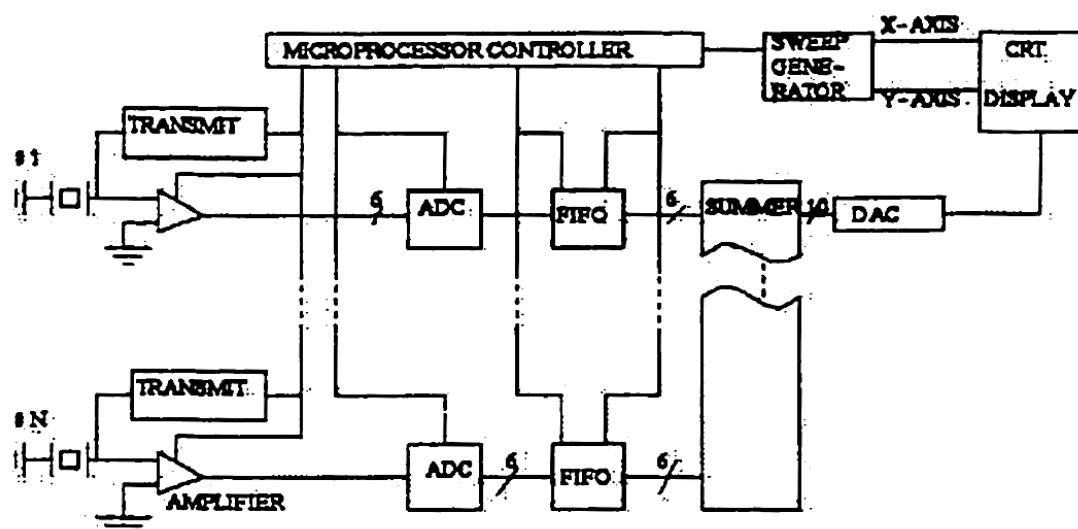


Figure 3.9- Block diagram of the ultrasonic imaging instrument when the analog circuitry is replaced by digital circuitry [39].

The delay in this element was controlled by the microprocessor to provide focusing and steering at the receiver. The signals were then summed together to form the reconstructed image. One of the major problems in medical ultrasound imaging was the imaging of the dynamic movements of organs such as the heart. The systems that were developed made use of one delay line per channel, providing the required delay in a discrete quasi-continuous manner. Each delay line provided hundreds of delay taps to provide the overall delay. So real-time scanning of the heart required fast switching to continuously track the echoes, which required an especially complex control system and introduced undesirable switching noise. In order to track the variable returning echoes efficiently, novel methods for implementing a programmable delay system were developed [40, 41]. The technique was based on separate and independent processing of the carrier and of the envelope of the echo pulses. Carrier phasing was accomplished by electronic phase-shifters, while delay lines varied the envelope delay. The approach adopted was based on mixing the echo with a digitally phase-controlled coherent local oscillator, followed by filtering of the upper or of the lower sideband. Once phase coherence of signals was established, the increment of the delay line required for time-shifting the signal envelope is no longer dependent on the carrier frequency value  $f_0$ , but on the extent of signal bandwidth around  $f_0$ . O'Donnell et. Al., [42] proposed a digital beamformer with autonomous channel control in place of the conventional delay and add architecture. The fully digital beamformer used the principle of baseband interpolation. A block diagram of the processing performed on each channel is presented in Figure 3.9.

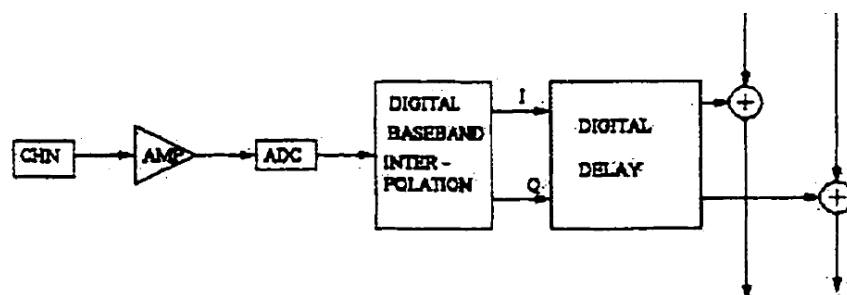


Figure 3.10 - Fully digital beamformed using baseband interpolation [42].

The digital baseband interpolation algorithm uses baseband demodulation followed by Low pass filtering and phase rotation to implement the delays. The phase is rotated using a CORDIC processor. While the earliest commercially available digital beamformers were available in the early 80's, they did not begin to have significant impact until the early 1990's. Much of this delay was due to the need for A/D converters (ADC) with sufficiently large number of bits and a high enough sampling rate for ultrasound signal digitization. In the designs discussed above [32, 41], 8-bit A/D converters were used which limited the using quantization of delay as well as the pulse fidelity. They tried to overcome this problem by analog shift registers [32] or by phase shifting [41]. Therefore an obviously important topic is the number of bits required for A/D conversion. The literature does not supply a real answer. Most expressions given are constrained by the assumptions mad. Now 12- bit A/D converters have been developed, thus increasing the dynamic range.

### 3.2.5.2 Digital beamforming existing technology comparison

In this section we will review the commercially available beamformers, and contrast them against the design developed in this thesis. Although most of these systems have been released since the beginning of this thesis work, each of them contains a number of trades-offs that make them unsuitable for our application. The majority of commercial development has focused on extracting raw sample data from a commercial system for post-processing. This serves the needs of a segment of the ultrasound community that is developing post-processing algorithms, but ignores the requirements of those working on transducer designs and front-end processing techniques. This trend began with the development of Ultrasound Research Interface (URI). The original URI was developed in 2003 by Siemens as an extension to their SONOLINE Antares Scanner, and was called the Axius Direct URI. Since that time, Siemens, GE, and Philips/ATL, have all produced add-on interface cards for researchers to access some parts of their system hardware. Most of these systems are not comparable to this thesis work as they do not allow the use of custom transducers, and contain a highly restricted interface.

In the last few years, Ultrasonix has made the open nature of its platform a selling feature. This began with the 500RP [43]. This platform contained a fixed number of channels (32) and a fixed sampling rate (40MHz), but allowed low level access to the beamformer through an open API framework. The system was still expensive (\$65k-\$100k USD), and could not support either the channel count or frame-rate required by some systems in our lab (288 channels, real-time 3D). Their more recent effort is the Ultrasonix SonixDAQ and SonixTOUCH Research system released in 2010[28][25]. The SonixDAQ is an add-on module to the SonixTOUCH that is intended as a data collection tool. The module can support a large, but fixed, number of channels (128), to capture a large, but fixed, buffer of data (16GB). The module is limited in that its external download link is restricted to USB 2.0 speeds, and is not intended for real-time processing of volumetric data. The SonixTOUCH itself can only be used with transducers it is designed for, and the processing hardware cannot be adjusted to account for transducers with differing numbers of elements. In addition, the cost of the SonixDAQ system (\$70-80k) is added on to the already high price of the base system.

The other major development in research platforms comes from developments in software beamformers. In 2007 Vera Sonics announced a commercially available software beamforming platform the Vera Sonics Ultrasound Engine [46]. This system can support a maximum of 64 channels, although only at reduced sampling rates. In comparison with the amount of data throughput used on a standard channel in this thesis, only 8 channels would be supported. This system is not competitive with the channel count and data rate required for our applications, and furthermore, would require additional layers of hardware to interface with our transducers.

Outside of commercial developments, individual research groups have contributed their own beamformer system designs to the store of academic knowledge available. C. Hu et al. developed an FPGA based high-frequency beamformer [47]. Their design was only for low channel count devices, and due to a low-speed USB PC connection, only for offline or 2D processing. The same group earlier this year reported a mixed analog-digital based system replacing their earlier design [48]. The design uses a commercial ADC capture board that digitizes RF data from an analog beamformer front-end. They were able to beamform a 64 element high frequency array at 400fps. This system is still restricted to 2D, and contained a fixed number of channels. The analog nature of the design also places considerable restrictions on the applications of the system; for example, parallel beamforming is impossible with this design, as is supporting lower frequency transducers.

Yasutaka et al. [49] have reported a high-speed FPGA based beamformer design, although no hardware has yet been produced. JA Jensen and S. Nikolov et al. have also reported several hardware beamformer designs. Most recently, they have begun to construct a large hardware capture beamformer [50], [51]. The hardware specifications presented have been impressive, however the design has not yet been presented as complete. Also the cost of the complete system places it out of reach of most researchers. In addition, many researchers have begun to attempt to use software based beamforming systems, however all have experienced the drawbacks described in the previous section [52].

In addition to the shortcomings given in the systems above, all of the shown solutions fail to be effectively scalable to support both large and small designs. If a system is designed for transducers with few elements intended for low-speed imaging, it is not expandable to high-end designs. If a system targets transducers used for high-speed imaging, it does not scale for use with low-end systems. The system given in this thesis provides an ideal match for both high-channel count designs for high-speed imaging, as well as the opposite end of the spectrum in low-cost, low-channel systems, due to its inexpensive and versatile design.

### 3.3 Summary

Beamformer design has been an integral part of the ultrasound system since the technology was conceived. We discussed in this chapter the meaning of the analog beamforming and the digital beamforming and described the advantages and the disadvantages of both. Furthermore, we discussed the main features of ultrasound digital signal processing by studying the ultrasound pulse Frequency Spectrum, Sample Rates, (SNR)Signal to noise ratio, Digitalization and Bit Depth, Arithmetic precision and Signal band width and Sampling rate also we studied the ultrasound digital beamforming different ways of implementations. At the end of the chapter we made a comparison between the existing technologies of the digital beamforming designs.

## **Chapter 4**

# **Ultrasound Digital Beamformer Hardware Design**

### **4.1. Introduction**

This chapter will describe the design of a digital beamformer Hardware. We will start by describing an overview of the complete hardware design, and how the different functions are segmented into separate hardware. Next, the hardware component choices made, and each of the hardware sections is discussed in detail to describe the key features of each design. Finally, the cost required to produce each board is detailed.

### **4.2. Hardware Design Requirement**

The beamformer design will need to excel in a number of areas. First it must be reconfigurable. This reconfiguration needs to allow it to create a nearly arbitrary image region, and should have the ability to vary nearly every parameter involved in the beamforming calculations. The device should also be reconfigurable on-the-fly, with no knowledge of hardware internals. Secondly, the design should be expandable or contractible, to fit with the size of device needed. Again this expansion and contraction should not require any understanding of the hardware internals. Thirdly, the system should be high-speed. This is required to allow for modern 3D and real-time 3D imaging. Finally, it should be inexpensive, with the cost scaling by the number of channels required for any given task. In addition to these requirements, it was our intention to make this design as high-quality as possible. Well-designed hardware can be difficult to identify, as it involves not just one area, but every part of the design process [53], [54]. A good design is not only tightly integrated, and elegantly arranged, it is also intentional in how these details are handled [3].

### **4.3. Hardware Design Architecture**

When the complete beamformer system was initially conceived, the most important consideration was how the signals will flow through the system. Typically, signals arriving at the beamformer from a single group of wires, or connector, will need to be spread apart for processing, and then routed back together for summation and display [3]. Figure 4.1 shows the three-dimensional arrangement of processing boards we used in order to solve this problem.

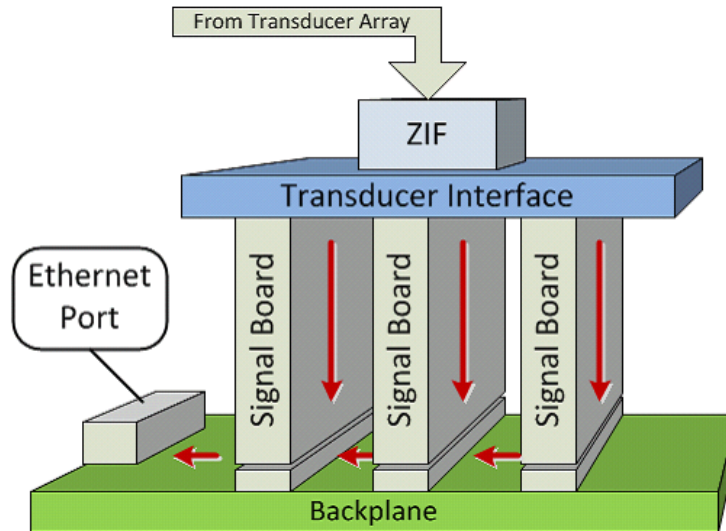


Figure 4.1 - Pictorial representation of beamformer system PCB connections[3]

The signals in the Figure originate at the ZIF connector, and are distributed through the transducer interface board to the signal processing boards. Each signal processing board quantizes and beamforms the signals passed to it, and then pass the results along the backplane to its neighbor board. The final beamformed signal is passed to a PC for display using an Ethernet connection. The arrangement shown has several advantages. One significant benefit is that the design inherently divides the processing tasks among a number of identical signal processing boards. The number of boards included determines the number of channels that the system can support. This allows the system to expand or contract by the addition or removal of signal processing boards. The vertical arrangement also makes efficient use of space reducing the amount of routing required to distribute and recombine signals, which will improve the performance of the system [3].

#### 4.4. Component Selection

Decision of the component selection are made by weighing multiple factors which include design performance, but also cost and availability, or more difficult to quantify factors such as footprint design and pin out. The two components that have the greatest influence on the design and system performance of the signal processing board are the Analog to Digital Converters (ADCs), and the FPGA. In selecting the ADC device used, many options were considered from various vendors. For the ADCs we select The AFE5801 is an analog front end, targeting applications where the power and level of integration are critical. The device contains eight variable-gain amplifiers (VGA), each followed by a high-speed (up to 65MSPS)

ADC, for a total of eight ADCs per device. Each of the eight differential inputs is buffered, accepts up to 2V<sub>pp</sub> maximum input swing, and is followed by a VGA with a gain range from -5dB to 31dB. The VGA gain is digitally controlled, and the gain curves versus time can be stored in memory integrated within the device using the serial interface.

Typically, FPGA beamformer designs are limited by RAM resources as well as the number of I/Os available on the FPGA device. In evaluating the available options, only Xilinx devices were considered due to previous design experience with their products. The latest devices released at the start of this design were the Xilinx Virtex 6, and Spartan 6 series devices [55], [56]. Both of these series of devices use 40/45 nm lithography CMOS and have lower power consumption than previous generations [57]. Both also make use of an advanced configurable logic block (CLB) design that allows six input look up table (LUT) connections compared to four input LUTs of previous generations. This increase results in more compact and efficient device routing. The major difference between the Virtex and Spartan devices is that the Spartan series is optimized for cost, while the Virtex series is optimized for performance. The Virtex typically offers higher clock speeds, and some additional advanced features such as hardware MAC Blocks, HTX transceivers, and faster maximum clock speeds compared to the Spartan, but at added expense. For the beamformer architecture, none of these additional features were critical, allowing the choice of a Spartan series device for this design.

When the Spartan 6 product table is considered [58], the most common and versatile package used is the FGG484 package. One advantage of this package is that it makes use of a 1mm pitch Ball Grid Array (BGA) footprint. Additionally, the FGG484 footprint is available as an option for devices as small as the LX25 device (24k available logic cells), to the largest LX150 and LX150T devices (147k available logic cells). Each of the devices is drop-in pin compatible with others of the same footprint, provided that the additional I/Os available in larger sizes are not used. However, for the cost saving factor, we select LX45 as our design package besides, we used the Atlys Spartan 6 FPGA Development board as our testing board a pictorial diagram for the board shown in Figure 4.2.

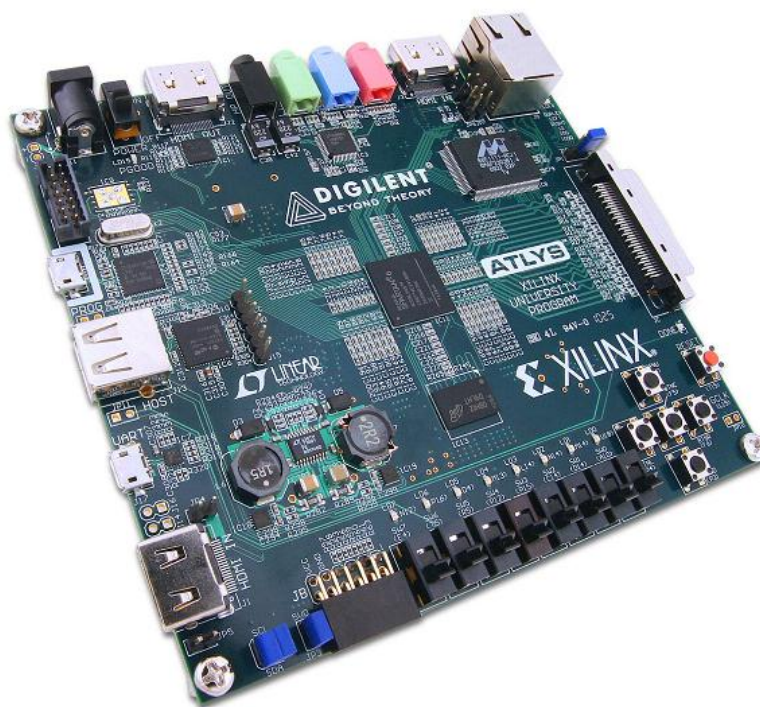


**Figure 4.2-The Digilent Atlys Spartan 6 FPGA Development Kit[62]**

The on-board collection of high-end peripherals, including Gbit Ethernet, HDMI Video, 128Mbyte DDR2 memory array, audio and USB ports make the Atlys board an ideal host for complete digital systems built around embedded processors like Xilinx's MicroBlaze. Atlys is fully compatible with all Xilinx CAD tools. Also we are taking the TI Digital beamformer design as our reference design which is used DSP C64+ which Digital signal processor With performance of up to 5600 million instructions per second (MIPS) at a clock rate up to 1.2 GHz.C64x+ core offers solutions to high-performance DSP programming challenges. The DSP core possesses the operational flexibility of high-speed controllers and the numerical capability of array processors.

## **4.5. Digital Beamformer Hardware Design**

The Hardware design is comprising of IP cores (Written by HDL) inside the FPGA interfacing with the other hardware by special interfaces and managed from the upper layers by a software processor (MicroBlaze). In this section, we will describe the FPGA banks and its interfaces with the outside world, as well as we will discuss the different system interfaces and its flow furthermore we will describe in brief the MicroBlaze architecture and its main components. We will illustrate the power section which responsible to generate the required power for all the system also we will illustrate the DDR2 memory system attached to the

FPGA which used for buffering the (delayed) data. At the end of the section we will describe the analog front end, including the transmitter circuit, receiver circuit and switches with isolators as well. Figure 4.3 shows the system design architecture:

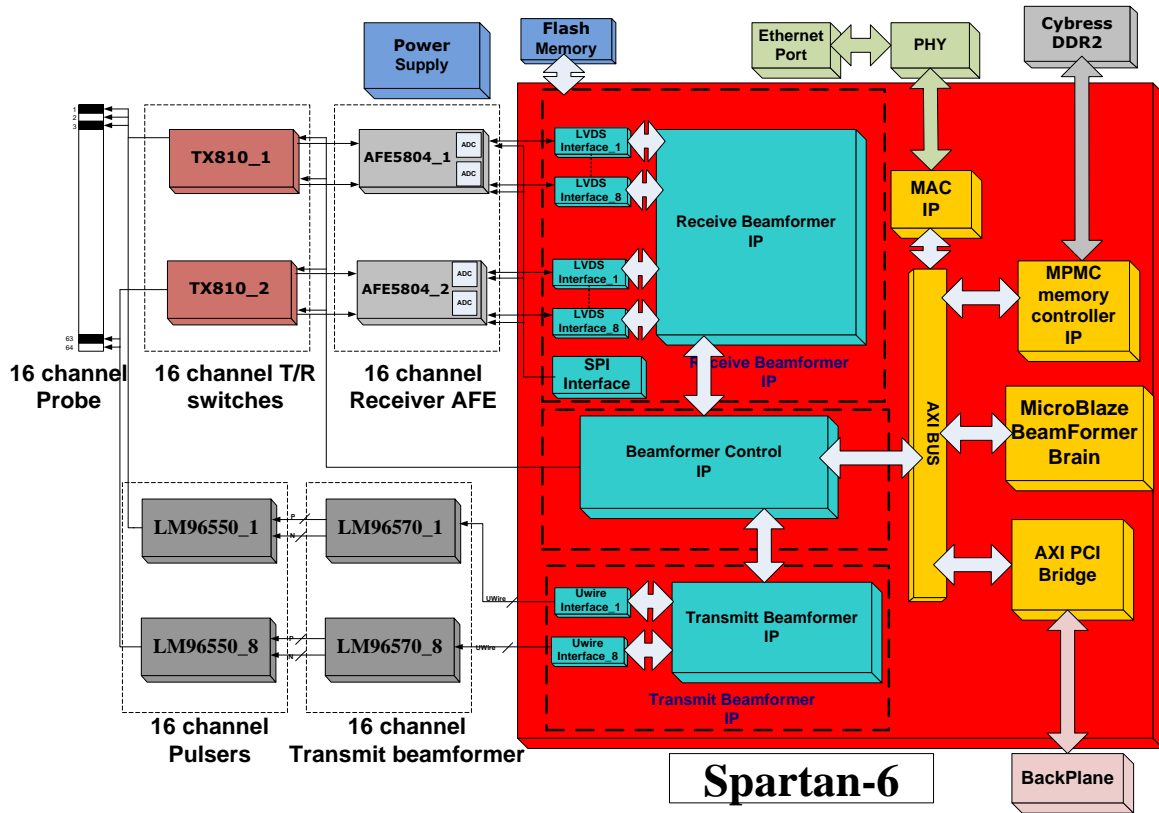


Figure 4.3-Digital Beamformer system architecture

#### 4.5.1. Overview

As we described before in figure 4.3, the proposed system architecture was designed for beamforming 16 channels, and it comprises two transmit beamformer ICs (LM96570) acting as pulse pattern control followed by two ultrasound pulser driver ICs (LM96550) this was for the transmitter circuit. For the receiver circuit, there are two ICs (AFE804) comprising all the receiver AFE functionality, both of circuits is isolated by HV switches. In the FPGA side, we can find two IP core controllers the receiver / transmitter circuits and there is control IP core synchronize between the transmitting and the receiving as well as control the HV switches. Besides there is PCI Bridge for interfacing with the backplane, as well as there is a memory controller for DDR2 operation controlling. The last interface is the MAC, and this is the responsibility of the MAC IP core. All the software operation (FSM) is managed by the MicroBlaze software processor through AXI bus. There is custom circuit consisting of a number of DCDC regulators for powering up the digital beamformer system.

## 4.5.2. Power system

One of the main points of failure of the Digital beamformer system was the power distribution system. In our designed, we are using three switched mode power supply. A switched mode power converter is a modern DC-DC converter design that uses a pair of matched power field effect transistors in order to regulate an input DC power supply into a different voltage with high conversion efficiency [59 - 61]. The input power rail for this design is 5V voltage regulator circuits from Linear Technology create the required 3.3V, 2.5V, 1.8V, 1.0V, and 0.9V supplies from the main 5V supply. The switch mode converters were designed using a buck converter topology. Please see appendix A for more details about the schematics.

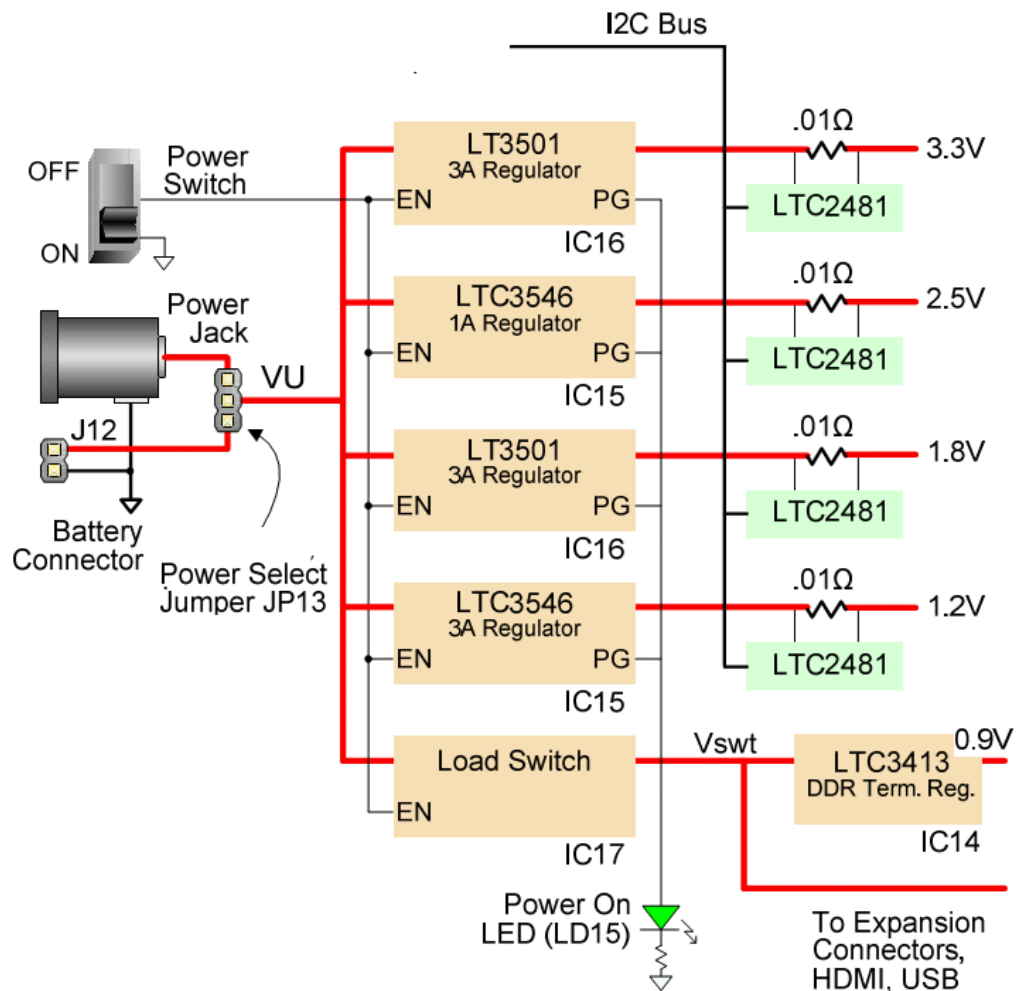
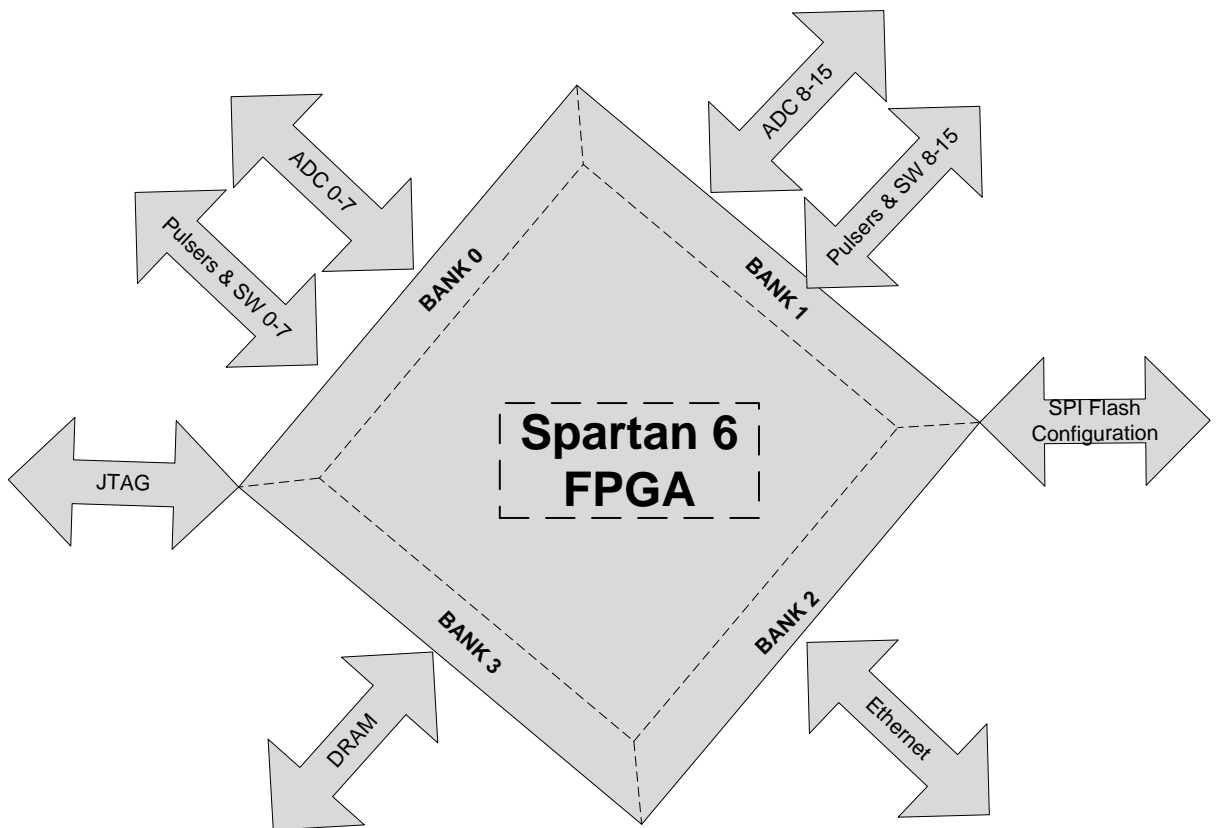


Figure 4.4- Digital beamformer power section [62].

### 4.5.3. FPGA

The Spartan 6 series FPGA provides the processing for each channel of digitized data. We are using VHDL as the internal hardware definition language (HDL) code, which defines the operation of the FPGA. Here I will present the FPGA hardware features. As the processing center of the card, the FPGA receives signals from, and delivers them to, multiple sources on the board. In the FPGA Banks section comprising the four banks of the SPARTAN 6 FPGA. These banks are controlling the whole operation of the digital beamformer as shown in the next figure,



**Figure 4.5 – Diagram showing major FPGA I/O bus connections per bank. ADC busconnections attach to Banks 3 and 0. Data is passed in to the card along the backplaneconnections to Bank 1, while beamformed data is passed out on Bank The Comm 2.bus is bidirectional, and attached to Bank 2. DRAM pins are allocated in Bank 1[62].**

Please see more details about the schematic in appendix A, as the processing center of the card, the FPGA receives signals from, and delivers them to, multiple sources on the board. Figure 4.5 shows the major bus connections that are handled by the FPGA, and indicates the I/O bank to which they are attached. I/O banking rules for the Spartan 6 devices can be complex [64], and the existing arrangement was created in order to accommodate those

rules, as well as to minimize the overall layout paths for each major bus. The highest speed bus signals (387MHz DDR) are generated by each of the ADC chips. Incoming transducer signals are passed to the FPGA through the ADC chips. The interface between the FPGA and each ADC device consists of 8 differential high-speed DDR LVDS signals, each differential pair containing a serial stream of data for a single transducer channel. Each ADC also transmits a high-speed serial clock that is synchronous to the serial data, and a lower speed frame clock that is synchronous to the beginning of each data word from the ADC. Both of these signals are also transmitted using LVDS.

The final bus shown in Figure 4.5 is the JTAG input bus. This is not associated with any input bank as it is only used to initialize the FPGA hardware when the power is turned on. The JTAG bus connects the FPGA to a Xilinx based flash electronically erasable programmable read-only memory (EEPROM) chip (XCF32P). The EEPROM stores the synthesized HDL code used to initialize the hardware state of the device, and can be reprogrammed through a JTAG port on the board. It should be noted that this port is operated as a serial master device, using the onboard oscillator circuit to control the programming sequence. This is in contrast to the more common mode in which the EEPROM is operated as a serial slave device. The serial slave mode is hardware selectable using an optional resistor connected to the Mode Select pin (R7/R8). It has been designed this way to make use of the hardware compression feature of the EEPROM. Hardware compression is required in order to fit the full configuration file for the largest LX150 device into the EEPROM. Aside from the hardware signal buses, the FPGA contains two oscillator mounting points, only one of which is used in the current design, with the second provided for future expansion. A signal is also provided to indicate the presence (or absence) of the previous card in the chain. The FPGA is supported by a large number of decoupling capacitors mounted on the reverse side from the FPGA, and incorporated into the BGA via footprint. Please see the appendix A for more details about the schematics.

#### **4.5.4. DDR2 Memory**

A single 1Gbit DDR2 memory chip is driven from the memory controller block in the Spartan-6 FGPA. The DDR2 device, a Micron MT47H64M16-25E or equivalent, provides a 16-bit bus and 64M locations. The DDR2 interface follows the spinout and routing guidelines specified in the Xilinx Memory Interface Generator (MIG) User Guide. The interface supports

SSTL18 signaling, and all address, data, clocks, and control signals are delay-matched and impedance-controlled as shown in the next Figure.

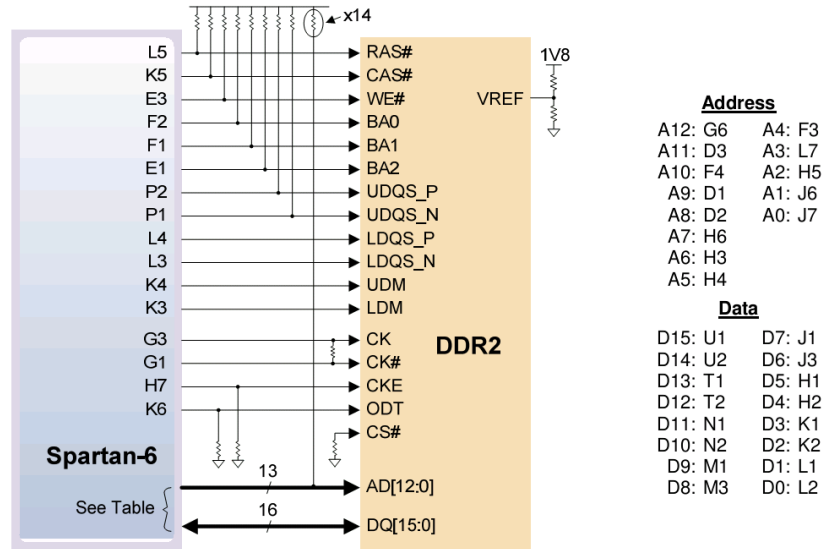


Figure 4.6- DDR memory section

Please see appendix A for more details about the schematics [62].

### 4.5.5. Flash memory (Configuration memory)

The Design uses a 128Mbit Numonyx N25Q12 Serial Flash memory device (organized as 16-bit by 16Mbytes) for non-volatile storage of FPGA configuration files. The SPI Flash can be programmed with a .bit, .bin, or .mcs files. An FPGA configuration file requires less than 12Mbits, leaving 116Mbits available for user data. Data can be transferred from a PC to/from the Flash by user applications.

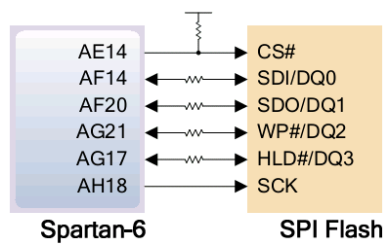


Figure 4.7- Flash Memory section [62].

### 4.5.6. Beamformer Transmitter

We are using LM96570 as our beamformer transmitter; it is a complete integrated solution for sending the Full controlled ultrasound transmitter signal over selecting beam directions and pulse patterns by programming individual channel parameters. Outputs interface seamlessly with positive and negative inputs on octal high-voltage pulsers ICs.

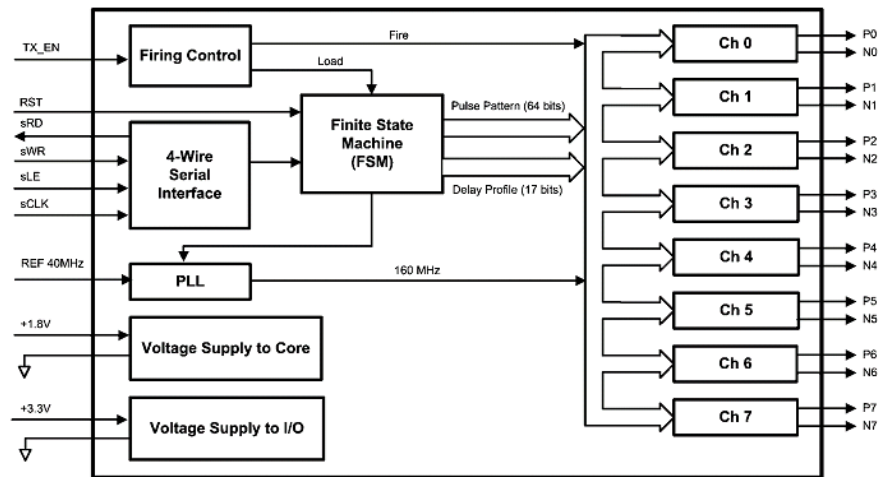


Figure 4.8-Digital beamformer transmitter IC [65].

Pulse patterns are locally generated with Sequences of up to 64 pulses Adjustable Pulse widths. So we can find with fewer signal interfaces we can have a complete four digital beamformer transmitter with 16 channels by 2 of them only. We are using 2 of them are being used in our design controlling by the Uwire IP core as shown in the next Figure.

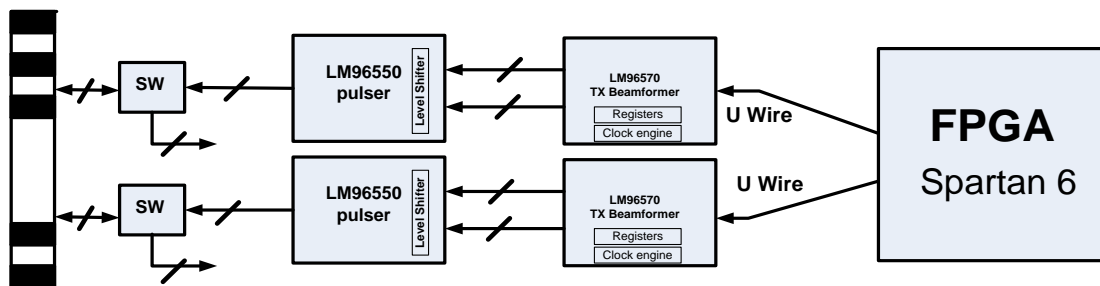


Figure 4.9-Digital beamformer transmitter interface with FPGA Please see the appendix A for more details about the schematics.

### 4.5.7. Beamformer Receiver

The AFE5801 is an analog front end, targeting applications where the power and level of integration are critical. The device contains eight variable-gain amplifiers (VGA), each followed by a high-speed (up to 65MSPS) ADC, for a total of eight ADCs per device.

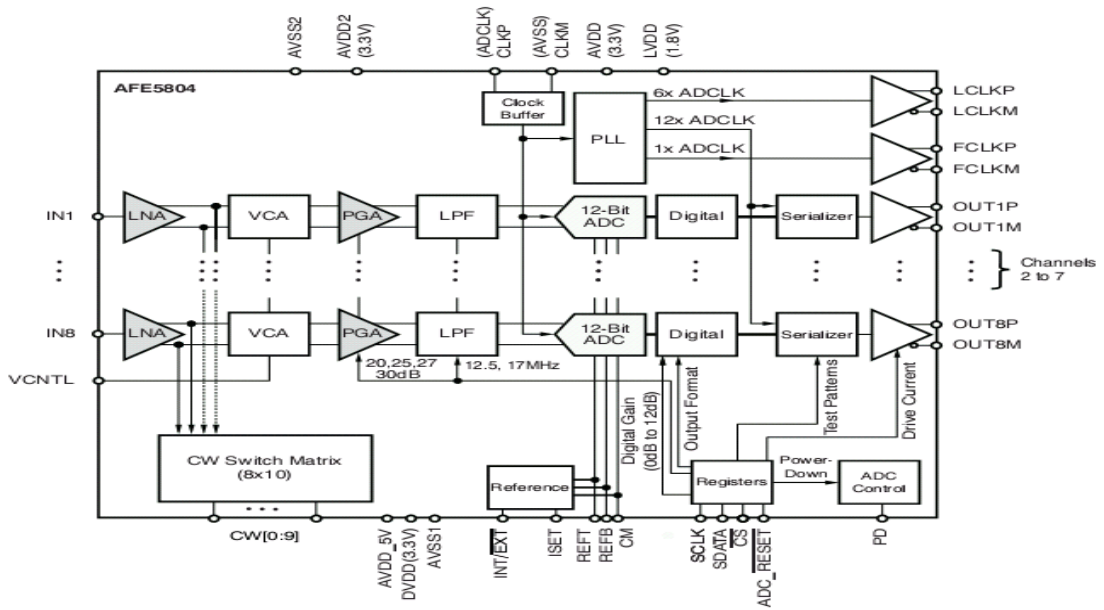


Figure 4.10- Digital beamformer receiver IC architecture[68].

Each of the eight differential inputs is buffered, accepts up to 2Vpp maximum input swing, and is followed by a VGA with a gain range from  $-5\text{dB}$  to  $31\text{dB}$ . The VGA gain is digitally controlled, and the gain curves versus time can be stored in memory integrated within the device using the serial interface. A selectable clamping and ant aliasing low-pass filter (with 3dB attenuation at 7.5, 10, or 14MHz) is also integrated between VGA and ADC, for every channel. The VGA/ant aliasing filter outputs are differential (limited to 2Vpp) and drive the onboard 12bit, 65MSPS ADC. The ADC also scaled down its power consumption should a low sampling rate be selected [68]. The ADC outputs are serialized in LVDS streams, which further minimize power and board area as shown in the next Figure

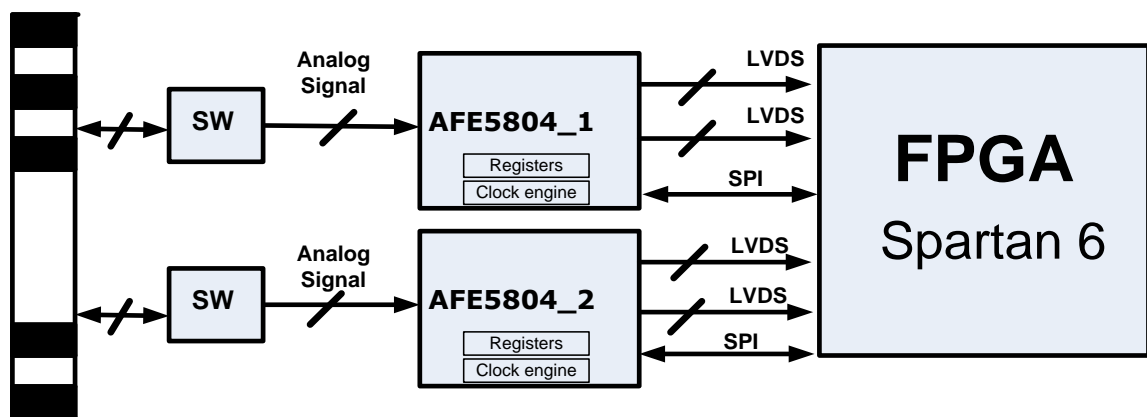


Figure 4.11- Digital Beamformer receiver interfacing with FPGA

Please see the appendix A for more details about the schematics.

## 4.6. Cost analysis

There are three primary expenses in a typical printed circuit board construction that need to be considered: the cost of the components, the cost of the circuit board, and the cost of assembly (or build-up). For the boards built for the imaging system in this thesis, the component costs dominate the expenses, although PCB construction and build-up costs are the more variable of the three. These costs would be reduced in volume production. We could not reach with our design to the manufacturing process, but we will have another manufacturing process for the digital beamformer as cost analysis reference for similar design except, they are using older and discrete chips, which cost more not like our design, which based on the integrated solutions also in their board. They used Xilinx SP605 Board, which cost around 500\$ but for us our diligent board cost 200\$.

Item		Unit Cost	Qty	Cost
Digital Board	Components	\$557.33	2	\$1,114.66
	Production	\$77	2	\$154.00
	Assembly	\$90	2	\$180.00
Backplane	Components	\$19	1	\$19.00
	Production	\$50	1	\$50.00
Xilinx SP605 Board		\$495	1	\$495.00
<b>Total</b>				<b>\$2,012.66</b>

**Table 4.1 - Cost summary for 64 channel systems[3]**

The digital signal board is the most expensive portion of the system, since it contains both the beamforming logic FPGA and ADC units. Their components on a single board were purchased for a combined price of approximately \$560 Canadian dollars per board. The PCB was produced for \$77 per board. Two components required assembly from outside of the lab, the FPGA, and TQFP ADC units. The overall system cost per channel of data decreases as more channels are added to the system as shown in Figure 4.13.

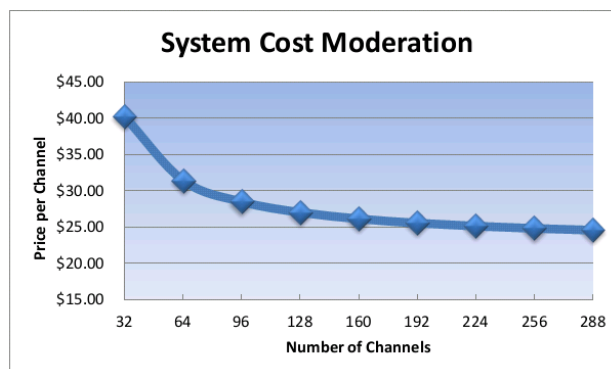


**Figure 4.12- System cost per beamformer channel compared as the size of the system is increased[3].**

For a small system of 32 channels or less, the cost is approximately \$40 per channel, while as the system size increases, per channel costs decrease to just under \$25 per channel.

## **4.7. Summery**

The proposed system architecture was designed for beamforming 16 channels. We discussed the overall architecture with highlighting the concept of multiple board integrations by one backplane. In general, the HW design comprises two transmit beamformer ICs (LM96570) acting as pulse pattern control followed by two ultrasound pulser driver ICs (LM96550) this was for the transmitter circuit. For the receiver circuit, there are two ICs (AFE804) comprising all the receiver AFE functionality, both of circuits is isolated by HV switches. In the FPGA side, we can find two IP core controllers the receiver / transmitter circuits and there is control IP core synchronize between the transmitting and the receiving as well as control the HV switches. Besides there is PCI Bridge for interfacing with the backplane, as well as there is a memory controller for DDR2 operation controlling. The last interface is the MAC, and this is the responsibility of the MAC IP core. All the software operation (FSM) is managed by the MicroBlaze software processor through AXI bus. There is custom circuit consisting of a number of DCDC regulators for powering up the digital beamformer system we go through the hardware design of the digital beamformer. We referenced our full detail HW schematics in the appendix.

## **Chapter 5**

# **Ultrasound Digital Beamformer Firmware Design**

### **5.1. Introduction**

Our proposed design is based on the field programmable gate arrays (FPGAs) in order to beamform the sampled transducer echo signal. Unlike ASIC designs, FPGA devices can be reprogrammed to perform different tasks. Because of its role in the system, the firmware design is just as important as the hardware design in determining system performance. We will describe in details the implementation the low level design of our digital beam former design by describing in details the design details for the composed components of the digital beamformer system the transmitter digital beamformer, receiver digital beam former and the controller.

### **5.2. Background**

In this chapter we will review how FPGAs function, and the role of hardware definition language (HDL) in producing a successful design. We will then describe the full system HDL modules used in this system and how they interact to create a beamformed image. Some of the key design features, along with their implementation details will then be reviewed. We will demonstrate the synthesis performance results achieved by the design, and finally review the HDL verification procedures.

#### **5.2.1. FPGA**

At its simplest level, a field programmable gate array (FPGA) is a reconfigurable logic device. The earliest versions of these devices provided little more than cross point connections between logic gates to define controllable logic. Modern FPGA devices use a mixture of configurable logic blocks (CLBs), which provide logic elements, MUXs and look up tables (LUT s), Block RAM buffers, Clock Managers, specialized single function hardware, and routing [69-71]. The connections between these elements are controlled so they can be configured in a nearly unlimited number of ways as shown in Figure 5.1. When the system is turned on, the hardware is programmed using a downloaded hardware definition file. The hardware definition file contains a description of how each hardware element needs to connect itself. During this initialization phase, the hardware cannot be used until the entire device is programmed.

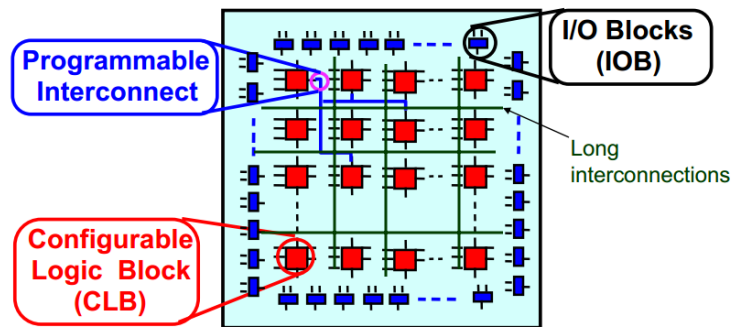


Figure 5.1-Shows the interconnection between CLBs [49].

One key benefit of an FPGA design is that since the hardware is reprogrammed at each time power is applied, the hardware state can be changed by altering this programming file. It is therefore possible to modify the FPGA code without making hardware changes.

### 5.2.2. Verilog HDL

The hardware definition file used to program an FPGA device is generally referred to as firmware. This file is written in such a way that each bit refers to a specific functional logic selection within the FPGA. In order to generate this file, a higher level description of the desired hardware logic must be created and processed. This high level file is written in a language called a hardware definition language (HDL). The HDL used in this development is the Verilog HDL language. Verilog is based on the “C” computer programming language syntax and structures. Much like in the C programming language, Verilog builds up a design by defining modules. Each module defines logic operations that occur within it, as well as defining any sub-modules used. A top level module contains the whole design. Unlike in a programming language where all operations are sequential, in a HDL all defined logic operations occur simultaneously and continuously, dependent on the logic structures built. Once a complete design is created in an HDL parsing that code is the next step to fit it into a specific FPGA device. There are several steps in this conversion process.

### 5.2.3. FPGA Synthesizing Process

There FPGA flow is mainly composed of five major phases, which are: RTL (or schematic drawing or IP porting), Functional Simulation, Synthesizing, Place and routing and finally Programming and testing. These phases are shown in Figure 5.2.

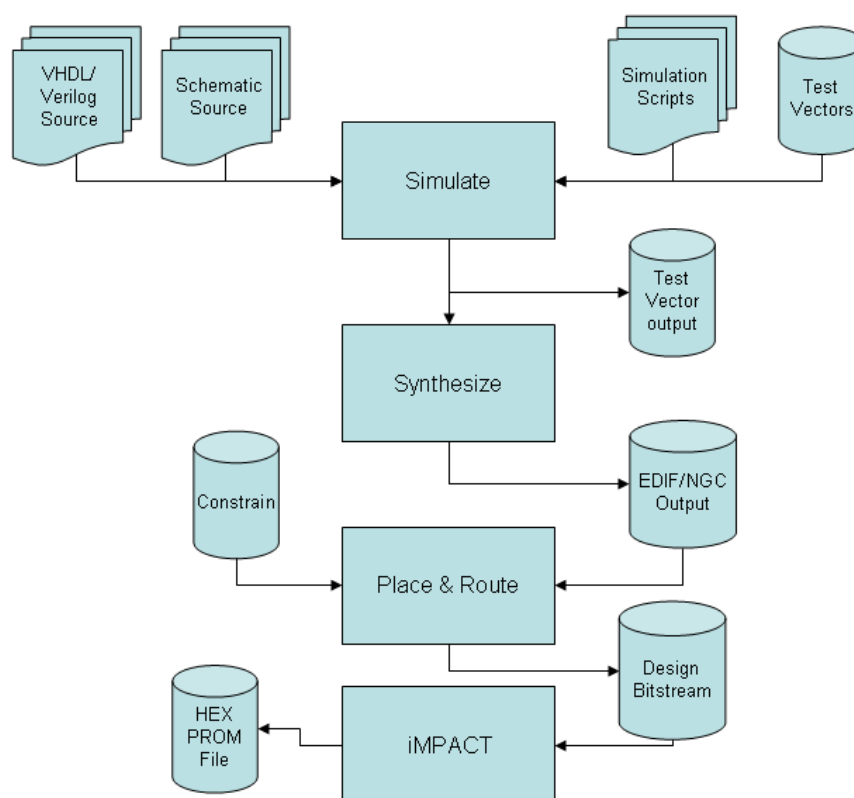


Figure 5.2. Shows the FPGA Design Flow [73].

First the HDL code must be synthesized, which converts it from a high level description to a gate level implementation. This also confirms that the HDL as written does have a hardware equivalent. The next stage is mapping, which takes the gate level description and assigns it into the hardware structures that are actually available in the chosen FPGA. Finally, the design must be placed and routed. This takes the mapped design, assigns it into specific hardware, and determines the path routes required to connect all of this logic. The place and route process also includes optimization, in which the design is rearranged to improve the distribution of the assigned hardware, to improve signal timing.

#### 5.2.4. Re-programmability

The use of an FPGA in any system, allows the hardware to be reprogrammed. The steps involved in reprogramming an FPGA device have been detailed in the previous section. In general, reprogramming an FPGA requires a high degree of knowledge of the hardware and a complete understanding of the currently implemented firmware design. Spartan 6 FPGA is characterized by its volatile memory, which means once the FPGA is being under reset, all logic inside will be erased. Thus, the need of non-volatile memory (SPI flash memory) has been raised in this kind of FPGAs. After resetting the FPGA it reconfigures itself

automatically from the flash memory and restores its configuration bitstream. So if we need to configure our FPGA, we do have need to create another section for beamformer configuration settings this section can be stored in different location of the flash as shown in the figure 5.3.

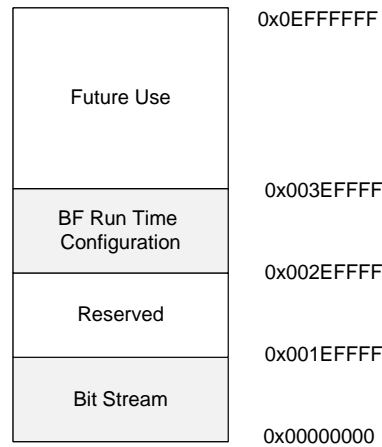


**Figure 5.3.**Shows the arrangement of the SPI FLASH.

We divided the flash memory (16 MByte) into three sections. The first section is the bit stream (configuration file), and it is actually limited by two MByte, and we reserved for it another two MByte in case of replacing the current FPGA capacity with bigger one. Moreover, we reserved two MByte of memory for the BF running time configuration, and we kept the remaining eight Mbyte for future expansion.

### **5.2.5. XILINX Embedded Development KIT (EDK)**

Embedded systems are complex. Getting the hardware and software portions of an embedded design to work are projects in themselves. Merging the two design components so they function as one system creates additional challenges. Add an FPGA design project to the mix, and the situation has the potential to become very complicated indeed. This is the reason for choosing MicroBlaze the software processor which responsible the house keeping operation like initializing the system, interfacing with the PC, etc. EDK is integrated development environment for designing embedded processing systems providing MicroBlaze and Power PC integration.

#### **5.2.5.1. MicroBlaze Software Processor**

The MicroBlaze embedded processor soft core is a reduced instruction set computer (RISC) optimized for implementation in Xilinx Field Programmable Gate Arrays (FPGAs). Figure 5-4 shows a functional block diagram of the MicroBlaze core. The MicroBlaze soft

core processor is highly configurable, allowing you to select a specific set of features required by your design. The fixed feature set of the processor includes thirty-two 32-bit general purpose registers, 32-bit instruction word with three operands and two addressing modes, 32-bit address bus [74].

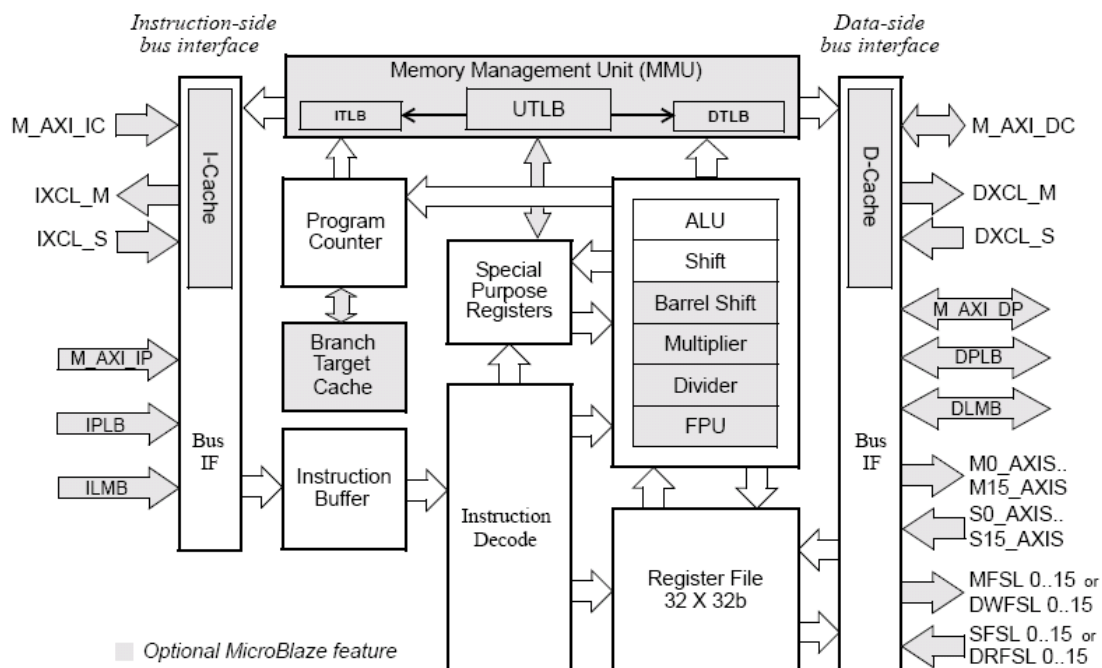


**Figure 5.4-** The figure shows a functional block diagram of the MicroBlaze core [74].

Finally, there are two options for the attaching BUS; we can use PLB bus or AXI bus. We used AXI bus because of its higher speed as well as it is little endian bus no need for any logic wrapper.

### 5.2.5.2.BF Embedded Development Kit (EDK) Platform

The Embedded Development Kit (EDK) is an integrated development environment for designing embedded processing systems. This preconfigured kit includes Xilinx Platform Studio and the Software Development kit, as well as all the documentation and IP that we require for designing Xilinx Platform FPGAs with embedded PowerPC hard processor cores and/or MicroBlaze soft processor cores as shown in Figure 5.5. It Provides a Xilinx Platform Studio (XPS) Tool Suite which Included Graphical IDE and command line support for developing hardware platforms for embedded applications [75]. The Base System Builder wizard enables creation of a working embedded system within minutes. XPS also includes other intelligent design wizards to quickly configure the embedded system architecture, buses and peripherals.

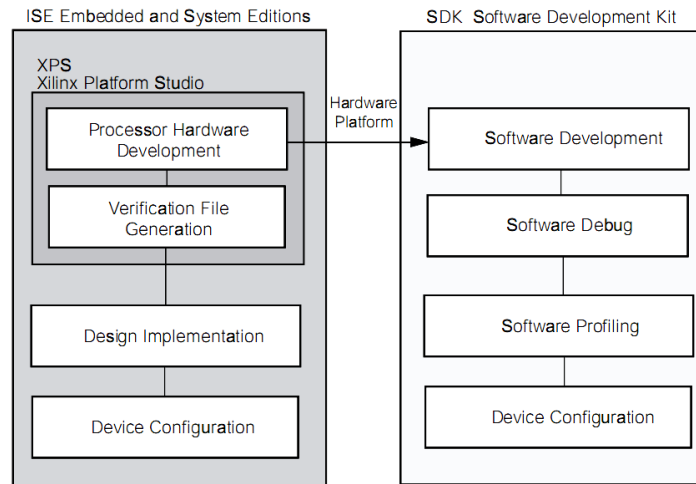


Figure 5.5 - Basic Embedded Design Process Flow [75]

Furthermore it provides Software Development Kit (SDK) for MicroBlaze and PowerPC - Including: GNU C/C++ compiler and debugger; Xilinx Microprocessor Debug (XMD) target server; Data2MEM utility for bitstream loading and updating. SDK is the recommended software-centric design environment based on the Eclipse IDE for more information you can refer to Appendix B. Below down in Figure 5.6 we can find the BF XPS platform it is AXI bus based.

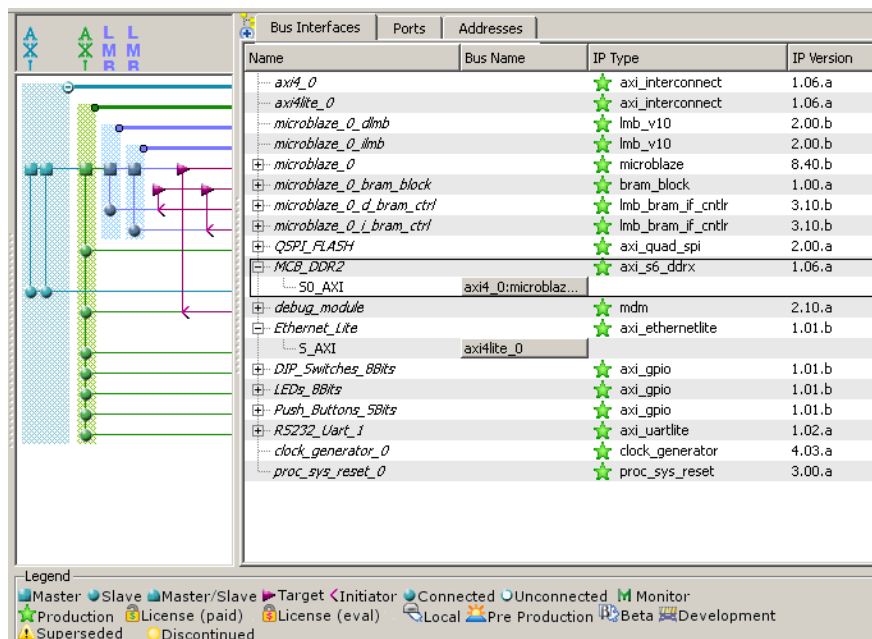


Figure 5.6 – Shows the BF XPS platform.

### 5.2.5.3. HW & SW Co-Design.

As we discussed before our proposed design divided into two layers hardware layer and Software layer. At present, hardware and software are mostly developed independently.

As a consequence there is little opportunity to optimize both hardware and software together. Moreover, it is also difficult to reason about a complete system (i.e. simulation, verification) these problems have been emphasized recently by several trends such as increasing complexity and increasing “personalization” of systems in software. . One basic approach can be characterized by identifying and implementing software parts, which consume high computing resources (usually time) in hardware [Henk92]. The dual approach seeks to identify complex system parts, which are good candidates to be implemented in software [Gupt92]. Firmware is meant by the code running on the MicroBlaze processor, but the Hardware is meant by IP hardware cores on which the logic is describing by the HDL. Hardware designs implemented in the same technology can in principle be compared. Criteria used for comparison of synchronous hardware designs are size (area) and time (delay). Furthermore, testability, design time and probably power consumption must be taken into account. Software applications are evaluated by the amount of source code (lines of code), the size of the executable code and the necessary data size. The runtime is mostly data and system dependent. Figure 5.7 Shows the Co-design diagram of the EDK.

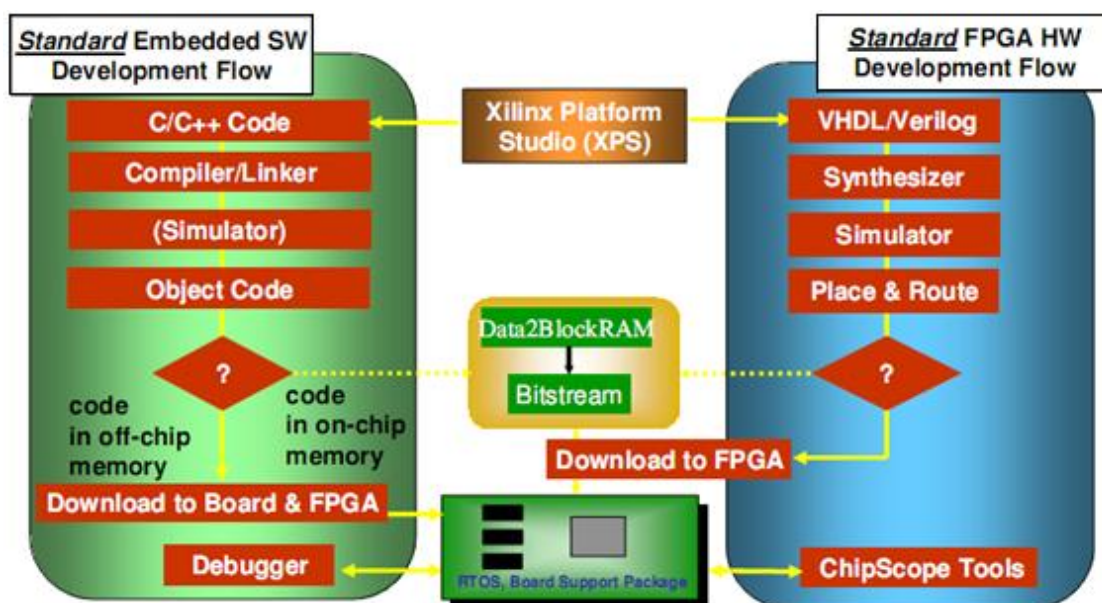


Figure 5.7 – EDK Co-design diagram [76].

Both interact to perform the beamformer operation this interacting or dividing the rules called coo processing. Both of the HW and Firmware can do some of the share jobs and there are many methods to determine which section will be implementing better in HW or in the FW according to the requirement of the target code we will decide on which platform it will be implemented.

### **5.2.6. Vivado High Level Synthesize (HLS)**

To manage the complexity of the digital design we need to move through new generation which is the high level synthesis , this tool will help us to synthesize our traditional code flow which written into C / C++ into the a complete IP core ready integration and testing as well.

#### **5.2.6.1. Overview**

The FPGA design community has moved through a few abstraction levels, to manage the complexity of the designs. Each new abstraction level hides some of the complexity of a design implementation step, offering productivity at the cost of less visibility in the challenges associated with the lower abstraction level [76]:

- A transistor layout database hides the challenges in mask making and wafer processing. The focus of the layout abstraction layer is to respect Design Rule Checks (DRC) which models the basic layout.
- For FPGA design, a net list avoids a detailed layout effort: the net list is constructed with instances from a pre-built library. The focus of the net list abstraction layer is to define the Boolean functionality of the design with appropriate area, performance and power.
- A Register Transfer Level (RTL) description captures the desired functionality by defining datapath and logic between boundaries of registers. RTL synthesis creates a net list of Boolean functions to implement the design. The focus of the RTL abstraction layer is to define a functional model for the hardware.
- A functional specification removes the need to the define register boundaries to implement the desired algorithm. The focus of the designer is only on specifying the desired functionality.

#### **5.2.6.2. High-Level Synthesis Architecture**

As shown in Figure 6.5, High-Level Synthesis accepts as input, a C-based design description, and directives and constraints, specified using the Graphical User Interface (GUI) or a Tcl batch script. A technology library specifying the timing and area details of all supported Xilinx device is built-in and is not required to be supplied. High-Level Synthesis outputs RTL design files in Verilog, VHDL and System C. In addition verification and

implementation scripts, used to automated the RTL verification and RTL synthesis steps are also created. For more details please refer to Appendix C.

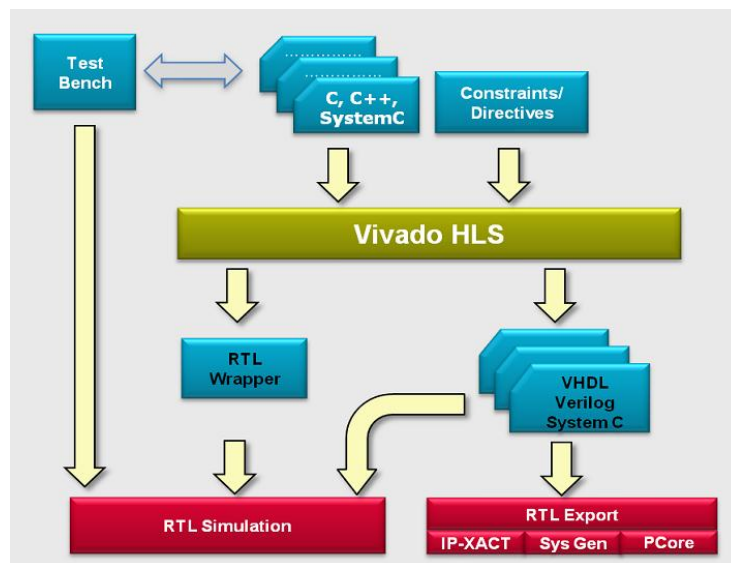


Figure 5.8. showing the block diagram of VIVADO HLS[76].

### 5.3. HDL Modules description

The HDL code modules divided into 2 main categories first category is the interfacing modules and the second section is the beamforming logic ctrl .the interfacing cores are LVDS core, Uwire Core, MAC core, SPI core and DDR core. The engine cores are the transmitter core and the receiver core.

#### 5.3.1 Interfacing Cores.

Interfacing cores are LVDS core, Uwire Core, MAC core, SPI core and DDR core. The engine cores are the transmitter core and the receiver core.

##### 5.3.1.1. Uwire Core

The top level block diagram for the Uwire IP Core is shown in Figure 5.4.This IP core responsible for beamformer transmitter IP interfacing

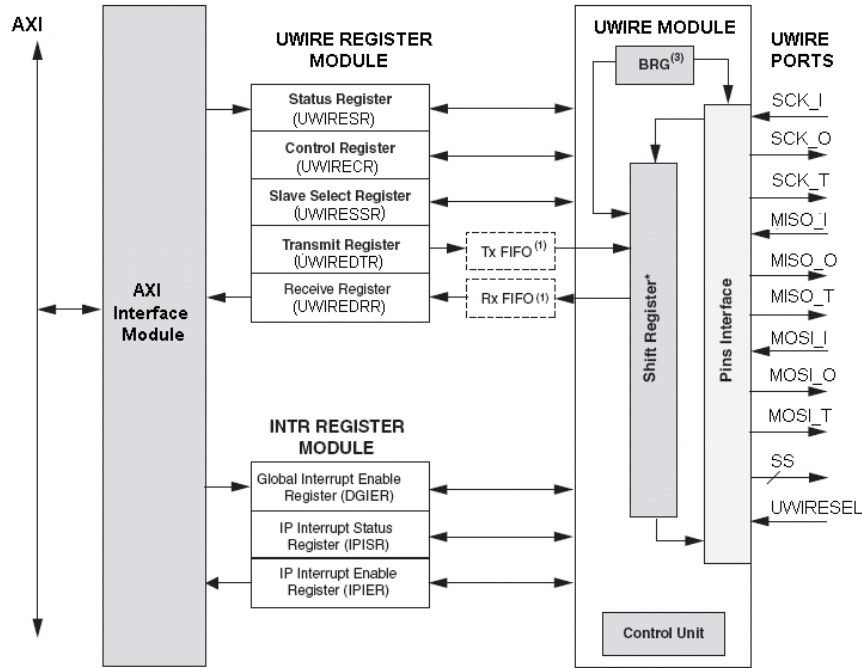


Figure 5.9- The top level block diagram for the Uwire IP Core.

The UWIRE IP Core is a full-duplex synchronous channel that supports four-wire interface (receive, transmit, clock and slave-select) between a master and a selected slave. The UWIRE IP Core supports Manual Slave Select Mode as the Default Mode of operation. This mode allows us to manually control the slave select line by the data written to the slave select register. This allows transfers of an arbitrary number of elements without toggling the slave select line between elements. The other mode of operation is Automatic Slave Select Mode. In this mode the slave select line is toggled automatically after each element transfer. The UWIRE IP Core modules are described in the sections below:

- **AXI Interface Module:** The AXI Interface Module provides the interface to the AXI V4.6 slave single. The read and write transactions at the AXI are translated into equivalent IP Interconnect (IPIC) transactions.
- **UWIRE Register Module:** The UWIRE Register Module includes all memory mapped registers .It interfaces to the AXI. It consists of Status Register, Control Register, N-bit Slave Select Register (N 32) and a pair of Transmit/Receive Registers.
- **INTR Register Module:** The INTR Register Module consists of interrupt related registers namely device global interrupt enable register (DGIER), IP interrupt enable register (IPIER) and IP interrupt status register (IPIISR).

- **UWIRE Module:** The UWIRE Module consists of a shift register, a parameterized baud rate generator (BRG) and a control unit. It provides the UWIRE interface, including the control logic and initialization logic. It is the heart of core.
- **Optional FIFOs:** The Tx FIFO and Rx FIFO are implemented on both transmit and receive paths when enabled by the parameter C\_FIFO\_EXIST. The width of Tx FIFO and Rx FIFO is same and it depends on generic C\_NUM\_TRANSFER\_BITS. The depth of these FIFO's is 16, which is FIFO design dependent.

A block diagram for our FPGA interfacing with the transmitter IC is shown in figure 5.11.

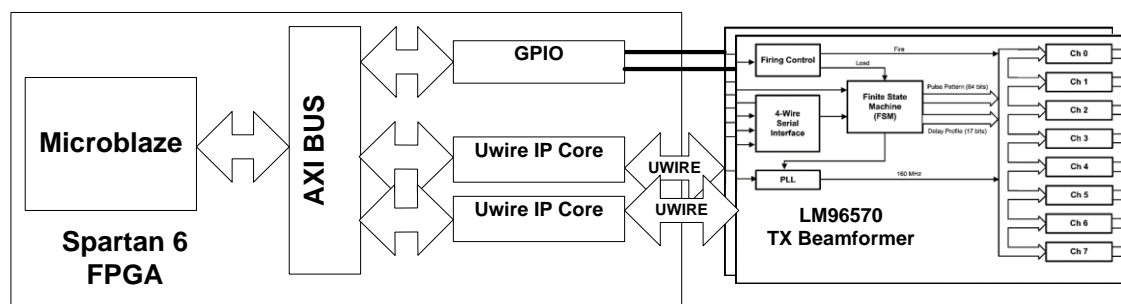


Figure 5.10-Interface between Microblaze AXI BUS and UwireIP Core of LM96570 TX Beamformer

### 5.3.1.2. Deserialization with Buffering IP Core

Eight differential inputs are sampled at a 70 MHz clock rate. The eight AFE804 has 8 ADC each has LVDS output, providing a serial 12-bit data bitstream with either MSB or LSB first. An LVDS high-speed clock output (LCLK) and an LVDS delayed repowered sampling clock (ADCLK) are also provided. The high-speed bit clock, LCLK, is six times the ADCLK sampling clock as shown in figure 5.12.

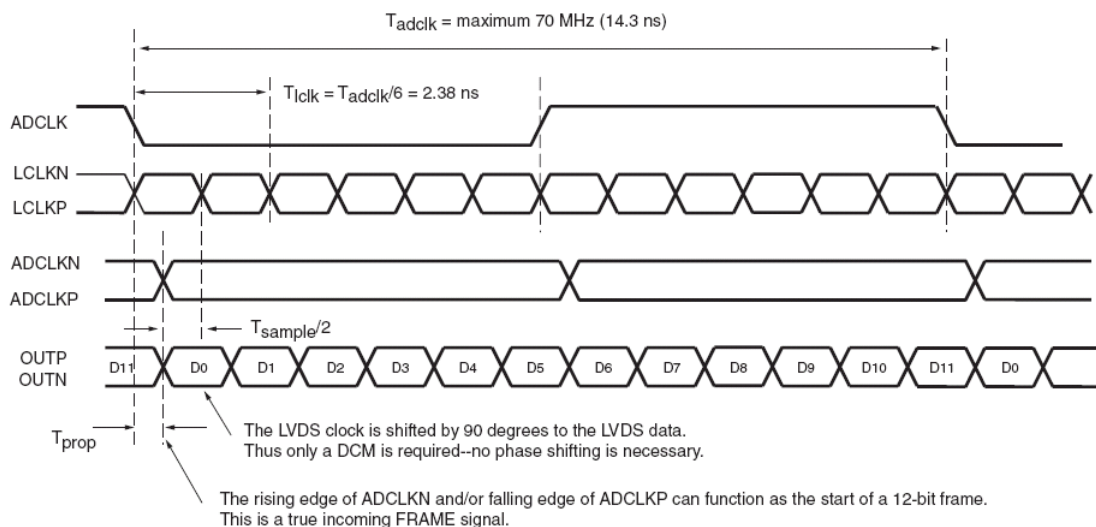


Figure 5.11- The high-speed bit clock, LCLK, is six times the ADCLK sampling clock[77].

### 5.3.1.3. Single Channel Interface

For a single-channel design, the ADC specifications are:

- 70 MSPS (70 MHz) with ADCLK 70 MHz (14.29 ns) and LCLK = 420 MHz (2.38 ns)
- 12-bit serial LVDS interface
- LVDS used in dual data rate (DDR) mode

DDR mode means that the bits are clocked at the FPGA at 840 Mb/s. The FPGA can receive LVDS data streams at that specified speed without problems when the interface design is carefully constructed. The AFE804 transmits edge-aligned data and sync signals with a 90-degree shifted clock. Taking into account the PCB layout, data, sync, and clock arrive at the FPGA pins shifted by 90 degrees. To register the received data into the FPGA with the receive clock, a digital clock manager (DCM) can be used in fixed phase shift mode. If doubt exists on the data-to-clock alignment; a DCM can be used in dynamic phase shift mode. Just we need to take care about that when the "Auto Phase Shift" design approach is used, a fixed shift parameter must be applied to the shift operation state machine to keep the 90-degree phase shift between data and clock[77]. Figure 5.11 shows a one-channel receiver module. This module takes in the serial differential data of one channel and outputs it, internal to the FPGA, as 12-bit parallel data. This module is used eight times for an 8-channel ADC device. For the single-channel design, the received clock is input to a DCM which aligns the internal clock to the external applied clock or phase shift the internal clock to the received clock.

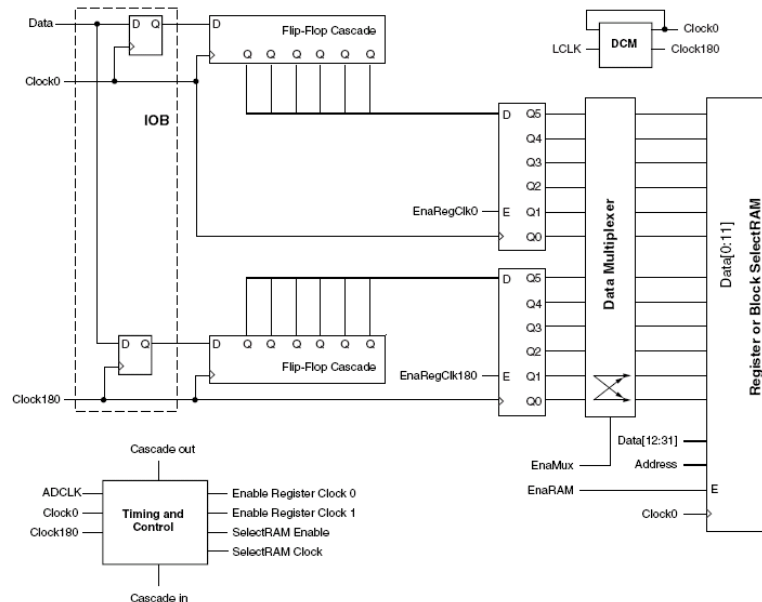


Figure 5.12- a one-channel receiver module[77].

The 12 incoming serial data bits of one channel are split into two sections. The even bits are clocked on the DCM clock, and the odd bits are clocked on the 180-degree shifted

clock. At a strobe pulse, ADCLK, these serial registered bits are stored in a parallel register. The result is a 12-bit parallel word with a jumbled data bit order.

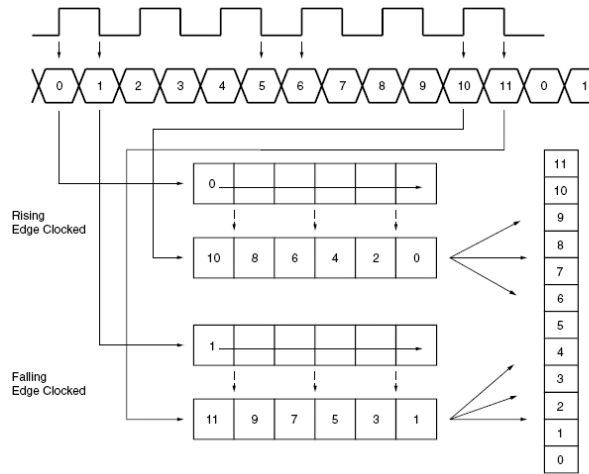


Figure 5.13- a12-bit parallel word with a jumbled data bit order[77]

After the bit ordering is resolved in the FPGA routing, this 12-bit word can be used as is by a backend application or can be fed to a set of registers, a Block Select RAM FIFO, or a Block Select RAM memory used as a register. When the 12-bit word is used as is, the backend application must run at a clock in phase with the received ADCLK clock. An easier solution is to let the backend FPGA design run at a clock rate similar, but not referenced, to the sampling clock, and uses a FIFO to cross the clock domains between the ADC receiver interface and the application logic.

### 5.3.1.4. Deserializing Timing

The high-speed LCLK is used as an interface clock and is therefore fed into a DCM. This DCM generates two phase-aligned clocks, CLK0 and CLK180. The data-aligned LVDS version of the ADCLK sample clock is used as a strobe signal to align the captured 12-bit words. The strobe signal is sampled on the positive and negative edges of the high-speed LCLK. Edge detection and phase detection are performed, when a rising edge of ADCLK is detected, two signals are generated to enable the parallel storage registers for the positive and negative clocked data. Normally, even bits (0, 2, and 10) are clocked on the rising edge of CLK0, while odd bits (1, 3, and 11) are clocked on the rising edge of CLK180. Figure 5.13 and 5.14 show the even bits clocked with CLK0 and CLK180, respectively.

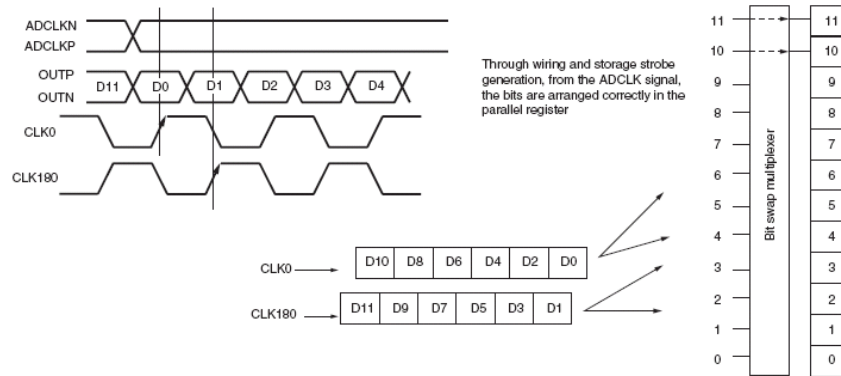


Figure 5.14-show the even bits clocked with CLK0.

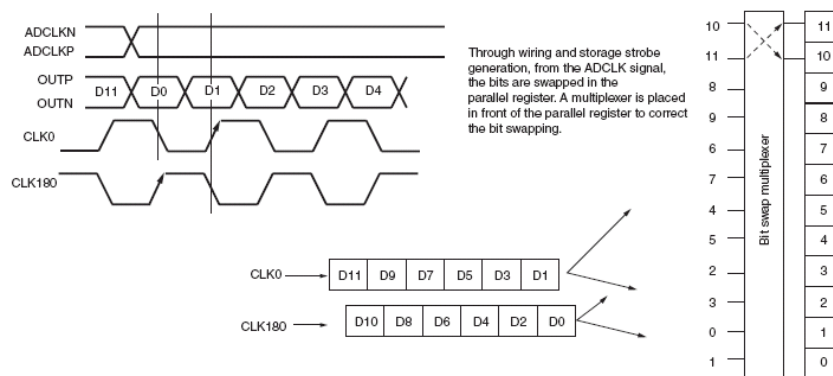


Figure 5.15- show the even bits clocked with CLK180[77].

To automatically prevent this bit swapping, a small multiplexer is placed between the parallel latch register and the storage register or Block Select RAM (FIFO). When the negative frame edge of CLK0 comes before CLK180, negative frame edge data is passed as is to the parallel register. When the negative frame edge is first detected with CLK180, data is normally bit- swapped when loaded in the storage register or FIFO.

### 5.3.1.5. Deserialized Data Buffering

When the basic reference design is used as provided, after the parallelized 12-bit values are clocked in a single register, they must be taken immediately by the backend application design. This design must function at a clock synchronous to ADCLK. Another approach is to store received parallel data in a FIFO and read it out with the backend application design. In this case, it is possible to run the backend design at an unrelated but frequency-similar clock. The FIFO is used to bridge the two clock domains. As in telecom applications, ADC converters produce a continuous stream of data, resulting in a continuous stream of parallel 12-bit words. The FIFO that best fits this application is called a self-addressing FIFO. FIFOs are constructed from memory, read counters (pop), write counters

(push), and flagging logic. With a self-addressing FIFO, the counters are replaced by the memory itself, and clock skew is no longer an issue.

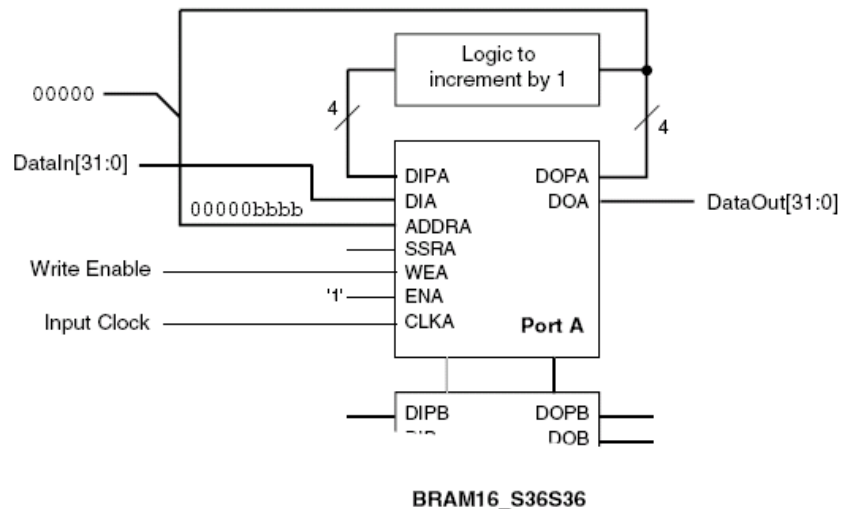


Figure 5.16- shows a standard self-addressing Part of the memory data output is fed back as memory address[77].

At the start of operation, the memory output is assumed to be all zeros. The RAM is addressed with this value from the feedback part of the output. At the same time, the data is incremented (in the LUT adder) by one, and the result is presented at the memory data input together with the incoming data. The next clock edge addresses memory space “zero” and writes the data value “zero+1 & input data”. Due to the construction of the memory blocks, this value appears at the output after a Clock-to-output (Tbcko) time. Now memory space “one” is addressed and a data value of two (output one + added one) is presented at the input. The address increment logic is built from a LUT and does not require a clock. Addition of a clock loses the advantage of direct data out. Block Select RAM memories have an ideal design for this mechanism. When a 32-bit wide FIFO is needed, the extra four bits (parity bits) can be used for the address storage-incremented functionality. A 16-deep FIFO can be constructed using four bits (the parity RAM bits) as shown in the next Figure.

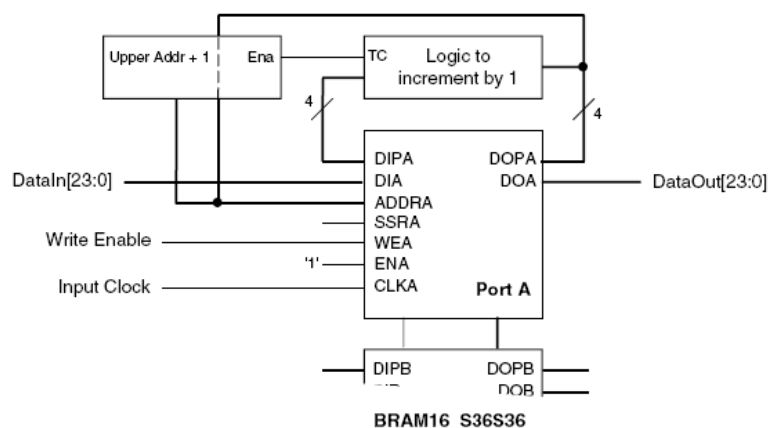


Figure 5.17- 16-deep FIFO can be constructed using four bits (the parity RAM bits)[77].

### 5.3.1.6. MAC

AXI Ethernet Lite MAC (Media Access Controller) is designed to incorporate the applicable features described in the IEEE Std. 802.3 Media Independent Interface (MII) specification, which should be used as the definitive specification. The Ethernet Lite MAC supports the IEEE Std. 802.3 Media Independent Interface (MII) to industry standard Physical Layer (PHY) devices and communicates with a processor using the AXI4 or AXI4-Lite interface. The design provides a 10 Mb/s and 100 Mb/s (also known as Fast Ethernet) interface. The goal is to provide the minimal functions necessary to provide an Ethernet interface with the least resources used. The top level block diagram of the XPS Ethernet Lite MAC is shown in Figure 5.18 and its attachment of this core to the AXI bus in Figure 5.19 [78].

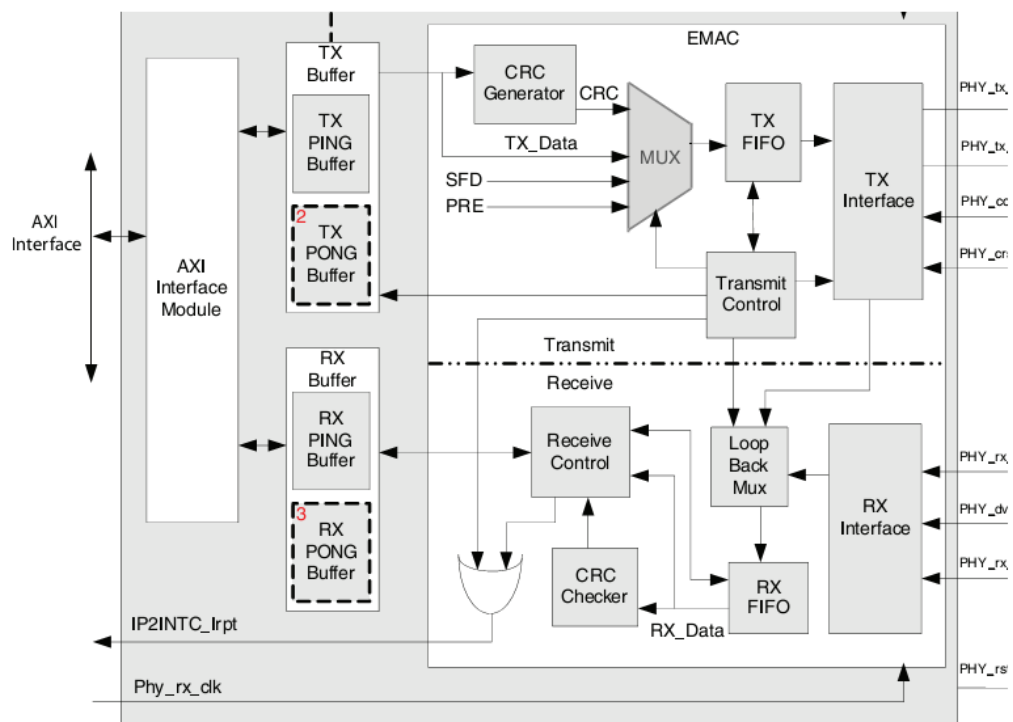


Figure 5.18 show the top level block diagram of the AXI Ethernet Lite MAC [78].

### 5.3.1.7. DDR Memory

In our system we are interfacing with DDR2 Memory for the operation of the digital beamformer. We are buffering the desterilized data from the receiver section then we continue the operation of the beamformer of the interpolation, delaying, Apodization and finally summing the data from the buffered data on the DDR2 memory. We are using the Spartan-6

FPGA memory controller block (MCB). The MCB is a dedicated embedded block multi-port memory controller that greatly simplifies the task of interfacing Spartan-6 devices to the most popular memory standards. The MCB provides significantly higher performance, reduced power consumption, and faster development times than equivalent IP implementations. The embedded block implementation of the MCB conserves valuable FPGA resources and allows the user to focus on the more unique features of the FPGA design [79].

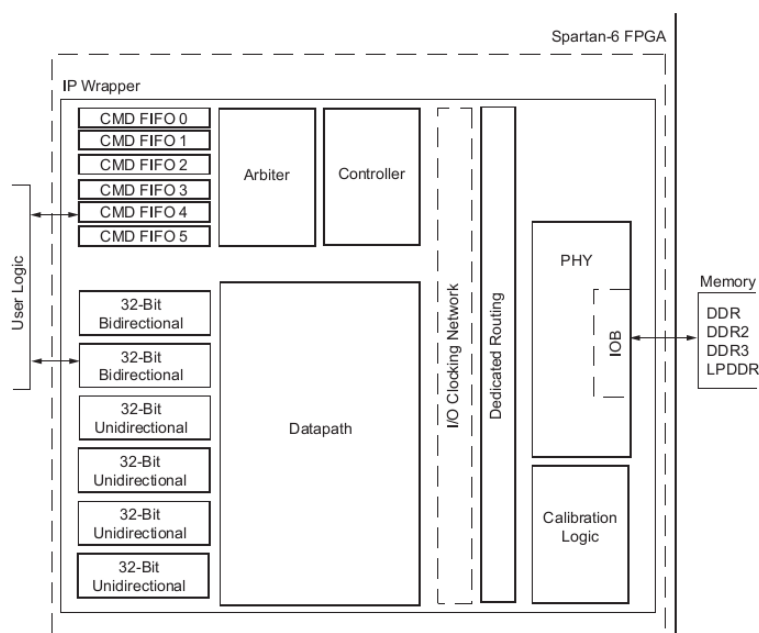


Figure 5.19--show the DDR memory controller block diagram[79].

The blocks diagram in Figure 5.20. Shows the major architectural components of the MCB core. Throughout this document, the MCB is described as provided to the user by the memory IP tools within the CORE Generator software or EDK environment. These tools typically produce top-level “wrapper” files that incorporate the embedded block memory controller primitive and any necessary soft logic and port mapping required to deliver the complete solution. For example, in Figure 5.20, the physical interface of the MCB uses the capabilities of the general I/O block (IOB) to implement the external interface to the memory. General I/O clock network resources are also used.

### 5.3.2. Engine Cores

Engine cores are the heart of the digital beamformer operation. They are responsible for the principle operation of the beamforming. The engine cores of the DBF are the transmitter DBF Core and the receiver DBF Core. In this section we will describe each one in detailed.

### 5.3.2.1. Beamformer Transmitter IP Core

The target of the beamformer transmitter core is to control over selecting beam directions and pulse patterns of the ultrasound transducer .we made graphical representation for this core shown in figure 5.21- The transmitter beamformer core can be divided modularly as three main components transmit level control, transmit focus delay and transmit sequence memory as shown in the next Figure.

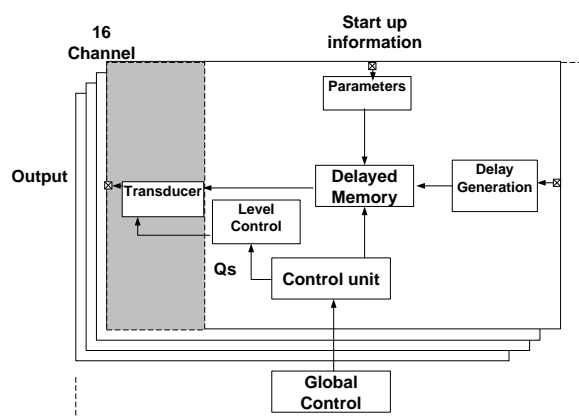


Figure 5.20- a complete transmitter beamformer Module.

#### 5.3.2.1.1. Beamformer Transmitter New IC

While our development progress we found a new solution which is a complete transmitter beamformer LM96570 IC. It has Full control over selecting beam directions and pulse patterns by programming individual channel parameters. And its outputs interface seamlessly with positive and negative inputs on octal high-voltage pulser ICs. Also it has the configurable timing provides Delay resolution of 0.78 ns and range of up to 102.4 US. And finally we could generate Pulse patterns with Sequences of up to 64 pulses Adjustable Pulse widths. , these integration functionality allowing us to remove these function from our design so the final design will be just send triggering the transmitter with preprogrammed delaying fires , figure 5.22 shows the block diagram of the beamformer transmitter after removing the beam selection control .

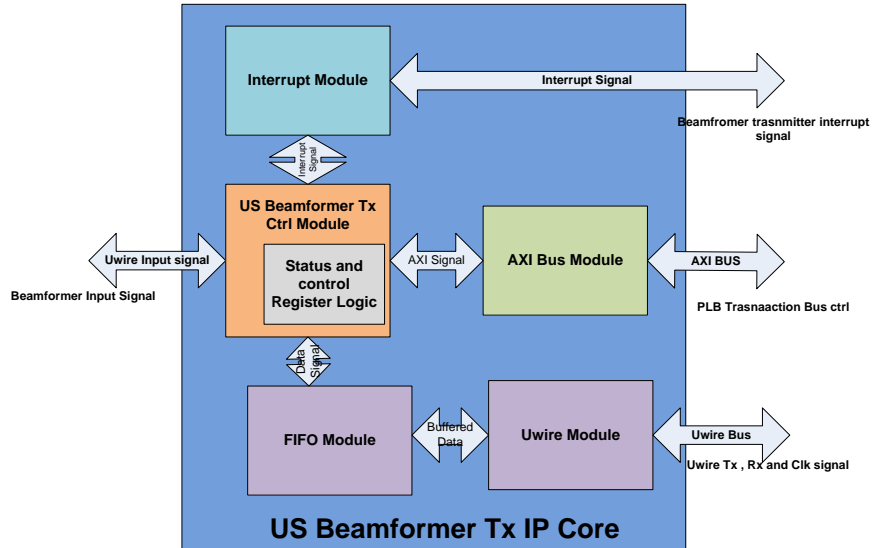


Figure 5.21- US beamformer Tx IP core architecture.

In the Figure 5.23 there is detailed architecture of the beamformer transmitter from inside we can see the main component of the module which are AXI Interface Module provides the interface to the AXI slave single, the Uwire Register Module which includes all memory mapped registers and the INTR Register Module which consists of interrupt related registers, Uwire Module which consists of a shift register, a parameterized baud rate generator (BRG) and a control unit.

### 5.3.2.1.2. DBF transmitter algorithm

After utilizing the new IC in our design and removing the beam pattern control from the design, the transmitter core task changed to be an easy task. Only it is required from us the LM96570 transmitter IC programming only. Our process for beamforming transmitter can be summarizing in the following procedures steps:

- Before scanning certain line, all the pulsers should be fired.
- Before firing the pulsers we first setup the delays for all the pulsers.
- Moreover we can make benefit of the 64 pattern option in the IC to save processing by programming in 64 burst instead of single burst.
- Also For every pulser we have to fix the central frequency by which we are transmitting.

### 5.3.2.2. Beamformer Receiver DAS IP Core

In this section we will describe the IP cores which being implemented by HDL on the FPGA, these cores implementations are hardware dependent and thus there is now way to be implemented by the FW.

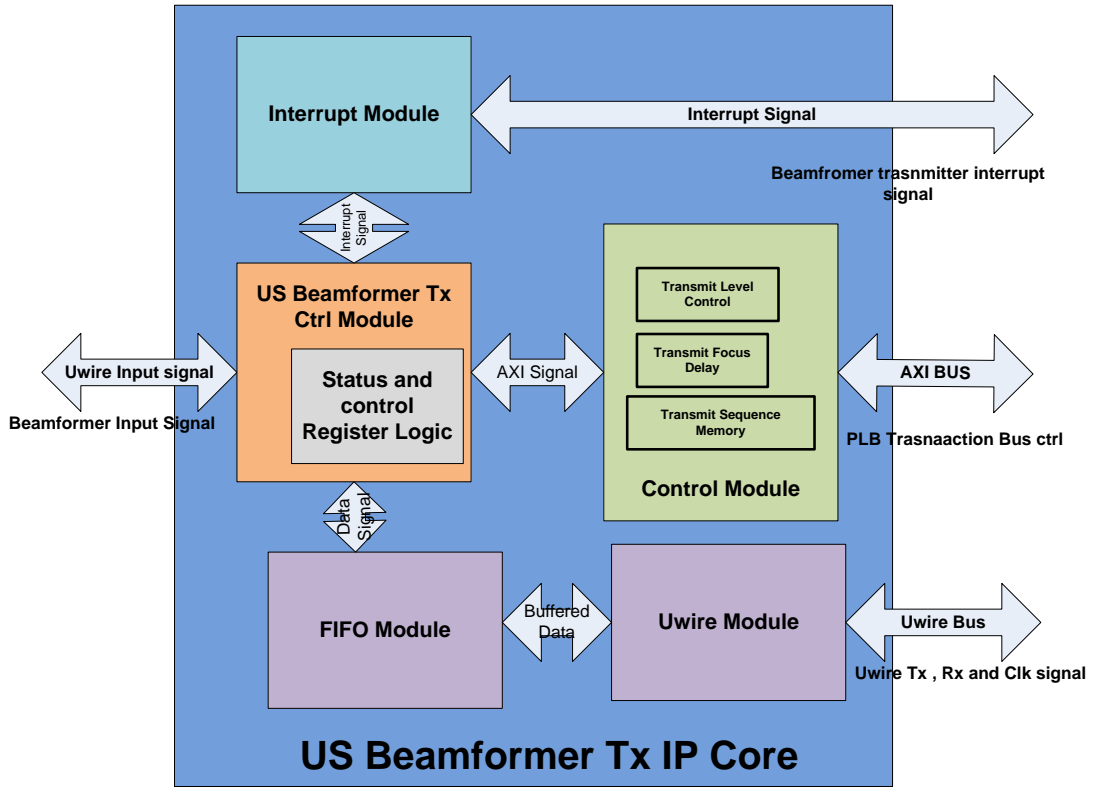


Figure 5.22 Internal architecture of the US beamformer receiver.

We can see that in figure 5.24-the internal component of the digital beamformer receiver is almost the same as the transmitter except that the main module itself which is the beamformer receiver module which is the heart of the core we can see more details about in the next section.

### 5.3.2.2.1. DAS core module

The beamformer samples the pulse echo received at each array element and stored prior to the delays being applied. The stored samples for all array elements. For a particular steering direction are delayed according to the receiving time delays for the focal point and summed to obtain the constructive interference. The amplitude of the envelope of the focused signal is displayed with corresponding brightness.

The function of receiver is to delay and sum the signals from the transducer elements. The analog signals from each transducer converted to digital samples. Then filtered to provide the desired integer and fractional sample offsets before the samples are scaled by the apodization factors then they are summed together to give a sequence of beamformed samples. The mathematical representation of each receives signal's response in the DAS is:

$$y_i[n] = \sum_{k=-\infty}^{\infty} h_i[n, k]x_i[n - k - d_i[n]], \quad (5.1)$$

Where  $y_i[n]$  is the filtered receive signal for the channel at time sample  $n$ ,  $h_i[n, k]$  is the coefficient of the channel interpolation filter at time sample  $n$ ,  $x_i[n]$  is the receive signal from the channel at time sample  $n$ ,  $d_i[n]$  is the integer delay for the receive signal from the channel at time sample  $n$ . The DAS beamformer will be the reference design for this software implementation [1,2]. After each channel of data is filtered, all of the filtered receive signals are summed together as shown in equation 5.2:

$$y[n] = \sum_{i=1}^M y_i[n] , \quad (5.2)$$

Where  $y[n]$  is the beamformed signal at time sample  $n$ ,  $M$  is the number of data channels. The basic block diagram for time domain beamforming, shown for a sonar system, is provided as Fig. 5.23. The top portion of the figure is common to both the time and frequency domain beamformers. The output of this portion of the figure, labeled “X”, then provides the input into the next stage of the beamformer, “X” for the time domain.

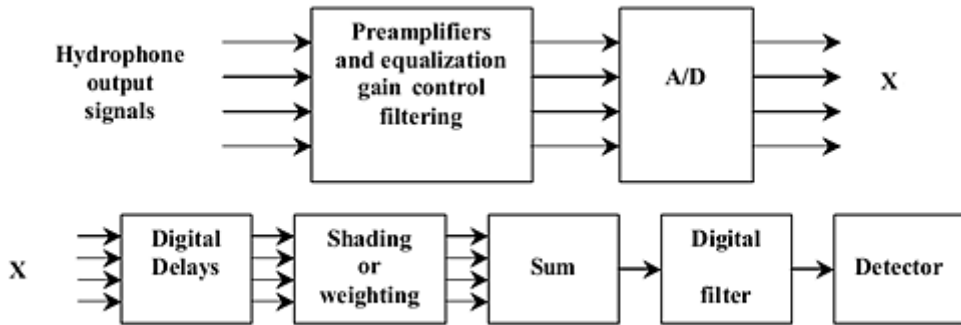


Figure 5.23- Basic methods of time domain beamforming for passive (and active) systems [4].

We will take TI software development kit as our reference in the development and we will extract all the information related to the interpolation filter and their tested data to verify our design. The previous equation should be transformed into logic design so we can implement it in the FPGA. so in the digital design view we can look it as IP core which will be attached to the AXI bus of the MicroBlaze. In principle Beamformer Receiver core comprising the following parts:

- Manager Unit
- Delayed Data Filter
- Interpolation filter
- Apodization gain generator
- Summation

We will describe each component in brief in the next sections

### 5.3.2.2.1.1. Manager Module

The Manager Module controls the flow of data through the entire beamformer. Although it operates on each channel, it is instantiated in hardware as a global module, meaning there is only a single module that interfaces with each of the individual channel processing hardware. This module contains a store of all of the information about the data points required for beamforming. It tracks the time elapsed since transmission, and sends out requests for beamformed pixels when appropriate. It also contains and distributes interpolation and apodization values required for each pixel. By maintaining a central storage area for all beamforming related data and releasing this data as a unit, timing difficulties are greatly reduced. It is important to note that although each channel on the beamformer operates independently, in order to simplify timing, they all operate synchronously on data items. This means that a data point will only be requested to be beamformed by the Control Store when the region is in memory on all of the channels in the FPGA. The address store can also stall beamforming across the entire chip if this condition ever fails. In practice this means that spacing imaging lines far apart will result in long periods of stall between processing of lines, while spacing lines close together will make it impossible for the beamformer to keep up with the input data stream. In either case, the beamformer will operate correctly.

### 5.3.2.2.1.2. Interpolation

The interpolation function is integrated into the data buffer. Linear interpolation can be implemented as a FIR filter with two coefficients  $h[0] = 1-D$  and  $h[1] = D$ . This is the same as a 1.order Lagrange filter. The higher the order of the filter the closer it gets to the ideal sinc filter. The formula for generating the coefficients for an nth order Lagrange filter is

$$h[n] = \prod_{k=0, k \neq n}^N \frac{D - K}{n - K} \text{ for } n = 0, 1, 2 \dots N \quad (5.3)$$

$$l_q(x) = \prod_{i=0, i \neq q}^n \frac{x - x_i}{x_q - x_i} \dots \frac{x - x_{q-1}}{x_q - x_{q-1}} \cdot \frac{x - x_{q+1}}{x_q - x_{q+1}} \dots \frac{x - x_n}{x_q - x_n} \quad (5.4)$$

Figure 2.8 shows the results from the filter-test program for Lagrange filters of order 1,2,3,4 and 5. One thing to point out is that the filters of even order, i.e. 2nd and 4th order, seems to perform better than the odd ordered filters. Figure 2.9 shows that magnitude and phase response of Lagrange filters with delay=0.5 samples.

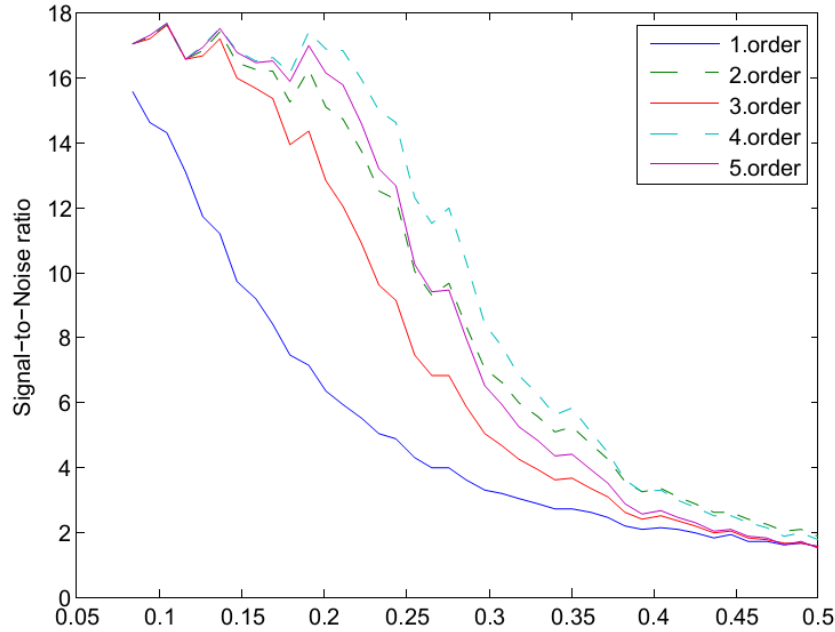


Figure5.24 Signal-to-Noise ratio using Lagrange filters[22].

The even-ordered filters, i.e. those with length  $L=3$  and  $5$ , have a poor phase delay response but a better magnitude response. The reason why the poor phase response does not affect the filter-test result is connected to the fact that the delays are evenly distributed between  $0$  and  $1$ , causing an equal amount of phase shift in both directions. Indeed, when delays are limited to the range between  $0$  and  $0.5$  there is no difference in the test-results for even and odd length Lagrange filters. How the filter's phase response affects the image quality of an actual ultrasound image is still unclear.

### 5.3.2.2.1.2.1. Generation of the filter coefficient

We generate the filter coefficient depending on many parameters which are the number of the filter coefficient tab , coefficient order and the fractional delay , below down there is our C routine for generate the filter coefficient :

```
for(filterCnt=0;filterCnt<numIntFilters;filterCnt++)
{
  uint_least8_t n;

  int_least32_t D = filterCnt * fracDelay;

  // compute the numerator coefficients
  for(n=0;n<numNumFilterCoeffs;n++)
  {
    uint_least8_t k;
    int_least32_t h_n = 1 << numFilterCoeffs_qFmt;

    for(k=0;k<numNumFilterCoeffs;k++)
    {
      if(k != n)
      {
```

```

uint_least8_t qFmt = 0;
int_least32_t sf_num = D - (k << fracDelay_qFmt);
int_least32_t sf_den = n-k;
int_least32_t tsf;
uint_least32_t numPnts = 1;

    math_div_cor_32b_32b(&sf_num,&sf_den,numPnts,qFmt,&sf);

h_n *= sf;

h_n >>= fracDelay_qFmt;
    }
} // end of k for Loop

// store filter coefficients in reverse order
pIntFilters[filterCnt].pNumCoeffs[numNumFilterCoeffs-1-n] = (int_least16_t)h_n;
} // end of n for Loop

// store numerator parameters
pIntFilters[filterCnt].numNumCoeffs = numNumFilterCoeffs;
pIntFilters[filterCnt].numCoeffs_qFmt = numFilterCoeffs_qFmt;

// store denominator parameters
pIntFilters[filterCnt].numDenCoeffs = numDenFilterCoeffs;
pIntFilters[filterCnt].denCoeffs_qFmt = denFilterCoeffs_qFmt;
} // end of intFilterCnt for Loop

```

### 5.3.2.2.1.2.2. Interpolation Filter Placement

The optimum placement of the interpolation filter also is an important consideration. The filter can be placed either before delaying the receive signals or after they are delayed and summed.

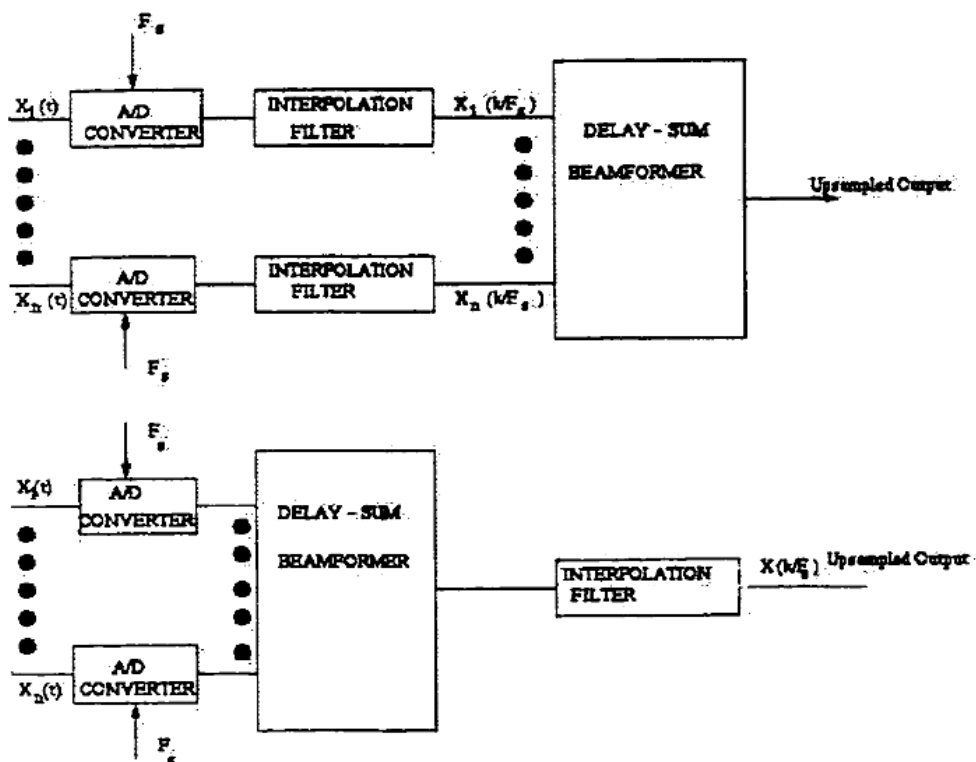


Figure 5.25-showing generation of the filter coefficient[21].

### 5.3.2.2.1.3. Apodization

Applying an apodization function to the received signals can improve the quality of beamformed images by reducing side lobe levels in the radiation pattern of the array. Apodization reduces the amplitude of the received signals based on their location on the array. We are using hanning window for generating our FIR filter coefficient:

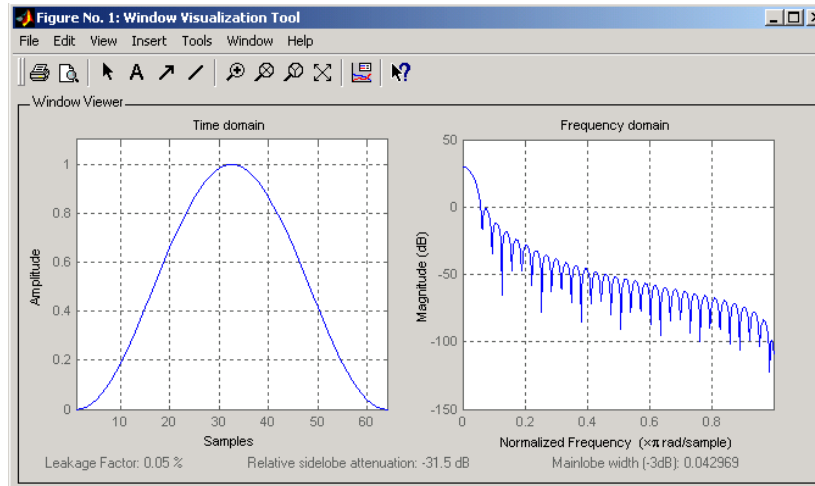


Figure 5.26- showing hanning window for generating our FIR filter coefficient.

#### 5.3.2.2.1.3.1. Generation of the apodization values

Generation of the apodization values using hanning algorithm need 3 parameters which are number of samples, number of iterations and the selected active transducer. Generation of the apodization routine is shown in the next c code.

```

int_least16_t twoPi = TWO_PI_16B;
uint_least8_t twoPi_qFmt = TWO_PI_16B_QFMT;
uint_least8_t tnumIterations = 20;

if (apodGain_qFmt < twoPi_qFmt)
{
    twoPi >>= (twoPi_qFmt - apodGain_qFmt);
}

for (sampleCnt=0; sampleCnt < numOutputSamples; sampleCnt++)
{
    uint_least16_t cnt = 1;

    for (channelCnt=startChannelNumber; channelCnt <= stopChannelNumber; channelCnt++)
    {
        int_least32_t num = twoPi * cnt;
        int_least32_t den = numActiveChannels + 1;
        uint_least32_t numPnts = 1;
        uint_least32_t index = channelCnt * numOutputSamples + sampleCnt;
        int_least16_t tcosTh;
        int_least32_t tth;

        // compute angle
        math_div_cor_32b_32b(&num, &den, numPnts, 0, &tth);
    }
}

```

```

// compute the cosine
math_cos_cor_16b_16b((int_Least16_t
*)&th, numPnts, numIterations, twoPi_qFmt, apodGain_qFmt, &cosTh);

// store the value
pApodGains[index] = ((1 << apodGain_qFmt) - cosTh) >> 1;

// increment the counter
cnt++;
} // end of elemCnt for Loop
} // end of sampleCnt for Loop

break;
} // end of ApodGainType_Hanning case

```

#### 5.3.2.2.1.4. Delaying

The method by which a linear array may be excited in order for the wavefront to propagate in any desired azimuth angle is shown in Figure 5.27.

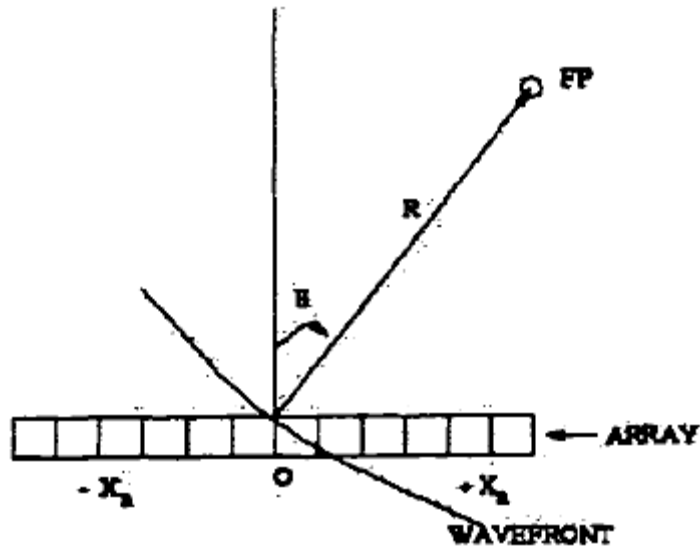


Figure 5.27- shows the coordinate system used to determine the time delay[19]

Needed for an element so that the summing of echoes from a target at a range  $R_{fb}$  and angle  $\theta$  produce constructive interference. For the calculation, it is assumed that the echo wavefront returning from a point scattered is of circular shape. The resultant delay  $\tau$ , required at an element that is at a distance  $x$ , from the center of the array for the delayed element's output to coincide in time with the center element output is given by[21]:

$$\tau_n = \frac{1}{c} \{ R_{fb} [ R_{fb}^2 - 2R_{fb}x_n \sin \theta + x_n^2 ]^{1/2} \} \quad [21]. \quad (5.5)$$

Here  $R_{fb}$  is the radial distance from the array center and  $\theta$  is the pointing angle relative to the array normal. The constant  $c$  is the velocity of sound in the medium. Two problems arise with the use of above equation in computing channel delay element times. First, the time delay becomes negative and therefore non-causal for negative steering angles i.e. to the left of

the center array. This can be overcome by adding a positive constant to the delays for all elements. Second is the inseparability of  $\theta$  and  $R_{fp}$  dependencies, Which make the direct computation of the time delays time consuming. This can be overcome by the use of parabolic approximation. Equation 6.1 can be approximated as[21].

$$\tau_n = \frac{1}{c} \left\{ x_n \sin \theta - \frac{x_n^2}{2R_{fp}} \cos^2 \theta \right\} \quad [21] \quad (5.6)$$

### 5.3.2.2.1.5. Delay filter coefficient Generation

As we described in the previous section Delay filter coefficient is a function of steering angles and the radial distance we can see in the next c routine how we can generate the delay filter coefficient.

```
for(channelCnt=startChannelNumber;channelCnt<=stopChannelNumber;channelCnt++)
{
// compute the radicand for the delay computation
rxBf_genRadValues(pRxBfParams,channelCnt,pRadValues);

// take the square root of the radicand
math_sqrt_cor_64b_32b(pRadValues,numOutputSamples,32,relSqrt_qFmt,pSqrtValues);

// compute the relative delay values
rxBf_genRelDelayValues(pRxBfParams,channelCnt,pSqrtValues);

} // end of channelCnt for loop
```

In this design, the total receive delay time in each receive channel is calculated and stored in a matrix array for each scan, representing a single b-mode scan.

### 5.3.2.2.1.6. Summation

The role of the adder module in the beamformer is to combine the outputs from each of the beamformer channels, and add them together with the output from the previous card in the chain. Since each card will be processing data independently, the summation of data between cards must be buffered such that it can be properly aligned, independent of the arrival of the data terms. This is accomplished by using two FIFO buffers within the Adder module. One FIFO Captures data passed from the previous card, while the second contains the summation of the data from the current card. Due to bandwidth limitations, the tracking of individual samples is not performed. Instead, with each transmit pulse all of the internal buffers are cleared. The module then relies upon processing order to align values between processing boards. The second stage of the adder module waits for both of these FIFOs to contain data

before pulling terms out of them, adding them, and passing them down the backplane chain as shown in the next Figure.

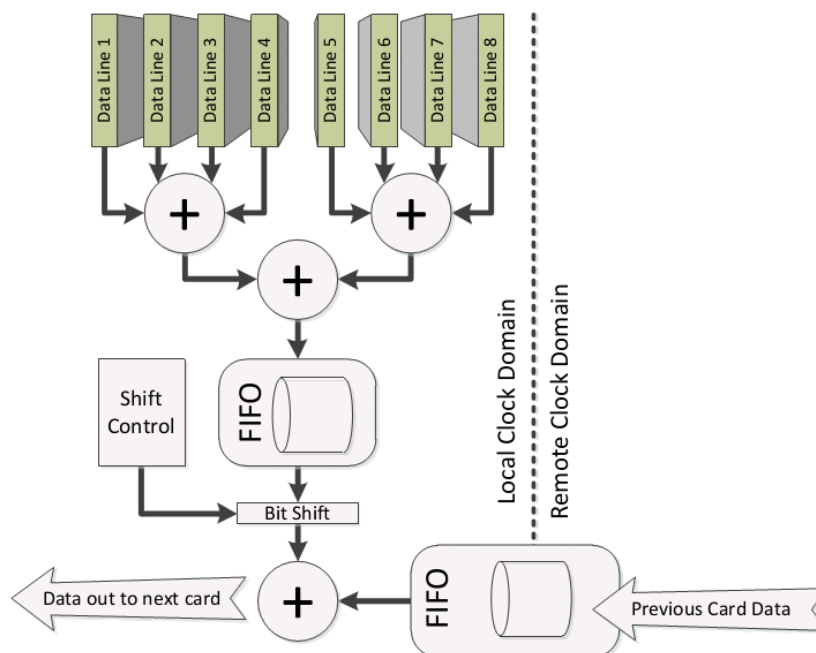


**Figure 5.28 - Adder module functional diagram.** Each beamformed data term is added to all others on the card, and then stored in a FIFO buffer. Data from the previous card is also stored in a FIFO. When both buffers are ready, the terms are summed together, and passed down the chain.

## 5.4. Challenges and Limitations

Many challenges were faced and solved in developing the beamformer HDL code. Most of these involved overcoming the limitations the hardware, such as removing speed bottlenecks, memory high speed buffering requirements, and reducing the need to use advanced mathematics. Although nearly any function could be coded, the added complexity may not be justified by the end results. Each of the final three tasks have varying degrees of mathematical complexity, and therefore the best place to perform these tasks needs to be considered. Using VIVADO High level synthesis tool was the edge of our design as it improve the dramatically the rate of our development due to overcoming the limitations the hardware of removing speed bottlenecks, memory high speed buffering requirements, and converting the advanced mathematics written in traditional C language into HDL language with all the degree of the optimization.

## 5.5. Summery

Here in this chapter we describe in details the architecture of the ultrasound digital beamformer, we go through all the firmware components and the system interfaces. The main

components is the FPGA we start the design with VIRTEX 6 but we could utilize the low price SPARTAN 6 for our system we discuss the main components in the FPGA and the meaning of CLB, LUT and BRAM also we introduce the MicroBlaze softprocessor as the house keeper for our system and its significant role in reducing the logic complexity. Also we introduce the Uwire interface which is the beamformer interface and also we give demonstration about this IP core and its components, also the deserializer using LVDS interface the ultrasound receiver interface also we describe in details the main components of the digital beamformer IP interface and its synchronizing and buffering techniques. We also illustrated ways of optimization techniques in the interpolation and the summation which being described in details in the next chapter. Also we give demonstration about the DDR memory core being used and the Ethernet.

## Chapter 6

### Ultrasound Digital Beamformer Implementation

#### 6.1. Introduction

This chapter describes the methods and procedures for investigating experimentally the proposed implementations of the digital beamformation. Moreover there is complete section for describing the optimization done for the design. The hardware and software procedures of each of all the design components are described below. Ultrasound images and testing vectors are obtained from TI ultrasound development Kit. It includes the raw scan lined and the parameters by which the scanning has occurred .

#### 6.2. System Parameters

This section presents the various design parameters like beam angle that decides the aperture length, temporal and spatial sampling periods, filter cut-off frequencies, and attenuation coefficients. We can find below a summery for each parameter with its default value which we are using in our testing as shown in table 6-1

Parameter	Description	Value	Unit
FsOverC_samplesPerUm	sampling rate divided by the speed of sound	4357718	Samples/um
FsOverC_samplesPerUm_qFmt	power of 2 used to scale up the sampling rate divided by the speed of sound	26	
Scan Line Number	scan line number	1	Line
Scan Line Spacing	scan line spacing of the beamformer	13422	M,Rad
Scan Line Spacing _ qFmt	power of 2 used to scale up the scan line spacing	24	
Current Pos_um	the current spatial position of the beamformer	0	um
CurrentPos_um_qFmt	the power of 2 used to scale the current spatial position of the beamformer	0	
CurrentAng	Current angular position of the beamformer	0	rad
CurrentAng_qFmt	Power of 2 used to scale the current angular position of the beamformer	15	
Num Input Samples	Number of samples per beamformer iteration	2536	Sample
Num Output Samples	Number of output samples per beamformer iteration	128	Sample
Max Lead Delay	The maximum lead delay <u>value</u>	1200	

Max Lag Delay	The maximum lag delay value	1200	
Num Scan Lines	The number of scan lines	50	
NumMlas	The number of multiple line acquisitions for the beamformer	1	
Num Channels	the number of transducer data channels in the x direction	192	Channel
Num Active Channels	the number of active channels in the x direction	64	Channel
Frac Delay	the fractional delay of the interpolation factors	3277	
fracDelay_qFmt	power of 2 used to scale up the fractional delay of the interpolation factors	15	
Int Filter Type	The interpolation filter type	Int Filter Type_Lagrange	
NumInt Filters	the number of interpolation filters	8	filter
IntFilterCoeffs_qFmt	the power of 2 used to scale up the interpolation filter coefficients	14	
Num Elements	the number of transducer elements in the x direction	192	um
Elem Spacing _um	The transducer element spacing in the x direction	501760	um
Elem Spacing _um_qFmt	the power of 2 used to scale up the element spacing value in the x direction	10	
Tr Type	the transducer type	Transducer Type_Linear	
Apod Gain Type	the apodization gain type	Hanning	
Apod Gain _qFmt	the power of 2 used to scale up the apodization gains	15	

**Table 6.1 Beamformer receiver configuration parameters default values**

In general this testing, a 192 element transducers only 64 element of them are active in the receiving the echoes with a center frequency of 5 MHz is used. From the previous calculation we get that that the signal from a 5MHz transducer would be too small to be detected at 17.1cm of depth and having determined the maximum depth possible, we can then use this to determine the maximum round trip time of flight (speed of sound in the medium is approximately the same as water (1510 m/s) .Using this speed we can estimate the time

required for a signal to penetrate to its maximum depth and return, it would require approximately 0.22ms ( $0.171\text{m}^2/1510\text{m/s}$ ) to complete the trip. By taking the reciprocal of this time-of-flight, we can determine another key limiting factor for any ultrasound system: the maximum number of pulses that can be completed per second. Again to continue our example, this system could achieve 4415 pulses per second.

### **6.3.DAS Implementation**

This implementation of digital beamformer is the earliest and commonly used beamformer in commercial ultrasound imaging instruments. All the beamforming was done after the data were acquired using the experimental imaging system. In this method, the beamformer samples the pulse echo received at each array element and stored prior to the delays being applied. The stored samples for all array elements. For a particular steering direction are delayed according to the receiving time delays for the focal point and summed to obtain the constructive interference. The amplitude of the envelope of the focused signal is displayed with corresponding brightness.

#### **6.3.1. DAS Image Formation**

The Image formation is composed of three main stages which are `rxBf_init ()` which responsible for initialize the beamformer with the proper parameters for the beamforming operations as well as generating the interpolation filter coefficient, the second is `rxBf_setup ()` which is responsible for starting the parameters for the specific new scan line and the third module which is `rxBf_run ()` this function is beamforming itself it makes the calculation and filtering to result beamformed data.

#### **6.3.2. Beamformer Initializing Module**

Beamformer initialization module is being used only one time at the start of the beamforming process for certain object , it is responsible for starting the operation from new scan line with the desired parameter for the specific region . A simple flow chart for this process is shown in figure 6.1.

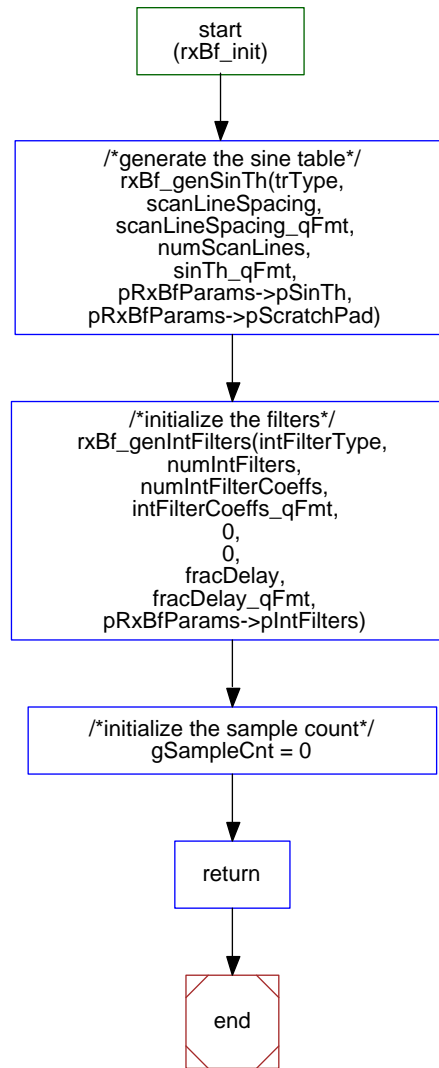


Figure 6.1-Shows the simple flow chart for the beamforming initialization module.

As shown in figure 6.1 there are 3 processes in the beamformer initialization module which are:

- **Initialize the sin table of the steering angles (in case of phased transducer)**
- **Initialize the interpolation filter coefficient**
- **Initializing sample count**

### 6.3.3. Beamformer Setup Module

This module is responsible for starting the operation from new scan line each scan line we need to do the following procedures:

- **Reset the sample counter again.**
- **Generate the start and stop channel indices.**
- **Generate the apodization gain factor.**

- **Generate the initial delays.**
- **Generate the compressed delay.**
- **Generate the Interpolation coefficient**

As shown in Figure 6.2, resetting the sample counter then we generate the start and stop channel indices according to the configuration parameters and depending on type of the ultrasound transducer type, then we generate the apodization gain then the compressed delay generation finally the initial delays generation

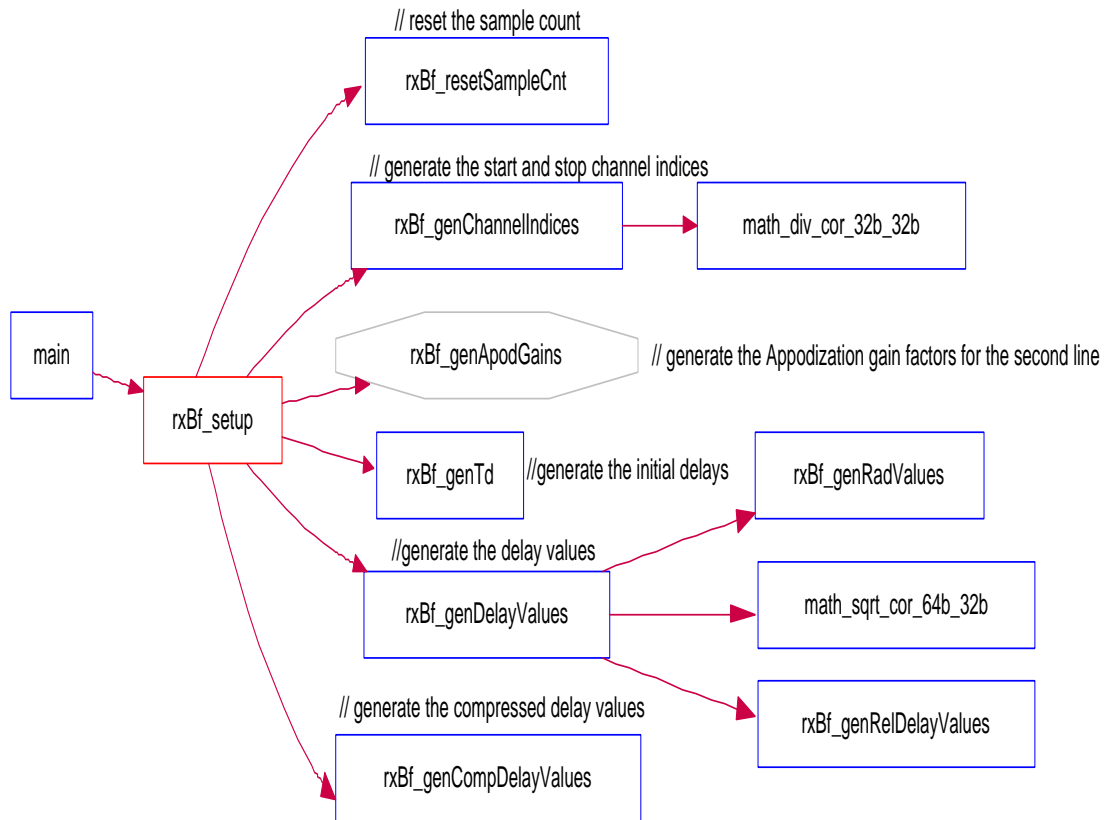


Figure 6.2-Beamformer setting up flow.

### 6.3.4. Beamformer Running Module

In this experimental investigation the total receive delay time in each receive channel is calculated and stored in a matrix array for each scan, representing a single b-mode scan. After all the received information has been suitably delayed, the outputs are then summed. The sum is then rectified, envelope detected and processed to obtain the brightness information. In case of multiple receive zones, the delays for each channel. Focal zone and B-mode scan are stored in a 3-dimensional array. The received information is first delayed for a range  $R_{fpl}$  along the same azimuthal orientation. Once all the echoes within that focal region associated with  $R_{fpl}$  are delayed. The delay in each of the channels is altered to produce a new focus some distance

beyond the first. This process continues until all echoes from the most distant focal region Rf<sub>pn</sub> have been delayed. This delay process is continued for each scan direction. For the DSA architecture, a high sampling rate is required, however, if temporal interpolation of the receive data is performed in conjunction with the beamforming operation, the received data needs only to be sampled at the Nyquist rate. This is called interpolation beamforming. The interpolation is accomplished by zero padding the original sequence, and passing the resulting sequence through a finite impulse response (FR) low pass digital filter. For single scan line in the running module we can summarize it by the following processes:

- **Zero out the summed data buffer**
- **Zero out the filtered data buffer**
- **Summing the resulted data**
- **Interpolating the data**
- **Combining the filtered data**
- **Updating the sample counter**

These processes are shown in figure 6.3.

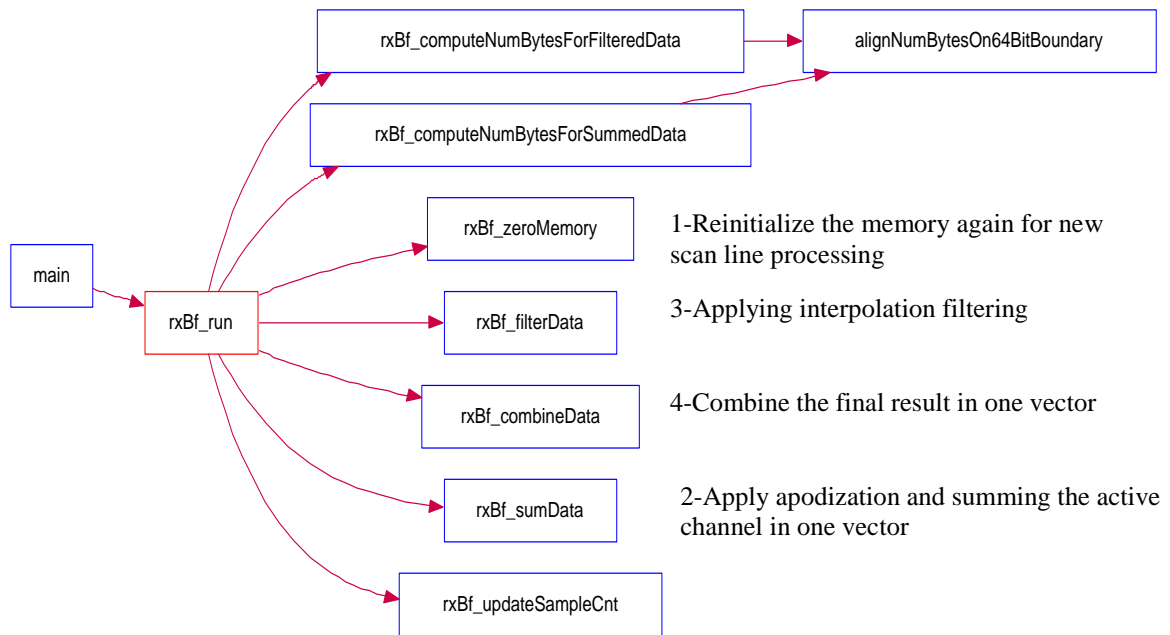


**Figure 6.3- Beamformer running flow.**

In the beamformer running module we can find that they are depending on each other first we are summing out the data then we zeroing out the filtered data then summing the result data then the interpolation stage and finally combining out the filter data .

### 6.3.4.1. Summing data

This stage comprises the following processes:

- **Initialization of the apodization parameters**
- **Getting the Delay value**
- **Apply Apodization**
- **Accumulate**
- **Packing the result data**

At the beginning of the apodization stage we should initialize it with the desired parameters which being adjusted to fit this target of the scan line, the second step is to get the delay valued generated in the beginning of the operation once we have both we can apply the apodization filter and accumulate with the last result of the apodization and finally packing the result into one vector.

### 6.3.4.2. Interpolation Filter

Interpolation filtering comprises the following 7 processes:

- **Interpolation Parameters Initialization**
- **For each output sample and For each coefficient element doing the following procedures:**
  - **Loading the filter coefficient**
  - **Loading the input data values**
  - **Apply the filter coefficient**
  - **Packing the result data**
  - **Scale the result**
  - **storing the result**

In the interpolation filter process we are using it to interpolate between each output sample and for each of the interpolation coefficient we are generating the required interpolated data and for each iteration we should load the filter coefficient, loading the input data from the apodization stage then applying the interpolation filter then pack the result and scale it with our maximum and finally storing the result data.

### 6.3.4.3. Combining the data

The combining of the beamformed data composed of two main steps:

- **Initializing the data**
- **Combining the data**

- **For each output sample and for each coefficient**
  - **Load the data**
  - **Accumulate the data**
  - **Round the data**
  - **Scale the data**
  - **Pack the result data**
  - **Save the result**

## **6.4. DAS Simulation and results**

As we did not have a complete implementation for our proposed design, we chose a study made for a system similar to our proposed firmware design (implementing almost the same the DAS algorithm). This study has been made by Sunil Vasudevan [21] for studying the differences between DAS and SAR DBF algorithms. He got Ultrasound images from a Aloka ultrasound machine (Aloka, Tokyo, Japan, model: SSD-246), manufactured in 1944. The transmit part of the system is a parallel real-time transmit system with a 3MHz, 64-element linear transducer array and pitch of 2 mm. The elements are 0.2mm from the probe surface. The transmit circuitry of the machine consists of a trigger which generates a gated square pulse. The amplitude is variable from 0 to 400 V p-p. This trigger pulse is applied to the transmit elements through a dual channel multiplexer.

### **6.4.1. Testing Phantoms**

The RF data that are used for experimental investigations are acquired from different phantoms. Since the receiving part of the experimental system described above is not real-time, it excludes investigations where movement distortion could be a problem. Hence all imaging is done on custom built and standard phantoms. Phantoms used in this thesis for the investigations may be classified into water phantoms and tissue-mimicking phantoms.

#### **a) Lucite block in water bath**

This phantom has a single Lucite slab of dimensions 12.5 x 9 x 1.5 mm which is immersed in a plastic tank holding de-mineralized and distilled water. Lucite is assumed to be a perfect reflector. This phantom is used to characterize transmit and receive beam patterns of the transducer array. The rf signals received are also used to set system parameters such as signal bandwidth, center frequency of transmitted signal and filter cut off frequencies.

**b) Lucite block holding tubes of different lengths.**

A Lucite block of dimensions 12 x 6.5 x 4 mm has holes drilled on the surface to hold hollow plastic tubes of 2 mm diameter. Copper wires are inserted in the hollow tubes to increase the reflectivity. The lengths of the tubes vary from 1 mm to 8 mm. This phantom is in a degassed water bath. It is used to find the point-spread function (PSF) of the different methods.

**C) Metallic sphere on Lucite slab.**

This phantom has a metallic sphere of diameter 2.5 mm on a Lucite block of dimensions 12.5 x 9 x 1.5 in a degassed water bath. This phantom is used to view improvements in edge detection with beam forming.

**d) Lesion and scattering phantom.**

This phantom is custom made (Ernest L. Madsen, Dept of Medical Physics, University of Wisconsin, Madison). It has a number of spherical lesions of diameter 6 mm and a backscatter coefficient 14 dB below their surrounding medium. The lesions have an attenuation slope of 0.5 dB/cm/MHz. The surrounding medium consists of glass bead scatterers of 45-53 microns in diameter range. There are 4 grams of beads per litre. It is used to compare overall image quality for different methods.

**e) Cyst and Wire phantom**

This is a wire and cyst tissue mimicking phantom (Nuclear Associates, model: #84-317). This phantom has a series of monofilament nylon targets, 0.375 mm in diameter that are separated over varying distances. It also has four simulated cysts of diameters 4, 6, 8 and 12 mm (cylinders of gel with no scattering). The filling medium is a hydrogel containing a scattering agent that simulates human liver parenchyma. It is used for comparing the overall image quality and finding the point-spread function.

**6.4.2. Testing configuration**

Configuration A simulated a single transmit focus and receive focus using 128 elements which were uniformly weighted. Configuration B simulated a conventional analog beamformer with single transmit focus and multiple receive focal zones. Each zone had a length of 20 mm. It used 64 active elements for transmit and Hanning apodization to weight

the elements (both transmit and receive). For configuration C, four transmit and receive focal zones were used. The length of the focal zones was 20 mm. 128 transmit elements were used. Configuration D simulated a typical digital beamformer, with multiple transmit focus and dynamic receive focus. The transmit had four focal zones of length 20 mm. Hanning apodization is employed to maintain a constant f-number over each focal zone. A f-number of 4 was used on transmit and 2 on receive. For configuration A, a point target at the transmit focus was used. For configuration B, C and D, a five point target with the points at the center of each focal zone was used. These configurations represent the gradual evolution of beamformer from analog to the present day digital beamformer

### 6.4.3. Testing Results

Figure 6.4 shows the point spread function (PSF) calculated at a focal range of 100 mm using the configuration. The plots showed the spatial variation of beam width and side lobe level without a) apodization, b) with rectangular apodization and c) with Hanning apodization, as a function of the lateral and the axial distances.

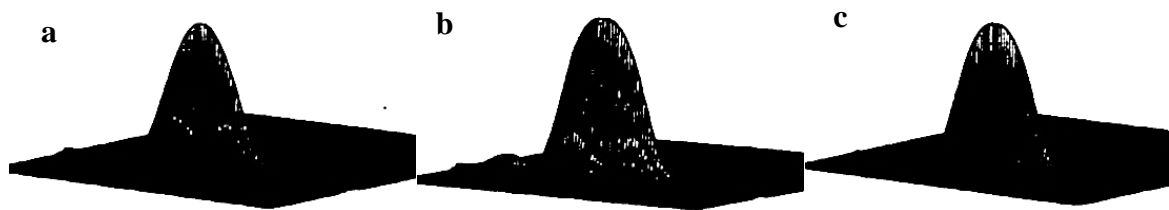


**Figure- 6.4 Images produced with single transmit and receive focus displayed over a 40 dB range. The data are collected from a wire object using configuration A with the object positioned at 100 mm: (a) without apodization, (b) rectangular apodization and (c) hanning apodization. All lateral and axial distances are in millimeters[21].**

To a large extent the performance of an ultrasound imaging system is characterized by the spatial response of the transducer. From the response, one can determine the spatial resolution as well as the image dynamic range, the two most important parameters of image quality. We see a decrease in beam width and side lobe level with apodization (Figures 6.4b and 6.4c), thus indicating a improvement in image quality when compared to the image without apodization (Figure 6.4a). The peaks of all the PSF's are normalized to one corresponding to the maximum value of the main lobe. Table 6.1 shows the beam width measured at -6 dB and the side lobe levels for each window versus the focal range.

Focal Range [mm]		100	103	105	107
Beamwidth [mm]	(a)	3.659	3.689	3.723	3.824
	(b)	3.349	3.620	3.584	3.543
	(c)	3.126	3.569	3.598	3.502
Sidelobe Level [dB]	(a)	-11.3	-9.2	-11	-11.54
	(b)	-10	-10	-10.9	-12.07
	(c)	-13.37	-12.07	-15.2	-12.83

Table -6.2 Beam width and side lobe level Vs Focal range: (a) without apodization, (b) rectangular apodization and (c) hanning apodization[21].

The values for beam width versus the focal range are plotted in Figure 6.5, indicating that apodization does help in controlling the beam width as we move into the far zone, where the gradual divergence of beams occur.

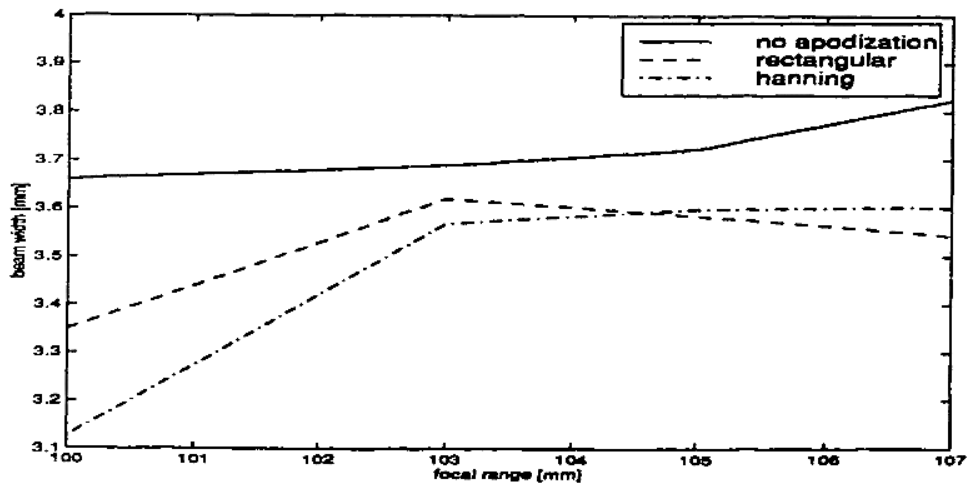


Figure -6.5 Comparison of 6-dB beamwidth versus focal range for a wire object obtained using configuration A[21].

Figure 6.6 shows the comparison of the -6 dB beamwidth versus the depth for the linear array in configuration A. The point spread functions for the wire object are calculated at distance of 3 mm, 5 mm and 7 mm respectively from the fixed transmit focus of 100 mm. The numerical values are tabulated in Table 6.2.

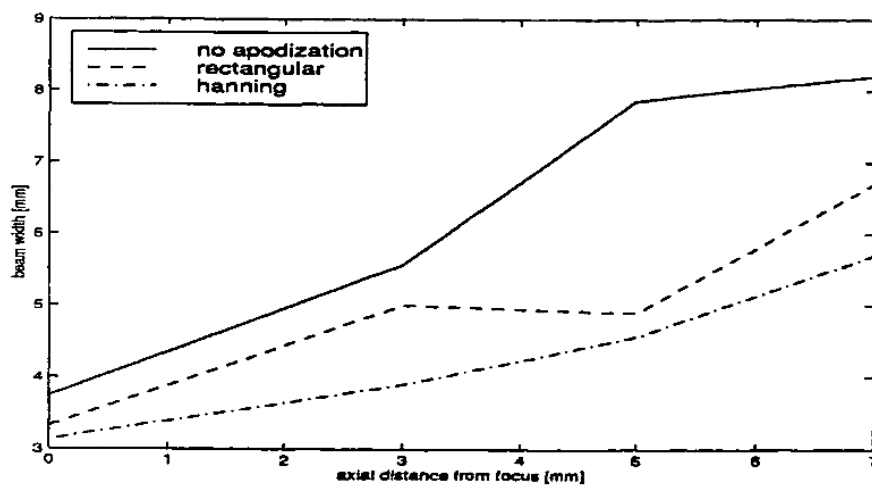


Figure 6.6 -Comparison of 6-dB beamwidth versus depth for a wire object imaged using configuration A[21].

These results indicate that apodization does help in improving the spatial response, when the objects appear beyond the focal region..

Axial distance from focus [mm]		0	3	5	7
Beamwidth (a)	[mm]	3.7	5.5	7.8	8.2
	(b)	3.3	5.0	4.8	6.77
	(c)	3.1	3.8	4.5	5.77

Table -6.3 Resolution of a wire target away from the focus of 100 mm for (a) without apodization, (b) rectangular apodization and (c) hanning apodization[21].

Figure 6.7 shows the surface plots of a 6 wire phantom obtained from configurations B, C and D. as described in Section 6.1, which shows the beam responses and side lobes for the arrays modeled. The surface plots are used to bring out the effect of various configurations on beam response and sidelobes, that may not be visible in gray-scaled images due to the scan conversion.

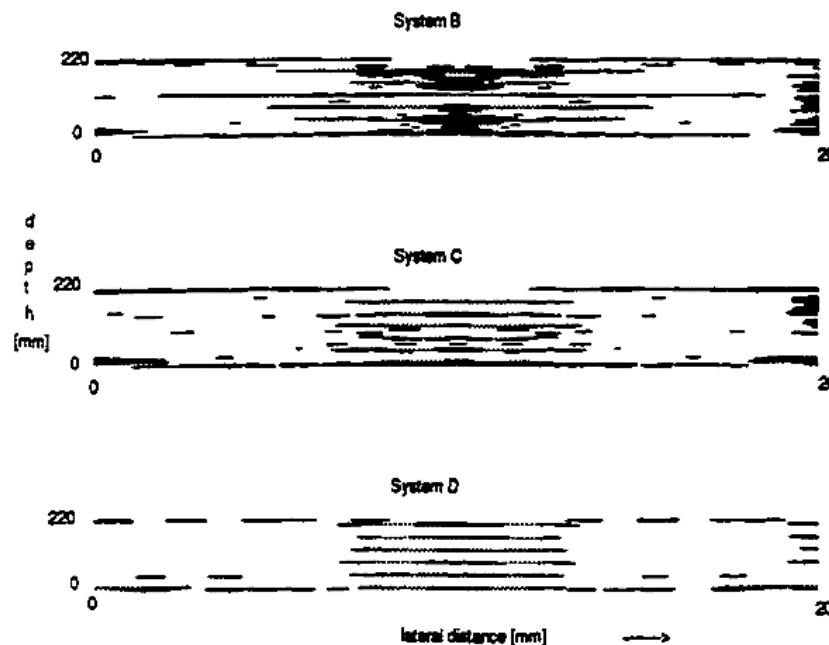
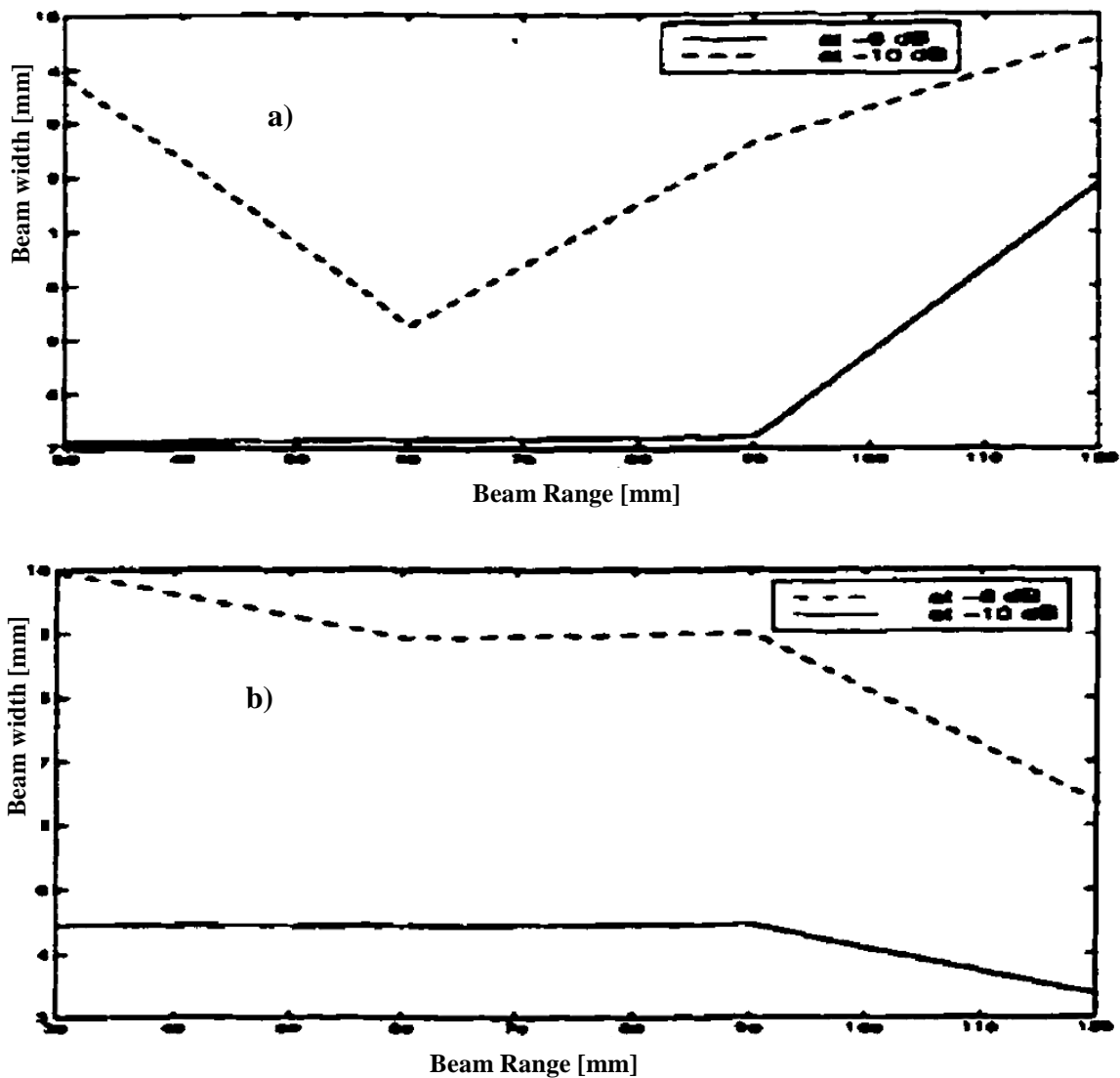


Figure 6.7-Surface plots of images of a six wire phantom obtained from (a) configuration B. (b) configuration C and (c) configuration D[21].

The six wire objects are at distances 35, 50, 65, 80, 95 and 110 millimeters. Figure 6.7a shows the surface plot for configuration B, that had a fixed transmit focus at 60 mm and five receive focal zones starting at 10 mm from the array surface and with a zone length of 20 millimeters. It uses 64 elements during transmit and all 128 elements for receive. Figure 6.7b shows the surface plot for configuration C that had four transmit points at 40, 60, 80 and 120 millimeters and five receive focal zones with same parameters as configuration B. All the 128 elements are used for both transmit and receive. Figure 6.7c is the surface plot for configuration D which employed dynamic apodization and dynamic receive that continuously 'tracked' the

receive echoes. The system had four transmit points at 40, 60, 80 and 120 millimeters and the data are sampled at a frequency of 25 MHz. These plots bring out the efficacy of a digital beam former in improving the image quality by limiting the beam spread and eliminating side lobes (Figure 6.7c), as compared to the other two configurations (Figures 6.7a and 6.7b). Also the ability of the digital beamformer to pick up signals in the far zone better than configuration C with multiple focus, is evident from Figure 6.7c. In order to generate the plots shown in Figure 6.8, a PSF is calculated at various ranges between 30 and 120 mm. The lateral response on millimeters at -6 dB and -10 dB were computed for each PSF.



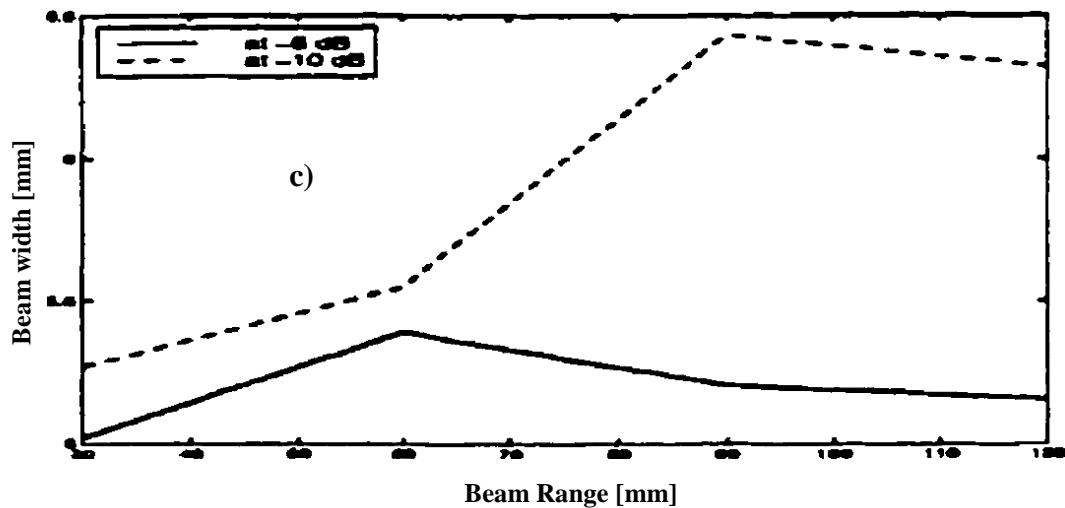


Figure 6.8- Simulated lateral beamwidth versus range for (a) configuration B (b) configuration C and (c) configuration D[21].

These beam widths were plotted versus range. Figure 6.8a shows the lateral response for configuration B with 64 active elements in transmit and 128 elements on receive. Figure 6.8b shows the performance of configuration C with 128 elements active on both transmit and receive. Figure 6.8c demonstrates the decrease in beam width over range when compared to Figure 6.8b, using dynamic apodization. One of the reasons for the popularity of digital beam forming is its ability to maintain good imaging capability at increasing distances from the array. This can be noted from the Figure 6.8c and table 6.3, where the beam width at lower signal levels over focal range is narrower than in configuration B and C (Figures 6.8a and 6.8b respectively).

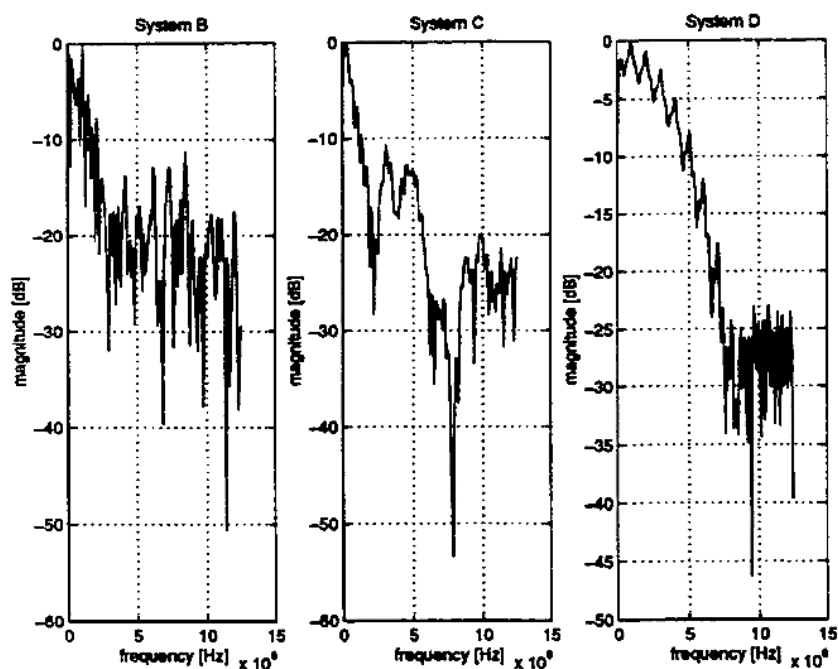


Figure 6.9 Frequency spectrum beam plot (single A-scan) of Images of a wire phantom using (a) configuration B. (b) configuration C and (c) configuration D[21].

Table 6.3 presents the results that provide a comparison of the three configuration B, C and D that are modeled. Figure 6.9 shows the lateral PSF's for the configurations B, C and D, obtained for the wire phantom described above. The magnitude is in dB and is normalized to the peak value. The PSF was calculated at range of 100 mm for each system. An increase in overall signal level is consistent with the discussion (Section 3.2) on digital beam forming (Figure 6.9c). when compared to analog beamformers (Figure 6.9b and 6.9c)

Focal range [mm]	Signal level	Improvement in lateral resolution	
		System C	System D
30	-6 dB	37 %	34 %
	-10 dB	19 %	61 %
60	-6 dB	38 %	24.5 %
	-10 dB	34 %	40 %
90	-6 dB	38.06 %	27.7 %
	-10 dB	28.7 %	49 %
120	-6 dB	71 %	56.6 %
	-10 dB	56 %	56.6 %

Table -6.4 The percentage narrowing of the lateral resolution of system C and D referenced to system B[21].

## 6.5. HDL Design Performance

The success of an HDL design can be measured in various ways. Commonly, design performance is measured by maximum clock speeds achievable, while device utilization is a measure of how well the design fits in the selected FPGA

### 6.5.1. HDL Clock performance

The clock speeds are determined by the slowest measured logic path combination in any clock domain. Often times the design can be run faster than is indicated by these results without noticeable effects since limiting paths may be non-critical, or only occasionally used. However, these provide a baseline for performance. These results are also calculated at the maximum (worst case) operating conditions of the devices, usually at 85 degrees Celsius, with core voltage -5% (1.14V). Again this provides a worst case performance achievable that is usually bettered in practice. Finally, if further performance gains are required, these results are entirely dependent upon internal logic placement and routing, and higher effort levels (or tailoring of design constraints) in the place and route engine may yield additional performance

improvements. The timing results for the complete design calculates that the maximum clock speed for the processing clock which determines the maximum beamforming speed, is 187MHz. In the current system this clock is only being run at 100MHz.

### 6.5.2. Device resources utilization & clock performance Tradeoff

FPGA utilization is how effectively and efficiently utilizes the internal resources of the FPGA. Normal coding techniques and synthesis tools implement every logic to LUT based architecture. Which utilizes more area on the chip and some fast and dedicated area of the chip remain unutilized. Which in turn results in slow clock rates and bigger critical path lengths, hence the design remains inefficient in terms of both speed and area. In this paper we will present and discuss some techniques to effectively utilize the FPGA resources in order to speed up the clock rates and reduce the area utilization. Although Device utilization is very important factor in reducing power consumption as well as the cost, this is due Choosing smallest package that fulfill design requirements have direct influence on the power consumption and the cost of the design.

### 6.5.3. Digital Beamformer Utilization

The RTL synthesizer is the next step after coding stage. In the synthesizer stage first we check the design flow diagram as shown in figure 6.10.

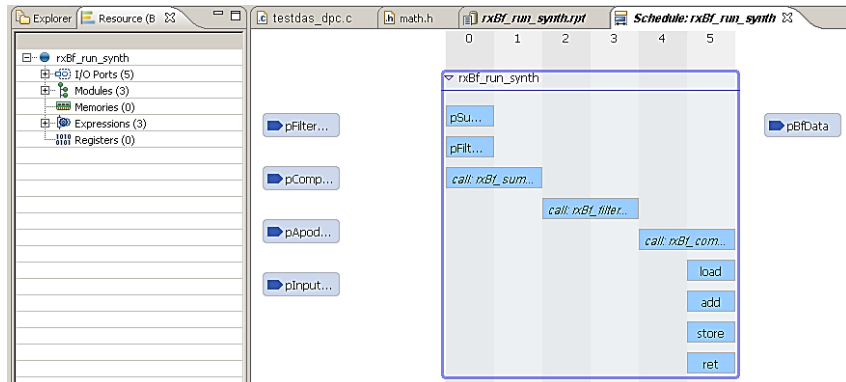


Figure 6.10- design viewer.

As shown in Figure 6.10 there is top level module which is rxbf\_run\_synth . This is the top level module of the DAS digital beamformer algorithm and composed of three modules the rxbf\_sum\_module , rxbf\_filter\_module and rxbf\_combined\_module.

#### 6.5.3.1. Default RTL Synthesizing

In this default synthesizer without any type of optimization we got a big latency of clock (Worst case 190,000 cycles). The result of the synthesized design shown in figure 6.11.

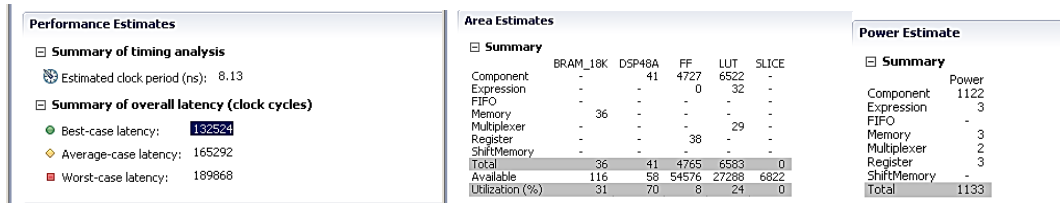


Figure 6.11- design viewer of the optimized synthesized.

Also we can figure out the device resource utilization is not encouragement for replacing this family with less FPGA , we can find DSP resources reached to 70% of the device without adding the remaining modules.

### 6.1.1.1. Performance Optimization

To utilize the device more in the area of the performance by making the best use of the parallelism of the FPGA. There are two important options in the VIVADO HLS to utilize the parallelism of the RTL synthesizer. These options are the pipelining and data flow behavior of the code flow. In figure 6-12 the designer view shows the top level module which is rxbf\_run\_synth embedded in the Dataflow option and the three modules the rxbf\_sum\_module , rxbf\_filter\_module and rxbf\_combined\_module are inside the top level function.

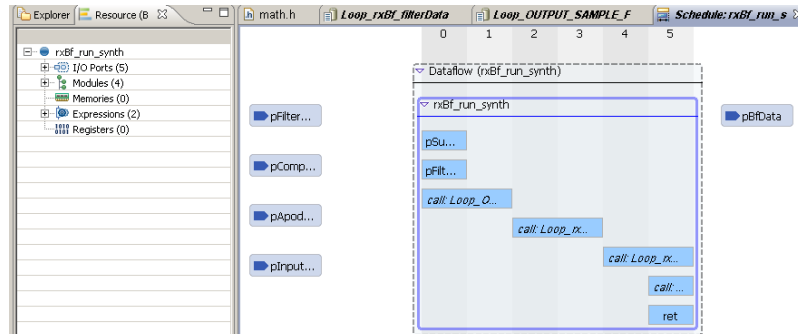


Figure 6.12 -design viewer after the performance optimization.

We can see the optimization results in figure 6.13 , in the performance estimate tape the clock latency reached to 44,000 cycles this leads to 5 times faster than the default synthesizing . Although we can find out increase in the resource usage: in the BRAM\_18K (62% instead of 32%), FF (11% instead of 8%) and the LUT (34% instead of 24%).

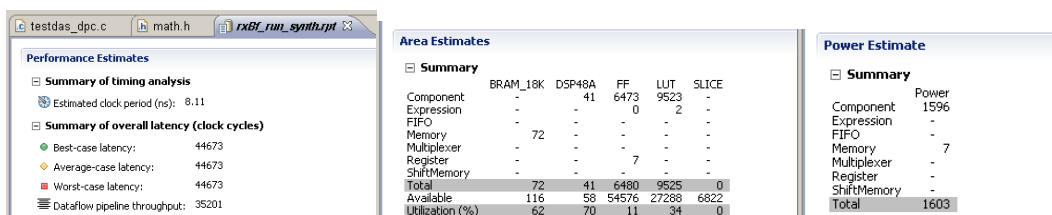


Figure 6.13- showing Project Performance Optimization.

### 6.5.4. FPGA VS DSP Performance

By measuring the DSP target performance (profiling result for performing digital beamformer operation with Kernel Complexity equal  $C64x+TM$  CPU cycles, based on CPU cycle accurate Simulator) we got result which is big than the proposed designed , the comparing is made in the table 6.5

Module	DSP	FPGA
rxBf_sumData	85,134	34,753
rxBf_filterData	9,682	8,821
rxBf_combineData	3,861	646
Total operation	100,000	44,225

Table 6.5 Shows performance comparison between FSP & FPGA

This comparing is done using the following parameters:

the number of scan lines	1
number of interpolation filter coefficients	8
number of interpolation filters	10
number of receive data channels	64
number of output samples per iteration of the beamformer	128

Module	DSP	FPGA
rxBf_sumData	85,134	10,625
rxBf_filterData	9,682	8,801
rxBf_combineData	3,861	721
Total operation	100,000	20,150

### 6.6.HDL Verification and Test Benches

Large and complex HDL code designs can be extremely difficult to debug. The approach taken with this project was to make extensive use of unit test modules to verify base functionality, along with full scale simulations to test the completed design. Register Transfer Level (RTL) code is simulated using an HDL synthesis package. For this project, the Xilinx ISE Simulator was used. A screen shot of the interface is shown in Figure 5.7. In this Figure,

modules are listed in the far left pane, selected signals to record are presented in the center, and their resulting simulated waveforms are on the right we have two simulation here Figure 5.7 show Edge and phase detect diagram for RxClk (CLK0) before RxClkNot (CLK180) for beamformer receiver and Figure 5.8 show Edge and phase detect diagram for RxClkNot (CLK180) before RxClk (CLK0) for beamformer receiver.

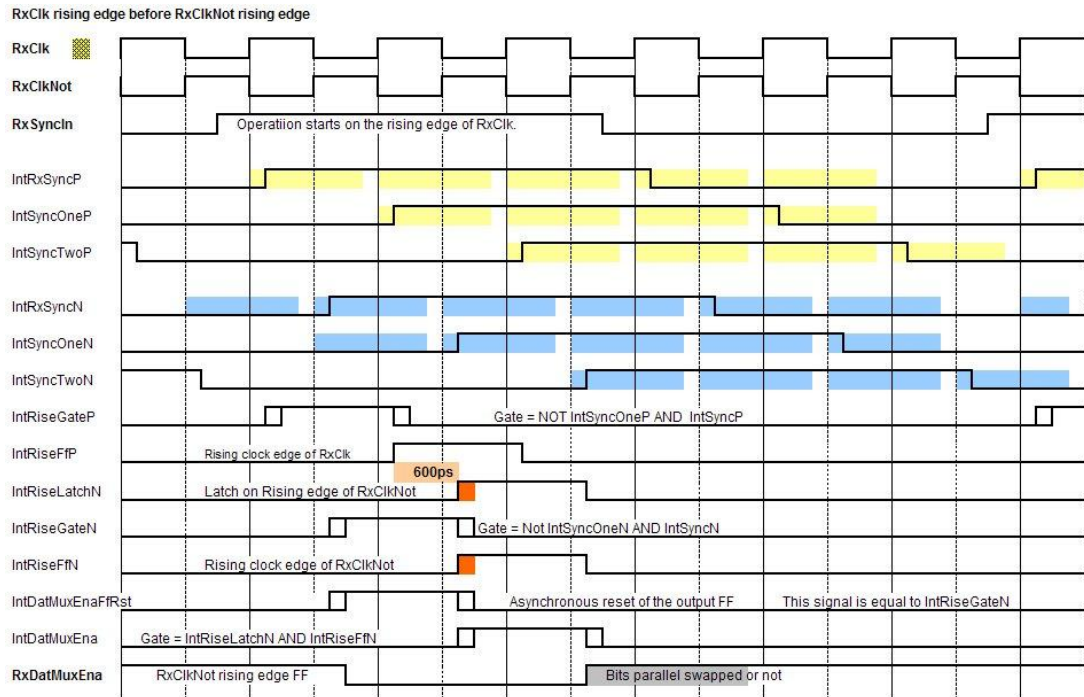


Figure 6.14- Test bench for Edge and phase detect diagram for RxClk (CLK0) before RxClkNot for beamformer receiver.

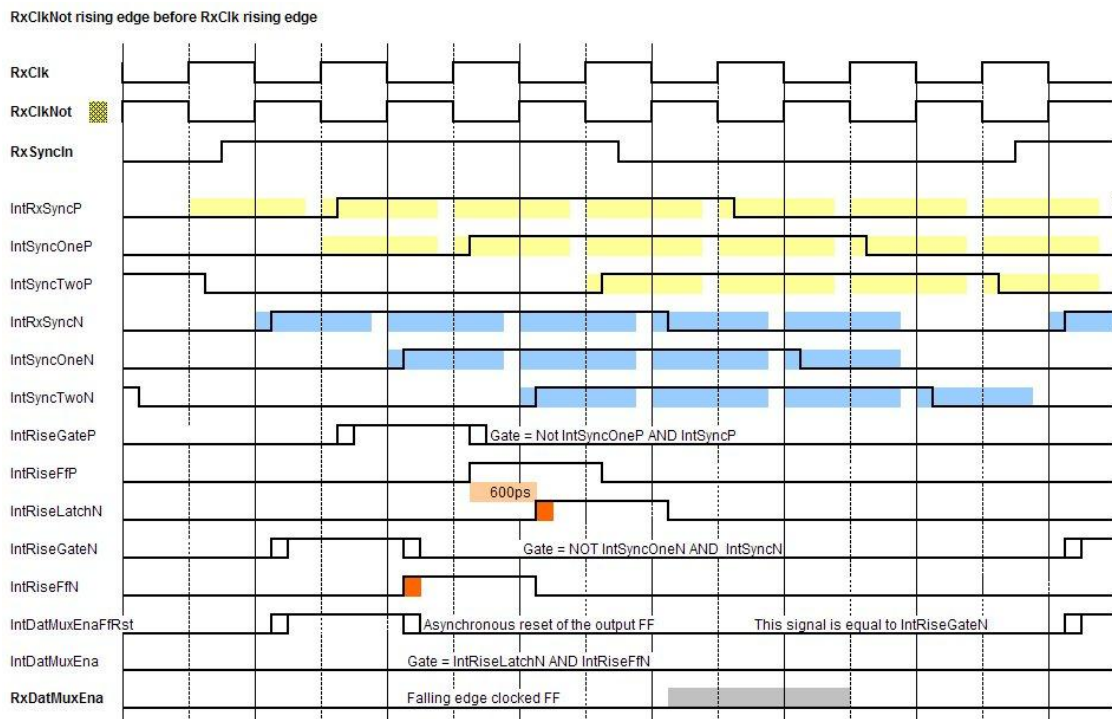


Figure 6.15 Test bench for Edge and phase detect diagram for RxClkNot (CLK180) before RxClk (CLK0) for beamformer receiver.

## 6.7. Software Simulation and Result Verification

In this section we are showing how we are simulating the digital beamformer receiver operation and how can we verifying our result.

### 6.7.1. Testing Environment

In this verification section we are using Code composer studio to prove our digital beamformer algorithm , code composer studio is integrated tool based on eclipse IDE.TI integrate all their controllers (MSP430 , DSP ,...) in this tool here we are using C64x as reference for our implementation. We can have a look in the code composer studio shown in figure 6.16

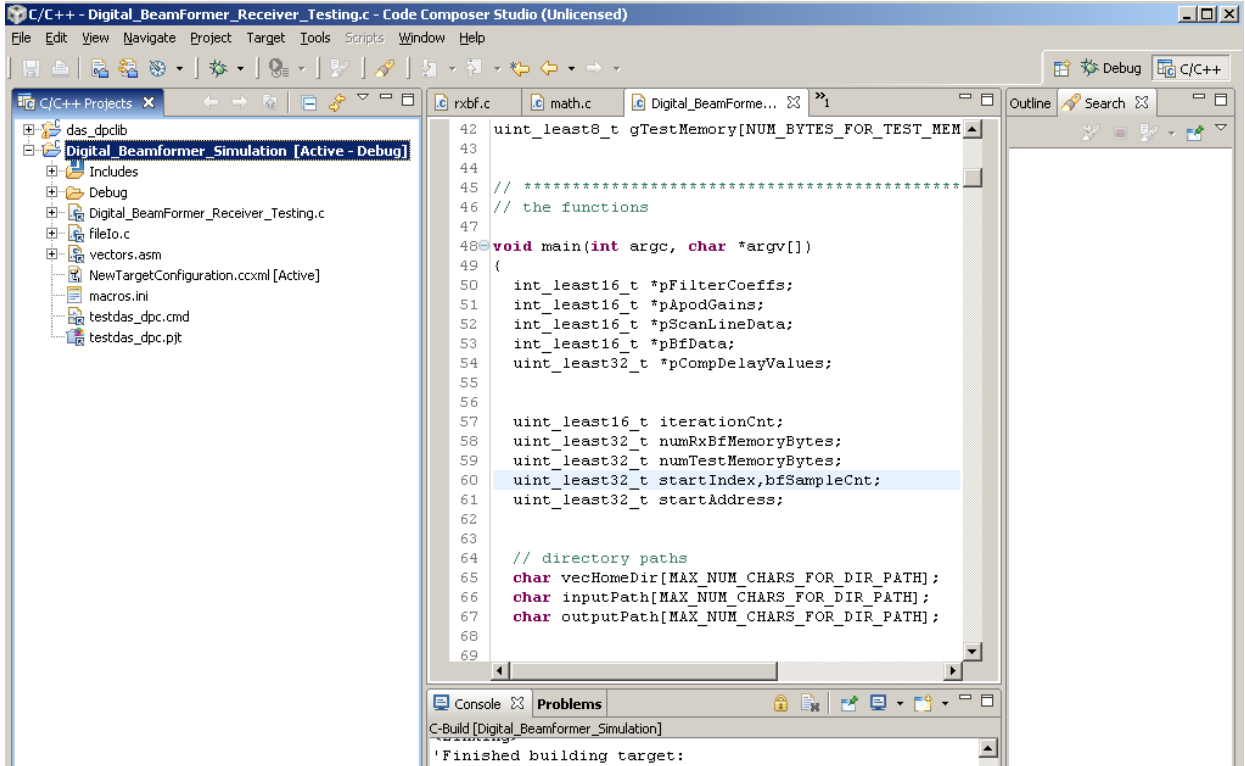


Figure 6.16- Code composer studio view.

### 6.7.2. Testing Vectors and reference

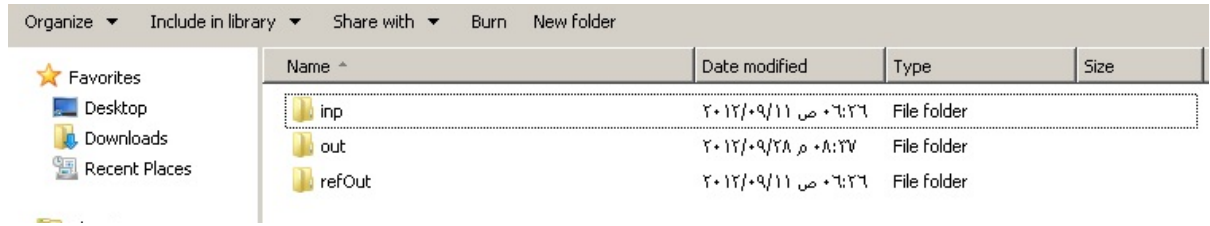


Figure 6.17- TI Testing & validation folder

Figure 6.17 shows many test cases reference result as shown in the left side and the right side our result which is empty before running the beamforming simulation and verification.

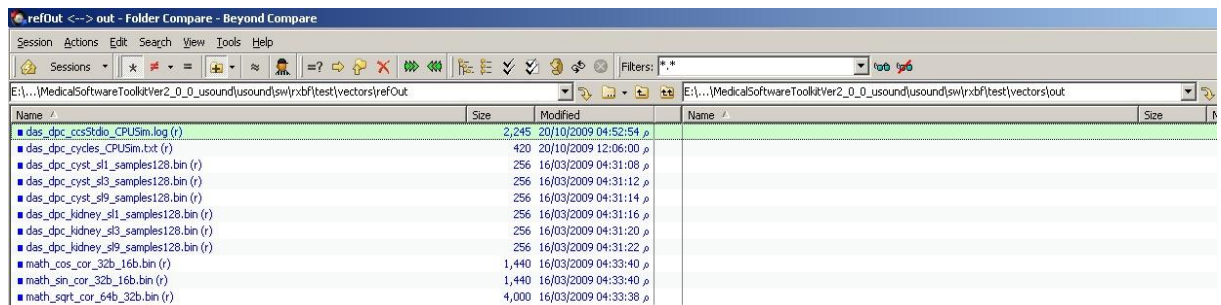


Figure 6.18-many test cases references for beamformer validation method

Figure 6.19- shows the content of the input folder with highlighting one test case vectors which include Scan line vector, apodization gain parameter vector, compressed delay vector, the filter parameters data vector and the generic parameters for this test case.

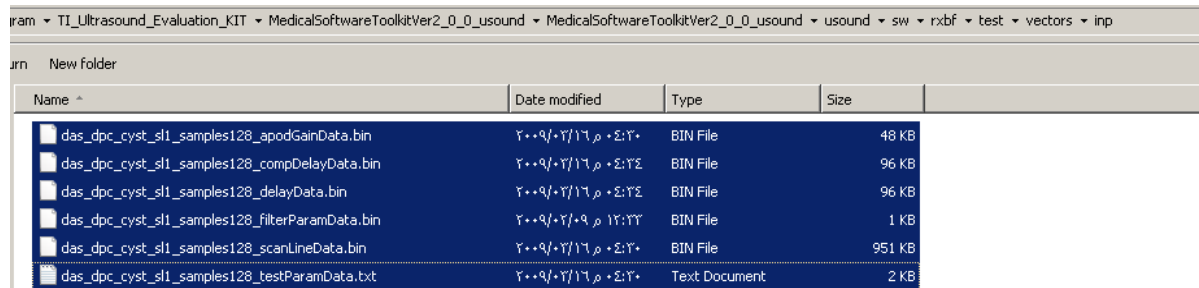


Figure 6.19-Content of the input folder.

### 6.7.3. VIVADO HLS Simulation and verification

For simulate the digital beamformer receiver we are simulating the hardware environment by feeding the parameters vectors into code composer studio then running it and out here in the next figure we will show the welcome message in the debugging.

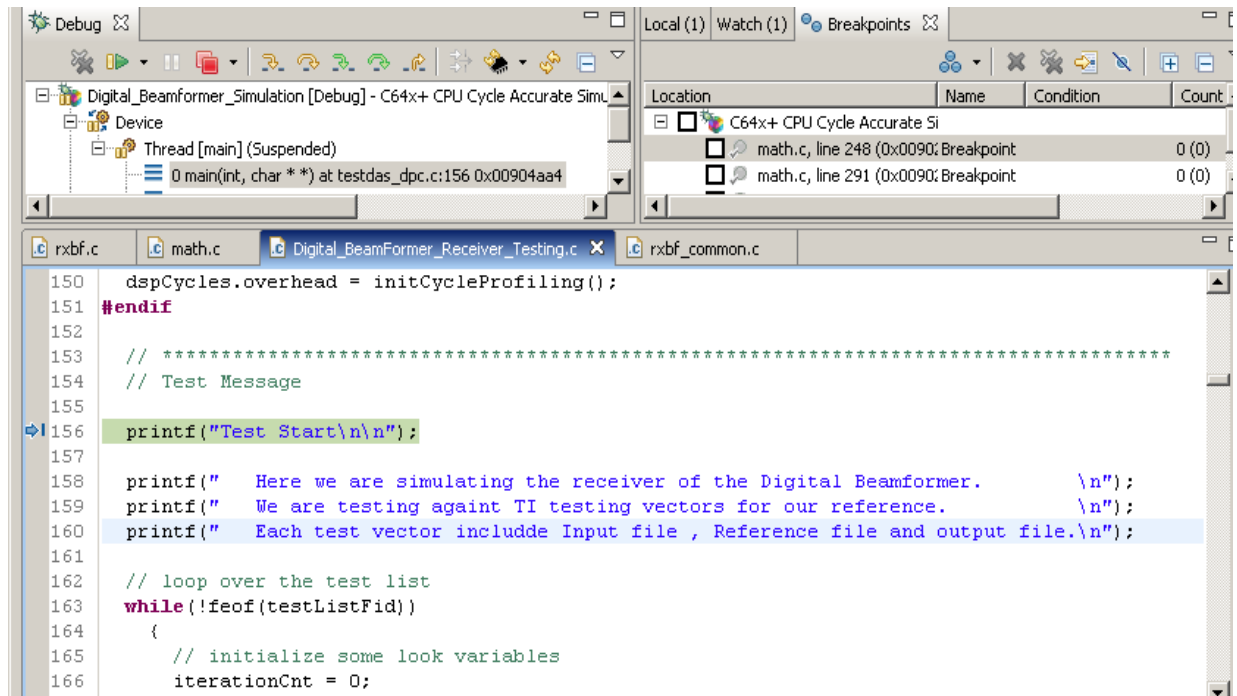


Figure 6.20-Testing welcome message.

In the debugging we are going into multiple of stages first of all beamformer parameters initializing is the first step in the beamformer as shown in figure 6.21 the initialization parameters is loading these configuration parameters which described in table 6-1 and this is one vector of the input files.

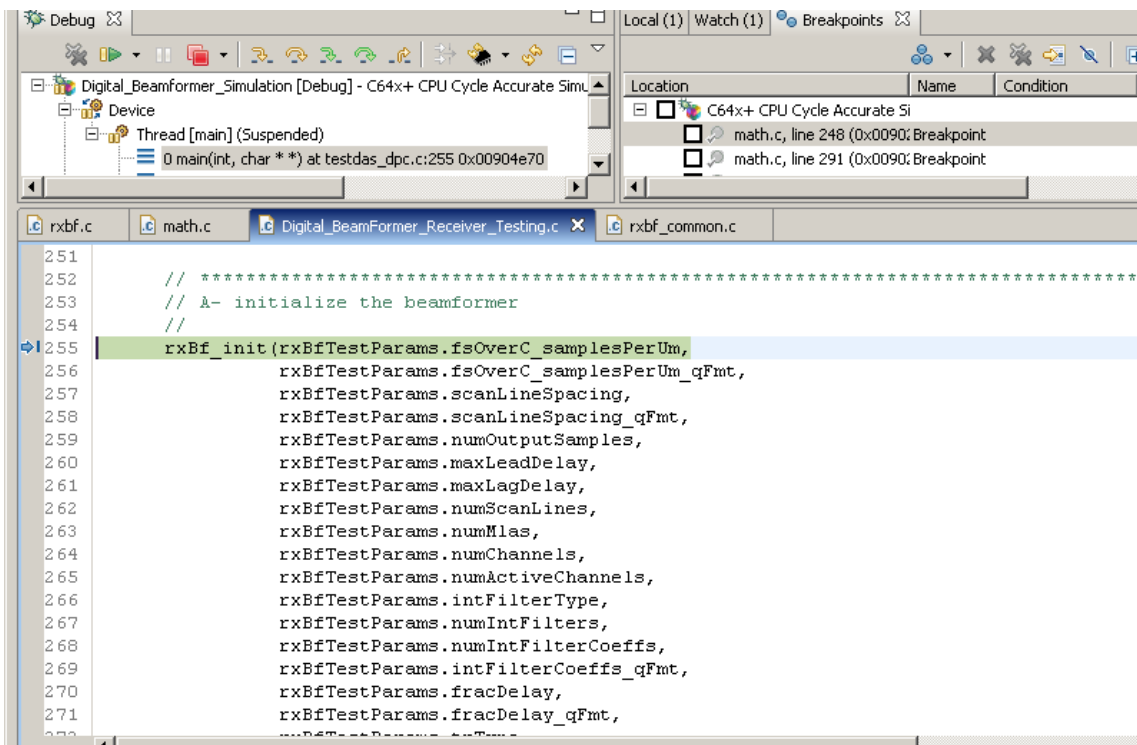


Figure 6.21-Initializing the beamforming stage.

The next step is the digital beamformer setting up in this stage we are start up the digital beamformer with the parameters being loading from the last step as shown in figure 6.22.

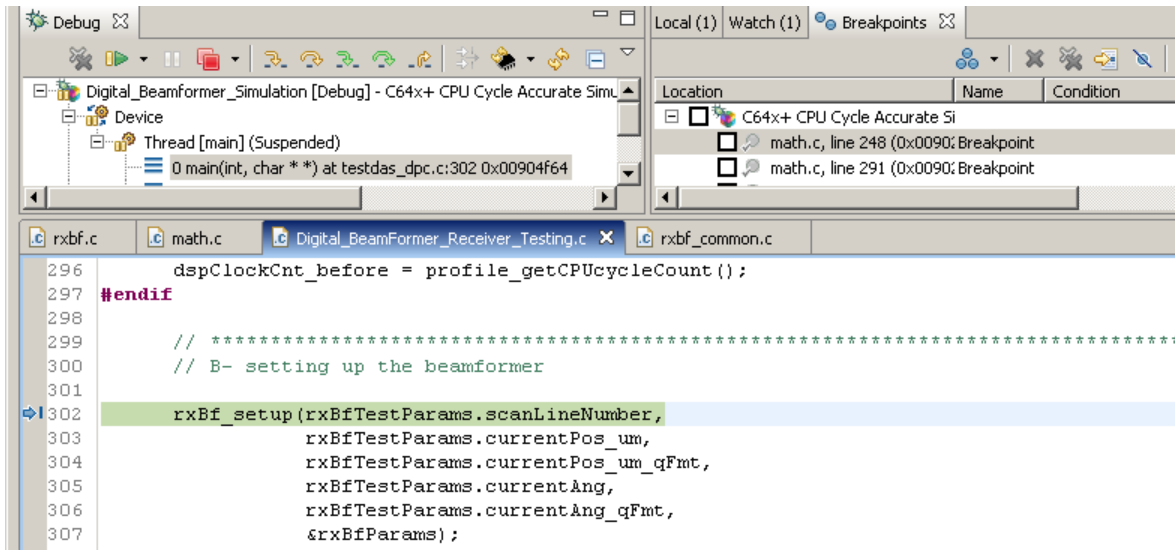


Figure 6.22-Configuring the beamformer with the general parameters.

The next stage is to allocate memory for this testing by calculating the space for filter coefficient vector, the apodization gain vector, compressing delays vector and scan line vector as shown in Figure 6.23.

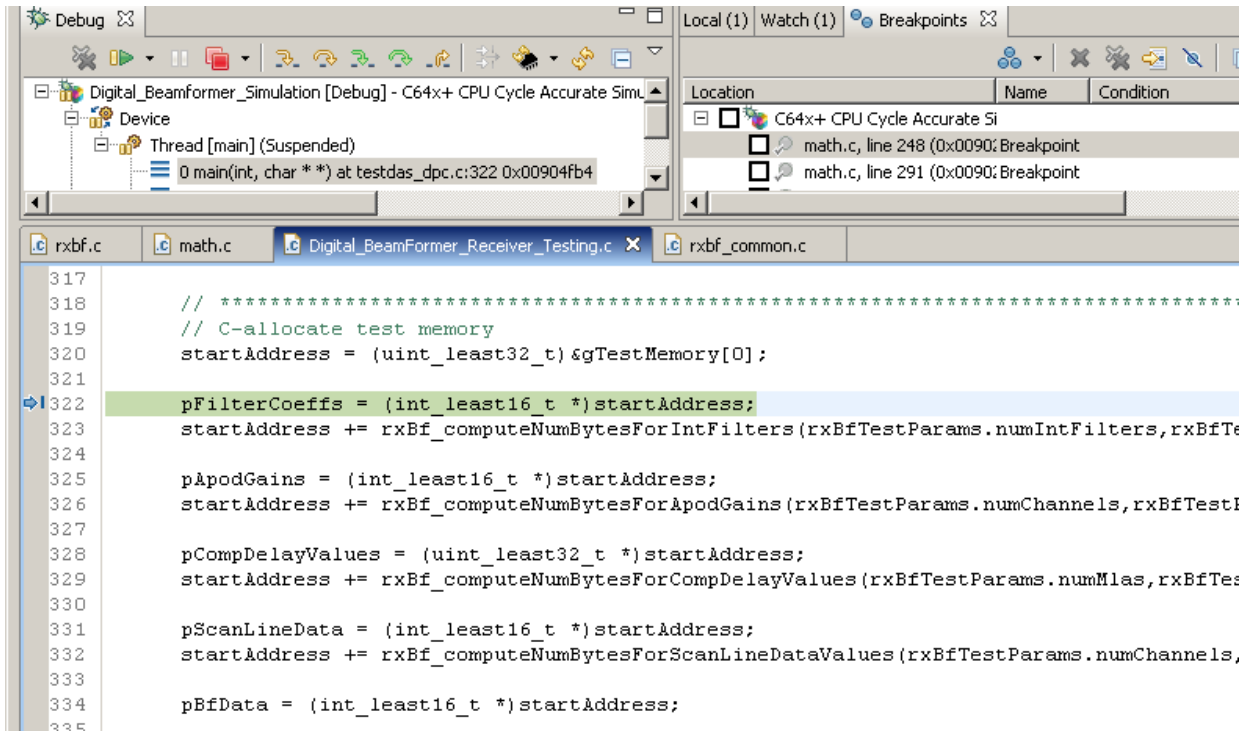


Figure 6.23-Allocating memory for different component of the beamforming.

The fourth stage is to setting up the filter coefficient vector with the input file as shown in Figure 6.24.

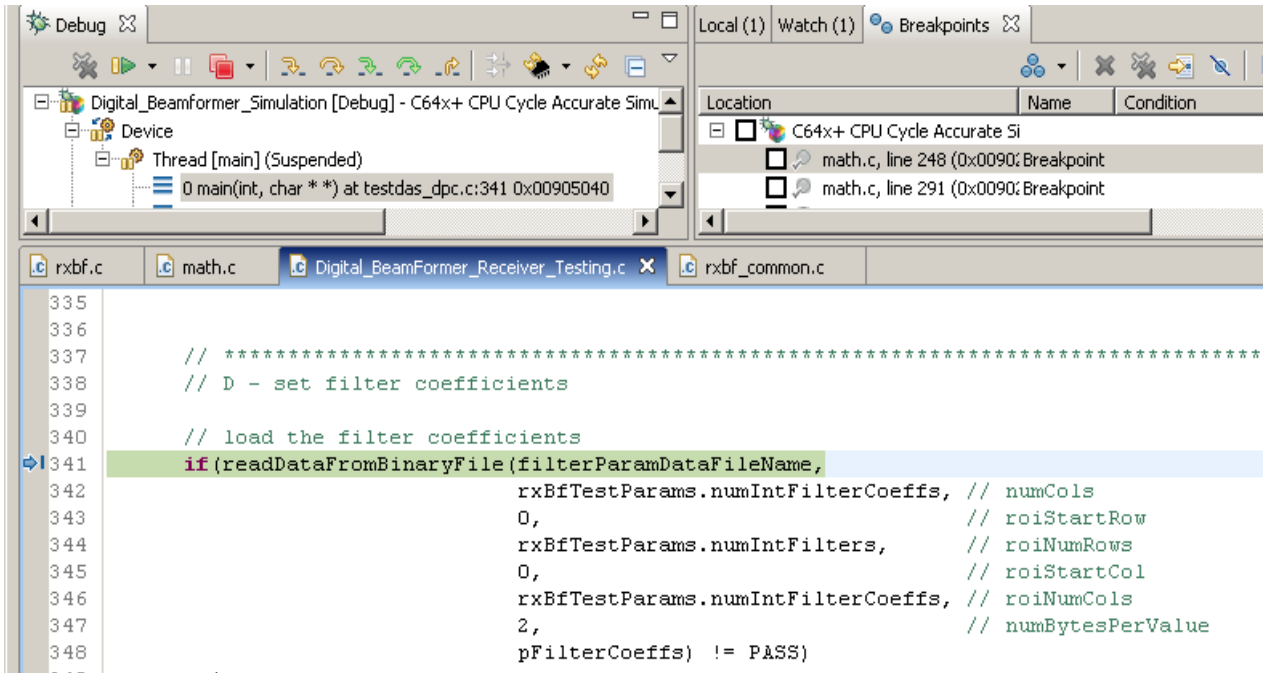


Figure 6.24-Loading interpolation filter coefficient.

All the previous configurations made for all the next scanning line but for each line we should configure it with different apodization and delaying values. Here down we start each scan line processing by applying apodization gain first. Figure 6.25 showing the while loop for the beamforming processing for each scanning line.

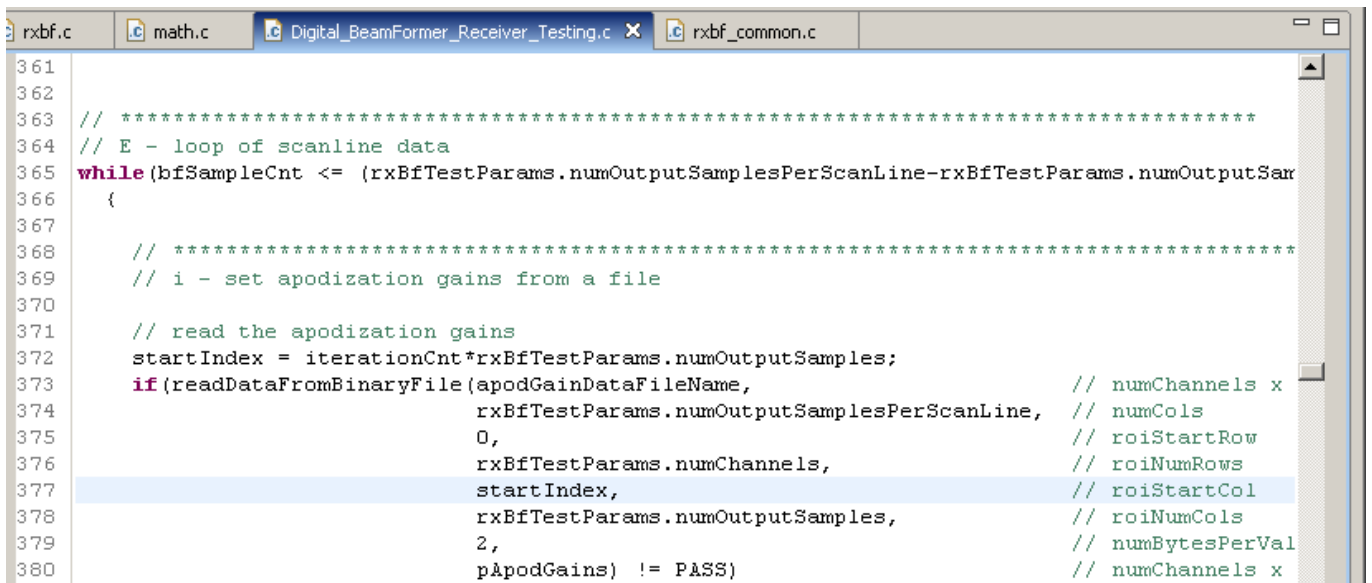


Figure 6.25-Configuring the apodization gain for each of scanning line.

The second stage for processing the scanning line is setting the compressed delay vector from the input folder this stage is shown in Figure 6.26.

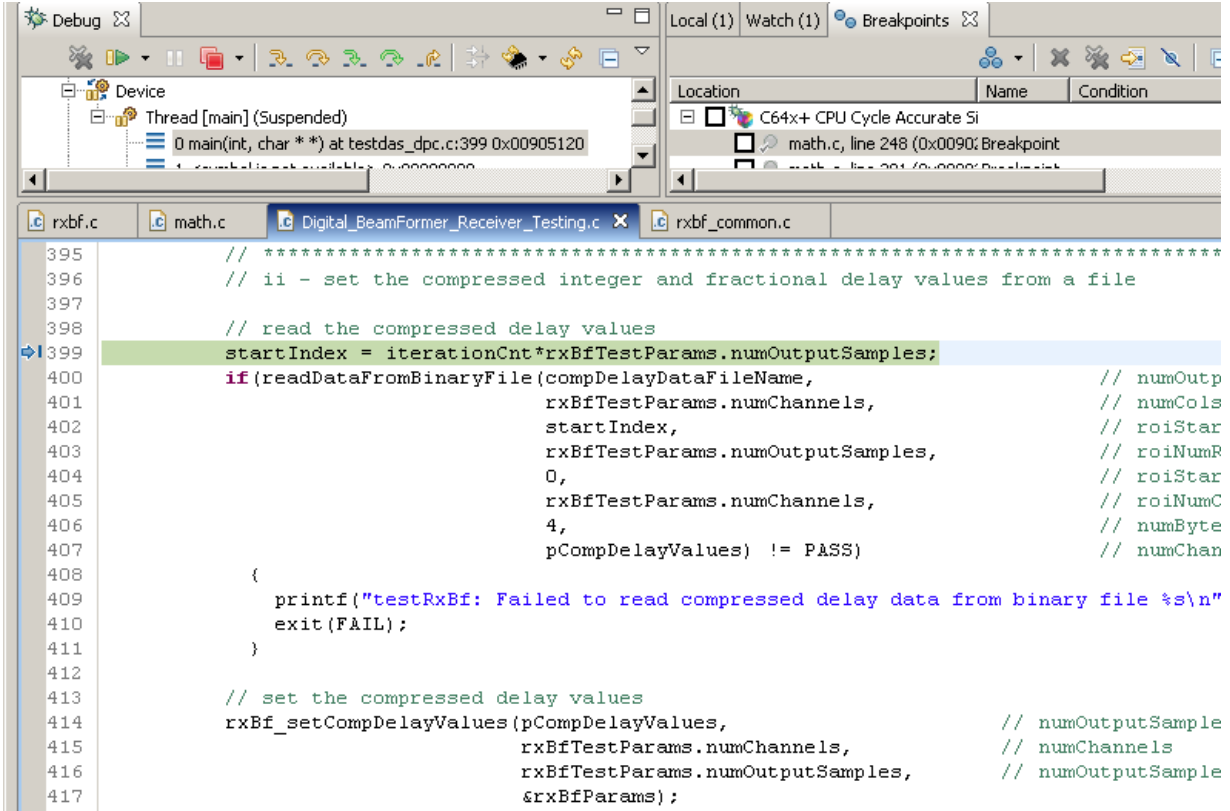


Figure 6.26-Configuring the delay values for each scan line.

The third stage for the scan line beamformer processing is the getting the input vector from the input folder as shown in Figure 6.27

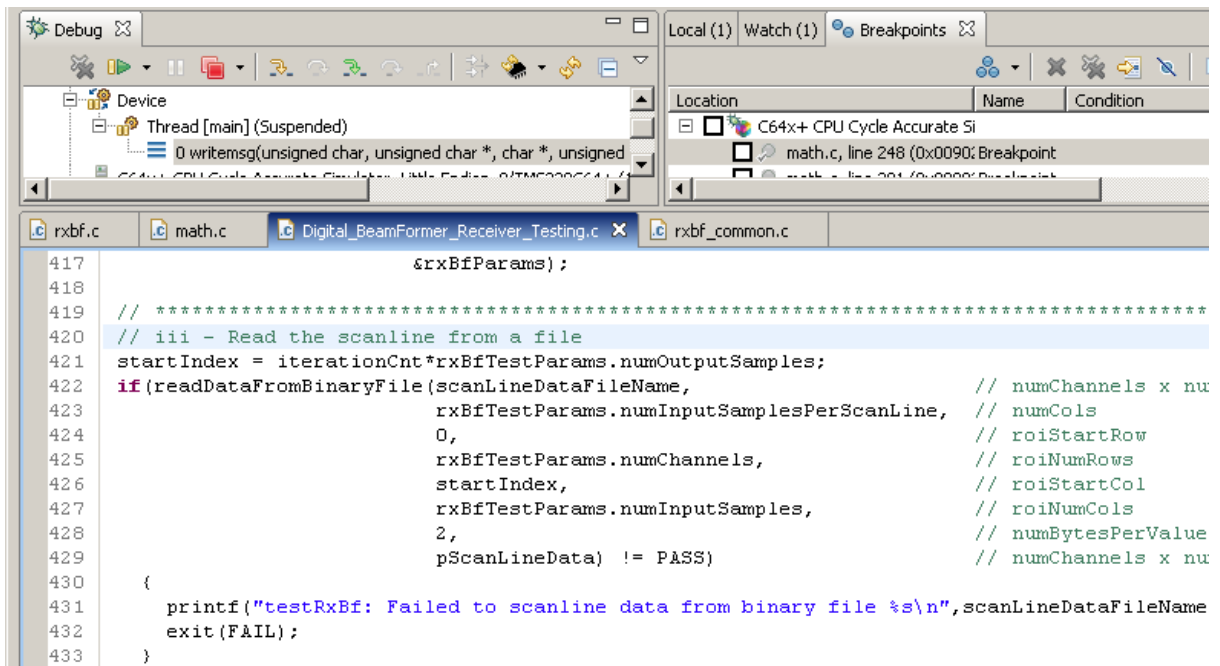


Figure 6.27-Reading the raw scan line vector from TI input folder.

Finally the last stage in the processing is running the beamforming after the proper configuration for the entire beamforming component as shown in figure 6.28.

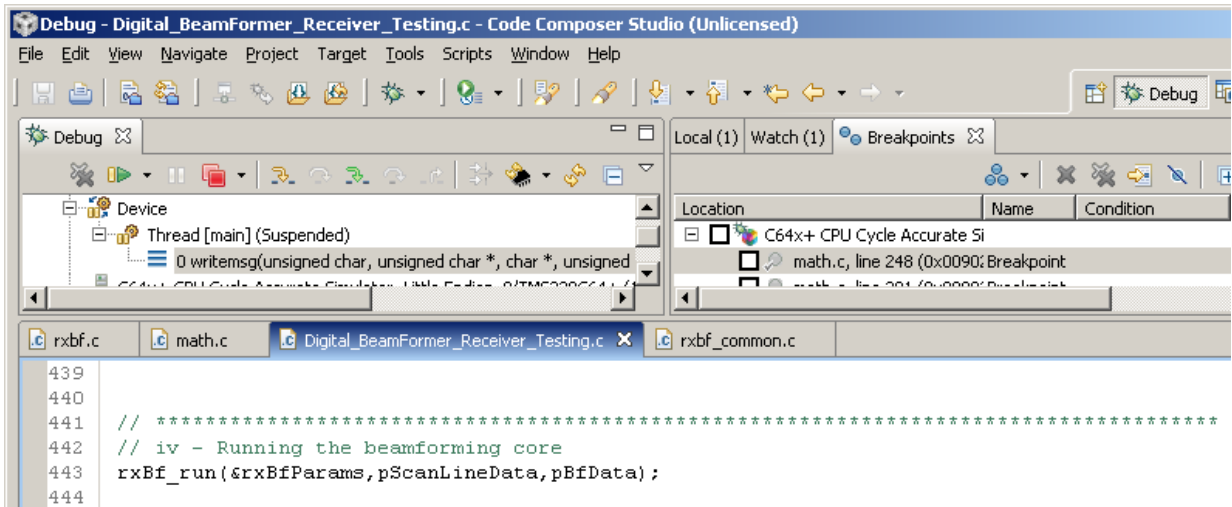


Figure 6.28- Running the beamformer operation on the selected scanning line.

After finishing the operation for the scanning line we stored the output of the result in the output folder for comparing as shown in Figure 6.29.

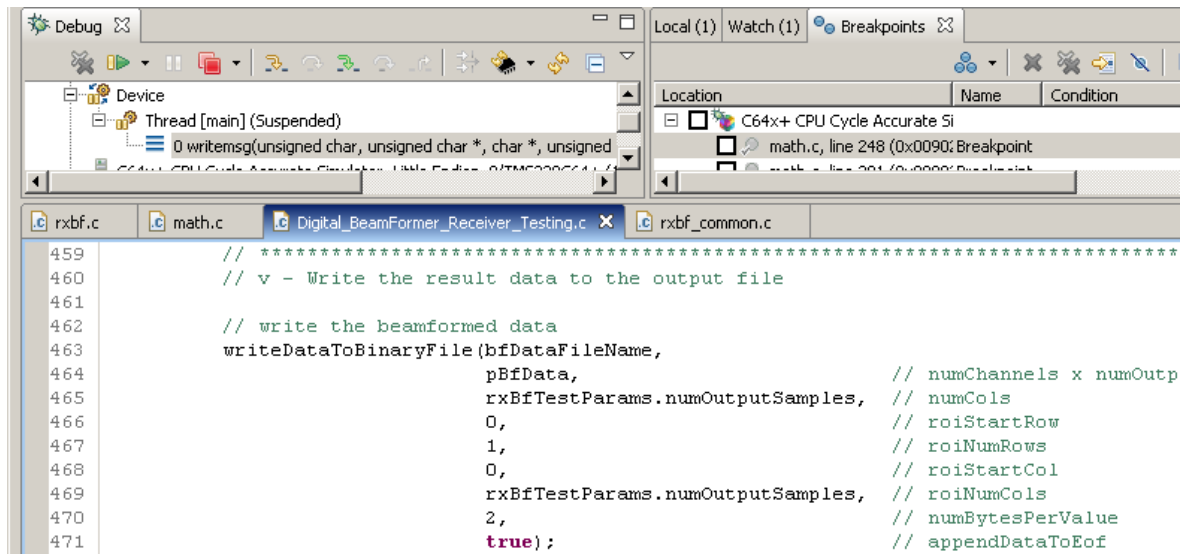


Figure 6.29- Writing the result output vector into file for comparing.

While the beamforming operation we are logging these events in the console output view we can see the logging events in figure 6.30.



## **6.8. Implementation Summary**

In this chapter we describe the digital beamformer Firmware implementation using a well-defined US development KIT from TI; it includes a reach library of test vector from which we could verify our development against its reference vectors. Moreover our design of the digital beamformer framework referenced from the TI US development kit developed and testing using VIVADO HLS IDE. We succeeded in utilizing the VIVADO HLS in developing our receiver digital beamformer to produce it in a ready-made IP core working in EDK. We succeeded in the optimization phase of the IP core. We decreased the complete design of the beamformer from latency of 400,000 cycle (11 nsec) to 41,000cycles (nine nsec) against 100,000 cycles (one nsec) of the TI C64X DSP for 64 channel operation. This means we could achieve (1/3) of the DSP processing for the 64 channel processing (almost the same processing time for our target at 16 channel beamforming processing). Moreover in the testing result the efficacy of the proposed Delay-Sum-Add architecture is compared with the common analog beamformer architecture. The images generated using the analog beamforming (Aloka, SSD-246) show poor lateral resolution because of the transducer array design of the ultrasound machine used. The DAS method does improve the image quality and lateral resolution. Properly delaying the samples and summing them, produces a coherent, strong signal with a narrow beam width and lower side lobes.

## Chapter 7

### DBF Discussion and DAS Limitations

#### 7.1. Discussion

Images have significant improvement in lateral resolution after apodization when compared with images produced with no apodization. The processed images show better resolution and lower side lobe level compared to unprocessed raw data. These figures show gray scale images of a typical wire object created using configuration A. The unprocessed image (without apodization) has wide lateral resolution due to the spreading of the beam. The other processed images which produced after processing exhibit progressively narrower lateral resolution, even though the differences between the rectangular apodization and hanning apodization cannot be distinguished easily from these figures. Apodization weights the elements to produce apertures, these apertures restrict the spread of the beam, thus produce narrower beams when compared to cases without apodization. The weighting also reduces the side lobe level resulting in an increase in dynamic range, where dynamic range is the ratio of maximum axial response to the maximum off-axis response. By comparing the previous results we found that images with no processing done on the RF data has wide beam at the focus and also higher sidelobe levels, on the other hand on the processed images the beam is narrower and also produces lower side lobes (hanning apodization produces lower side lobes and narrower beams when compared to a uniform rectangular apodization). The improvements in the sidelobe level results from the product of the apodized transmit beam pattern and receive beam pattern. It can be observed from Table-6.1 that the side lobe levels are around -10 dB when there is no processing and around -11 dB and -15 dB with uniform apodization and hanning apodization respectively. Also the side lobe levels after processing are progressively lower levels as the focal range increases. The reduction in side lobe level amplitude for hanning windows increases larger ranges, when compared with rectangular apodization. This can be attributed to the non-uniform nature of weighting. The results obtained are expected as discussed on in Section 4.2, except at 103 mm for rectangular window, which shows a higher level than the non-processed case. This may be due to errors (inaccurate measurements) in the simulations conducted. Figure 6.5 shows the improvement in beam width as a function of focal range with apodization. Although lateral resolution should be independent of depth, the resolution of the wire at 107 mm with rectangular apodization is worse than the two wires at shallower depths. In case of hanning apodization it

can be noticed that, the resolution remains almost constant with increasing depth. In case of resolution without apodization, there is a marked increase in the beam width as we move from the array. This is due to the broadening of the beam in the far zone, while in processed cases weighting controls the beam width. Figure 6.6 shows the lateral beam width versus depth. There is a gradual deterioration in the lateral resolution as the object is placed at increasing distances away from the fixed focus. This is expected, but as can be observed from the plots, the deterioration in the lateral resolution is far less when apodization is used and hence increase focusing. These beam widths are compared to the beam widths at the focus for both processed and unprocessed cases, which are found to be 3.1, 3.3, 3.7 millimeters without apodization, with rectangular apodization and with hanning apodization respectively. A hanning window has a gradually decreasing slope compared to the rectangular weighting. From Figure 2.4 (Section 2), it can be noted that the hanning window approaches zero in smoother fashion and hence contributes to better beam width control. Figure 6.7 is the surface plot comparison for a typical simulated analog beamformer with single fixed focus and multiple transmit focus and a digital beamformer with dynamic apodization and receive. The analog beamformer with single transmit focus (configuration B) show higher beam spread and side lobes around the deeper wire objects. The analog beam former is focused at one point on transmit and hence there is a gradual convergence of the beam around that focal point only, resulting good resolution at the focal point. Using a multiple transmit foci and receive method (configuration C) improves the axial and lateral resolution (Figure 6.8c). The beam widths are narrower when compared to configurations B and D due to the use of a larger aperture. However this causes an increase in number of side lobes. Figure 6.8 shows the remarkable improvement achievable by employing a digital beamformer. The side lobes are practically non-existent, which is due to the continuing focus maintained on receive. The beams show better focusing because of dynamic apodization, where the ratio of the aperture to the desired focal depth are greater than the ratio of array length to its focal length. Figure 6.8 plots the beam width versus the focal range at two signal levels. The advantages of using a digital beamformer are obvious. The lateral resolution deterioration at lower signal levels is higher in configurations B and C than in D. The beam widths are double when compared at the -6 dB level. The depth of field is significantly reduced when a single transmit focus is used. There is an increase in beam width see from Figures 6.8a to 6.8c of approximately 100% at -6 dB. Configuration C and D show narrowing of the beam at -10 dB for deeper distances. This is due to the use of multiple transmit and receive. At the -6 dB signal level, the beam width for configuration B increases dramatically beyond the fixed transmit focus while in configuration

C and D, they are nearly constant for the entire focal range except at later depths. The diffraction limited resolution at all ranges is because of the transmitting and receiving aperture are nearly in focus- However configuration D requires a complex scan converter and a large dynamic range for the ADC's. The beam width for configuration C is lower than for configuration D for all ranges, is due to the use of a larger receive aperture. Figure 6.9 shows the frequency spectrum for each system. Configuration D has lower side lobe levels around -25 dB. This is due to the dynamic apodization. Configuration C shows higher side lobe levels around -20 dB, which is due to the larger aperture being employed. Configuration B shows higher side lobe levels due to the lack of any control on transmit for deeper distances. Table 6.3 shows that there is an improvement in lateral resolution of about 50 % for configuration D when compared with B for all ranges. There is nearly a 30 % increase in lateral resolution for configuration C when compared with B but it is better at higher signal levels

## **7.2. DAS Algorithm Limitation**

There are certain limitations associated with the Delay-Sum-Add architecture. These limitations are:

- 1) target ambiguity caused by phase quantization errors**
- 2) limitations in delay line systems**
- 3) increased hardware complexity**
- 4) low frame rate**

The time delays for transmit and receive are usually discrete. This leads to quantization approximation to the ideal focusing and steering delay curves. This in turn can lead to a phase grating effect that produces grating lobes within the image field of view. These are independent of the amplitude grating lobes produced due to the inter-element spacing. Several approaches have been considered to minimize the grating lobes, one of the solutions being decreasing the time delay increments. Even though the digital delay systems have become practical and offer many advantages over analog delay lines, there are shortcomings primarily associated with sampling rate and noise in the digital circuitry. Since the sample rate is generally four to ten times to that established by the Nyquist criterion, the minimum delay increment is larger thus causing phase quantization error and also necessitates the use of A/D converters with large dynamic range, increasing the cost of the beamformer. This limitation can be avoided with use of interpolation beamforming as discussed above. The system complexity is directly related to the number of elements or channels in an array that is used for

transmit and receive. In DSA architecture since all the elements are used for transmit and receive, it increases the hardware needed for each channel i.e. each element would need a delay line, ADC, amplifier etc. All this increases the cost of the system. Reducing the number of active elements by employing synthetic aperture methods can reduce the system complexity and cost which is discussed next. The use of a large number of elements increases the number of beam lines which means better resolution but a slower frame rate. Thus DSA architecture is not suited for high speed imaging like 3-D ultrasound imaging.

### 7.2.1. Synthetic Aperture Imaging Architecture

The architecture for digital beamforming with synthetic apertures is described in section as well as the proposed designed for such system. The synthetic approaches can be separated into two classes:

- A. Synthetic receive apertures
- B. synthetic transmit or transmit / receive aperture

With synthetic aperture processing, the goal here is to achieve a level of performance without actually employing all the transmitting and the receiving channels. The approach used involves transmitting with two or more transmit sub apertures and receiving with two or more sub-arrays. Though this approach has received much attention in the literature, few if any results of practical applications have been reported. The approach used here uses partial beam sums that are obtained from signal subsets of overlapping receive sub apertures on consecutive firings. This architecture is called multi-element synthetic aperture focusing method (MSAF) [80]. The MSAF system is shown in Figure 7.1 with a five element active transmit ( $K_t = 5$ ) and five element active ( $K_r = 5$ ) subapertures.

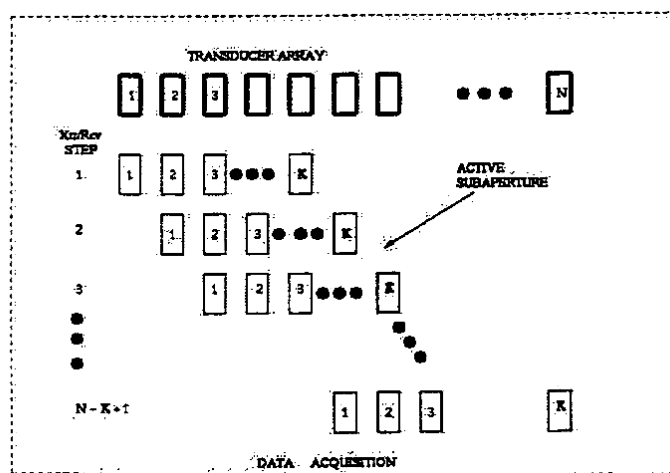


Figure 7.1 -MSAF system with a five element active transmit ( $K_t = 5$ ) and five element active ( $K_r = 5$ ) subapertures [80]

## **Chapter 8**

### **Conclusion and Future Work**

#### **8.1. Review of Work Completed**

This thesis has presented the work done designing, building, and testing a versatile ultrasound beamformer system. We Proposed a design based on the DAS digital beamforming implementation, it is consists of a 16 channel signal processing board. The modular nature of the design allows the hardware to expand to the size needed by any front-end transducer, from the largest 2D arrays, to the smallest annular devices. Even with this expansion, the on-board power distribution, and self-contained processing hardware ensures that every channel will be as robust as every other. The allocation of an expandable on board RAM further extends the usefulness of the hardware for research. For all of these advantages, the hardware is small, efficiently designed, and leverages the best of consumer electronics in order to minimize the actual system cost. The total expected cost per channel is between \$25 and \$40 The HDL firmware that has been created for the signal processing card is extremely optimized using VIVADO HLS at processing ultrasound data. Limited RAM resources are over comed using DDRAM. High-speed 387MHz DDR inputs are reliably deserialized using a dynamic phase alignment on the. Both the programming framework used, and the availability of CPU resources allow the software to be extended to perform additional real-time signal processing Taken as a whole, the beamformer system is fast, robust, versatile, cost-effective, and easy to use. All tests performed on individual component of it, have shown that desired performance has been met or exceeded. In usage, the design has consistently exceeded design requirements, all while costing a fraction of commercial options. All tests indicate the current system is ready to be used in real-time 2D imaging, with up to 64 Active elements per scanning. This design will provide an ideal platform for development, into the foreseeable future.

#### **8.2. Future development ideas**

The future development plane can be divided depend on the execution time, we can be divided our plan into two terms: Long term Future Work and Short term Future Work. Both will be discussed in details in the following sections.

### **8.2.1. Short-Term Future development**

The short term development plan is based on enhancing & optimizing the current and it is divided into four areas where we believe opportunities exist to further improve the system. First thing we need to complete the digital Beamformer configurability using the standardized backplane idea, actually we did the PCI interface in the signal processing board but we need to design the backplane board itself we need to continue work in the completing designing the PCI commands, defining the rules and the actions of the backplane system i.e. our card is one unit and we can add more cards to make 32, 48 ... digital Beamformer with big number of active transducers. The second this we need is to develop GUI software on the desktop PC to manage the user parameters also it can be used for adding/removing certain digital Beamformer cards to extend/shrink the system channels ,This software is controlling our boards using the Ethernet or the PCI interface. The third thing is the Ethernet design is the network port for accessing multiple Beamformer from remotely device, already we did the interface implementation but we did not finish the application itself. This integration would be the final step in producing a completely self-contained reconfigurable ultrasound beamformer system. The existing buses would work just as well for the transmit electronics, and the Ethernet Port card would serve as a break in the high-speed backplane ports, between a downstream receive bus, and an upstream transmit bus, without any changes in the backplane itself. Finally the Image compression need to be implementing to increase the processing speed as it would allow for completely arbitrary image formation. Additionally, selecting an efficient algorithm that relies on more computational logic and less storage would balance the hardware resource usage better; this could possibly lead to an increase in processing speed and allow the use of a smaller FPGA device to further save on cost

### **8.2.2. Long-Term Future development**

The Long term plane is the development of the 3D digital beamforming .Due to high processing operation required for this type of development an alternate implementation of the digital beamforming (SAR) will be utilized for the next future plane.

#### **8.2.2.1. Proposed design of the SAR**

Svetoslav Ivanov Nikolov describes a design and implementation of a real-time delay-and-sum synthetic aperture beamformer [81]. The beamforming delays and apodization coefficients are described parametrically. The image is viewed as a set of independent lines

that are defined in 3-D by their origin, direction, and inter-sample distance. The delay calculation is recursive and inspired by the coordinate rotation digital computer (CORDIC) algorithm. Only 3 parameters per channel and line are needed for their generation. The calculation of apodization coefficients is based on a piece-wise linear approximation [82]. The implementation of the beamformer is optimized with respect to the architecture of a novel synthetic aperture real-time ultrasound scanner (SARUS), in which 4 channels are processed by the same set of field-programmable gate arrays (FPGA) as shown in Figure 8.1.

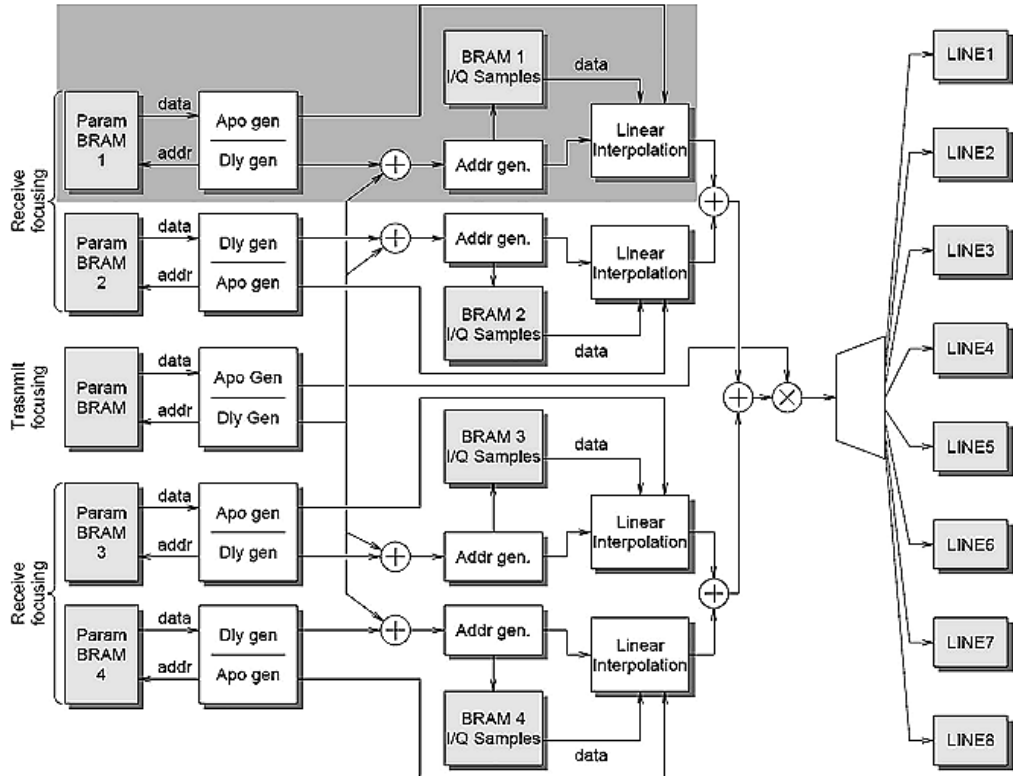


**Figure [8.1] - Overview of the beamformer is architecture. The beamformer is divided into blocks. Each block creates a part of a high-resolution SA image using data from 4 receive channels. Data are sent further in the system after all transmissions have been carried out [83].**

This design is modular, and a single beamformation unit can produce 4600 low-resolution images per second, each consisting of 32 lines and 1024 complex samples per line. In its present incarnation, 3 such modules fit in a single device. The summation of low-resolution images is performed internally in the FPGA to reduce the required bandwidth. The delays are calculated with a precision of 1/16th of a sample, and the apodization coefficients with 7-bit precision. The accumulation of low-resolution images is per-formed with 24-bit precision. The level of the side- and grating lobes, introduced by the use of integer numbers in the calculations and truncation of intermediate results, is below 86 dB from the peak. We are considering this system performance as an ideal solution for the 3D application, Thus we

consider this design is the next challenge for us in the future work to implement using our existing platform.

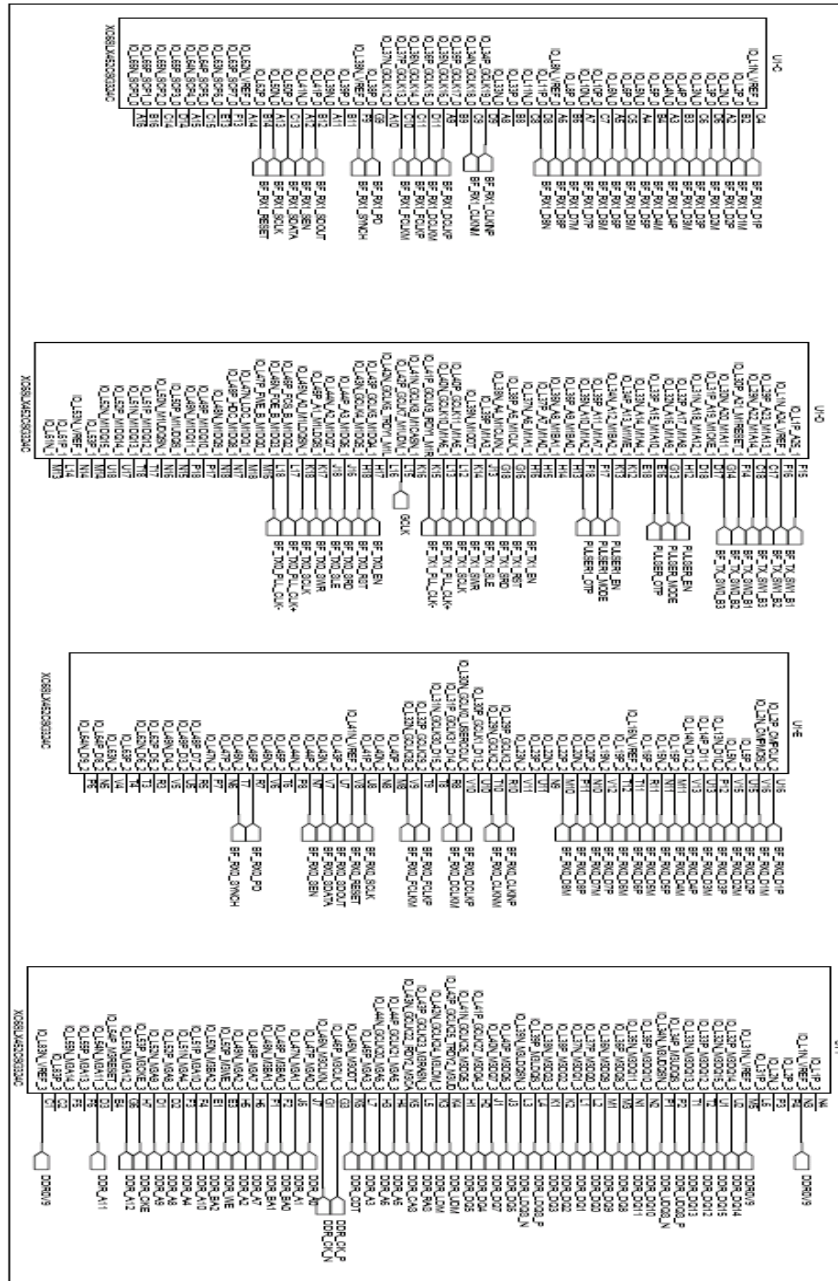
### **8.3. Conclusion**

This thesis has looked into a proposed low cost implementation of the digital beamformer based on the FPGA. We described a novel extendable Beamforming architecture design in the both of the system-level Hardware and Firmware design level. In the Hardware design, we were targeting the compactable application as well as the extendable applications where the power, level of integration and the feasible of the replication are critical. The three main components that have the greatest influence on the hardware design and system performance of the signal-processing board are the Analog to Digital Converters (ADCs), the Beamformer transmitter and the FPGA. Moreover we described gradual shift of beamforming from analog to digital and also traced the evolution of digital beamformers to its present day commercial implementations. Also the effect of apodization on lateral resolution and side lobes were studied. While rectangular apodization have narrower lateral resolution when compared with hanning apodization, it has higher side lobes. So a compromise between the two was used as apodization weight. With digital beamforming, the advantage of it over conventional analog beamformers has been brought out by comparing its performance with the simulated analog beamformer implementation. Digital beamforming does help in improving the image quality and has improved lateral resolution compared to analog beamformers. Also the increased dynamic range in a digital beamformer is due to the dynamic receive focusing and apodization. Our proposed design based on the DAS. The DAS architecture produces high resolution images but at a high cost due to the many parallel transmits and receives channels. Interpolation beamforming reduces the sampling rate, saving storage space but lowers the dynamic range and contrast. It had higher contrast levels when compared to the alternate architecture, synthetic aperture imaging where a large aperture is synthesized by multiplexing a smaller aperture over a large array. This method produced images with poorer lateral resolution and was susceptible to motion artifacts, but helped in increasing the frame rate that is suitable to do 3-D imaging. Also the system complexity is lower due to the low channel count. Thus with our proposed design, images of comparable quality of DAS architecture can be produced at a lower cost through synthetic aperture imaging.



## B. FPGA Banks

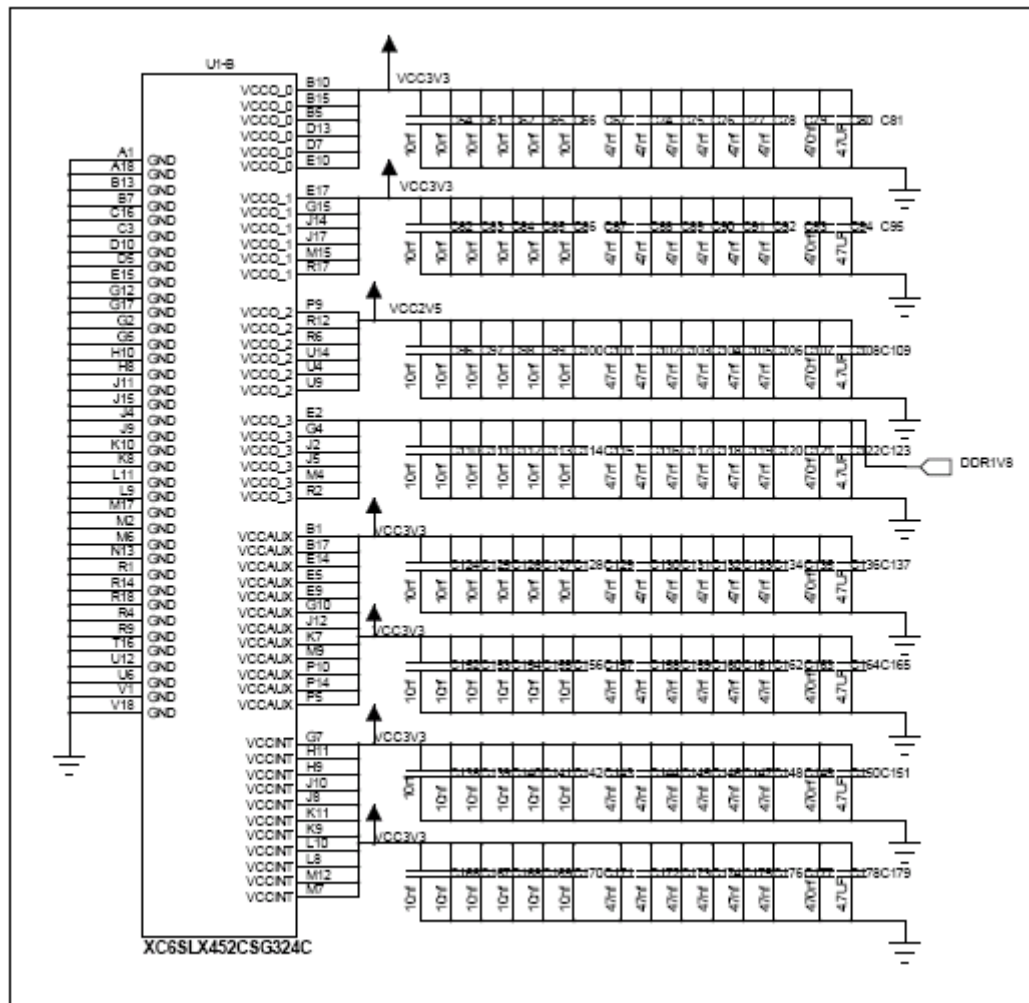
In the FPGA Banks section comprising the 4 banks of the SPARTAN 6 FPGA .These banks is controlling the whole operation of the digital beamformer.



FigureA.2-show the FPGA Banks section comprising the 4 banks of the SPARTAN 6.

### C. FPGA Power Rails

This section contains the power banks section, this section of the FPGA is responsible for powering up the FPGA with 3 different power suppliers +1V8 ,+2V5 and +3V3. Also there is a mesh of decoupling capacitors of different values to remove any noise in the FPGA power rail.

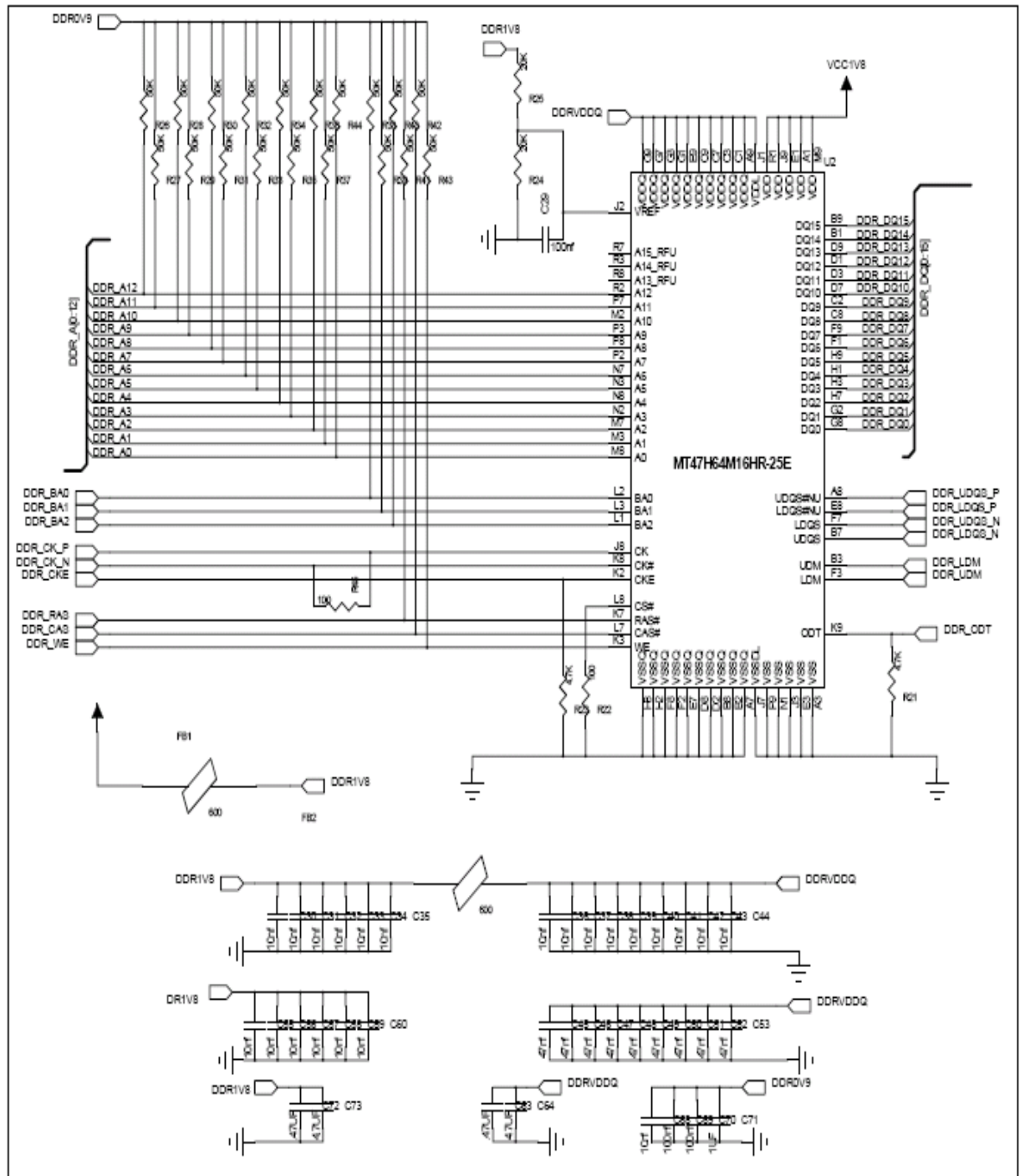


FigureA.3-show the power banks section which is responsible for powering up the FPGA with 3 different power suppliers +1V8 ,+2V5 and +3V3.

### D. FPGA Configuration and Programming

This section responsible for programming the FPGA using JTAG and the SPI flash which configure the FPGA with the bitstream and this needed for our SPARTAN 6 FPGA as it is volatile.

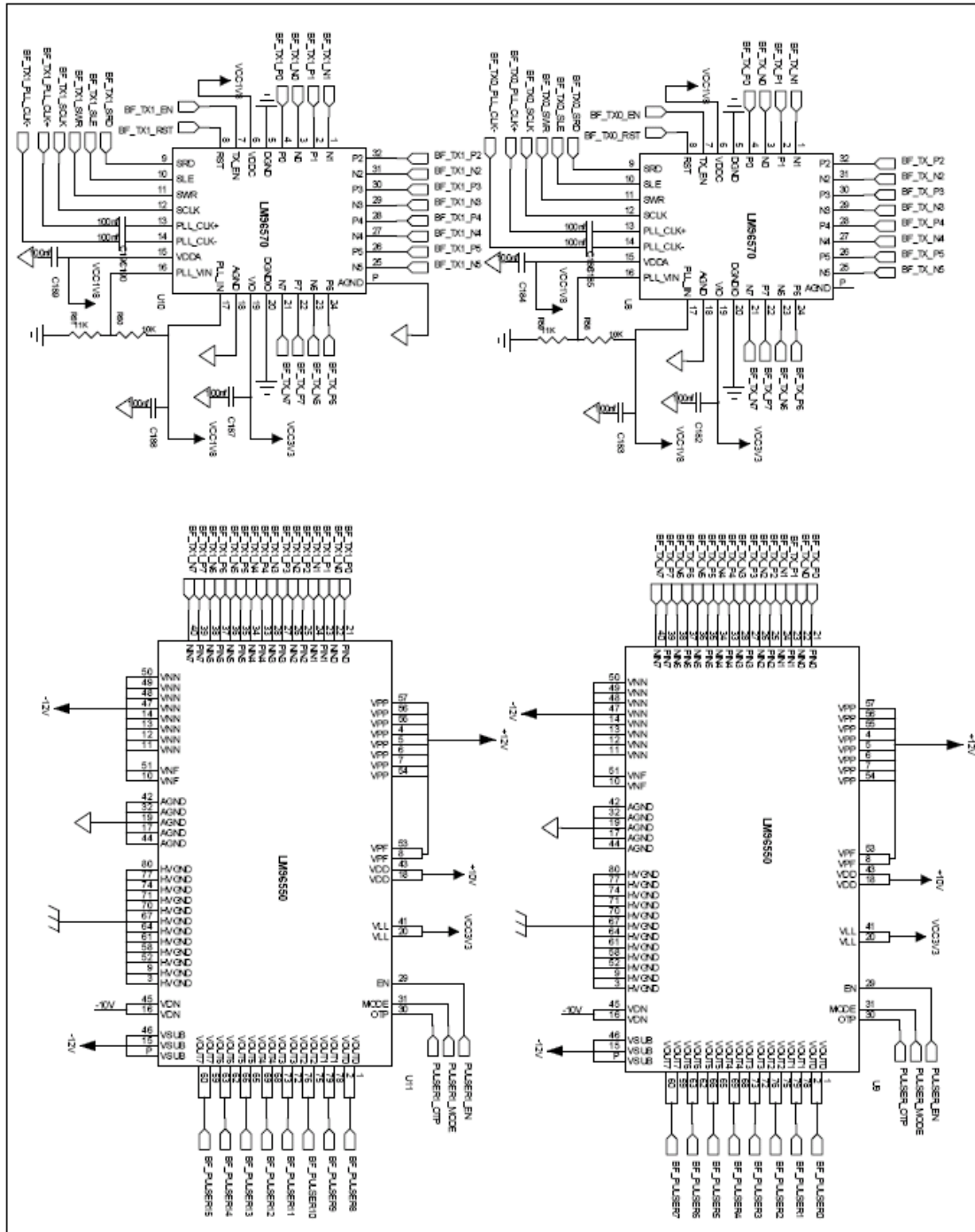




FigureA.5-show the digital beamformer operation for buffering and rest of DAS operation.

## F. Ultrasound beamformer transmitter

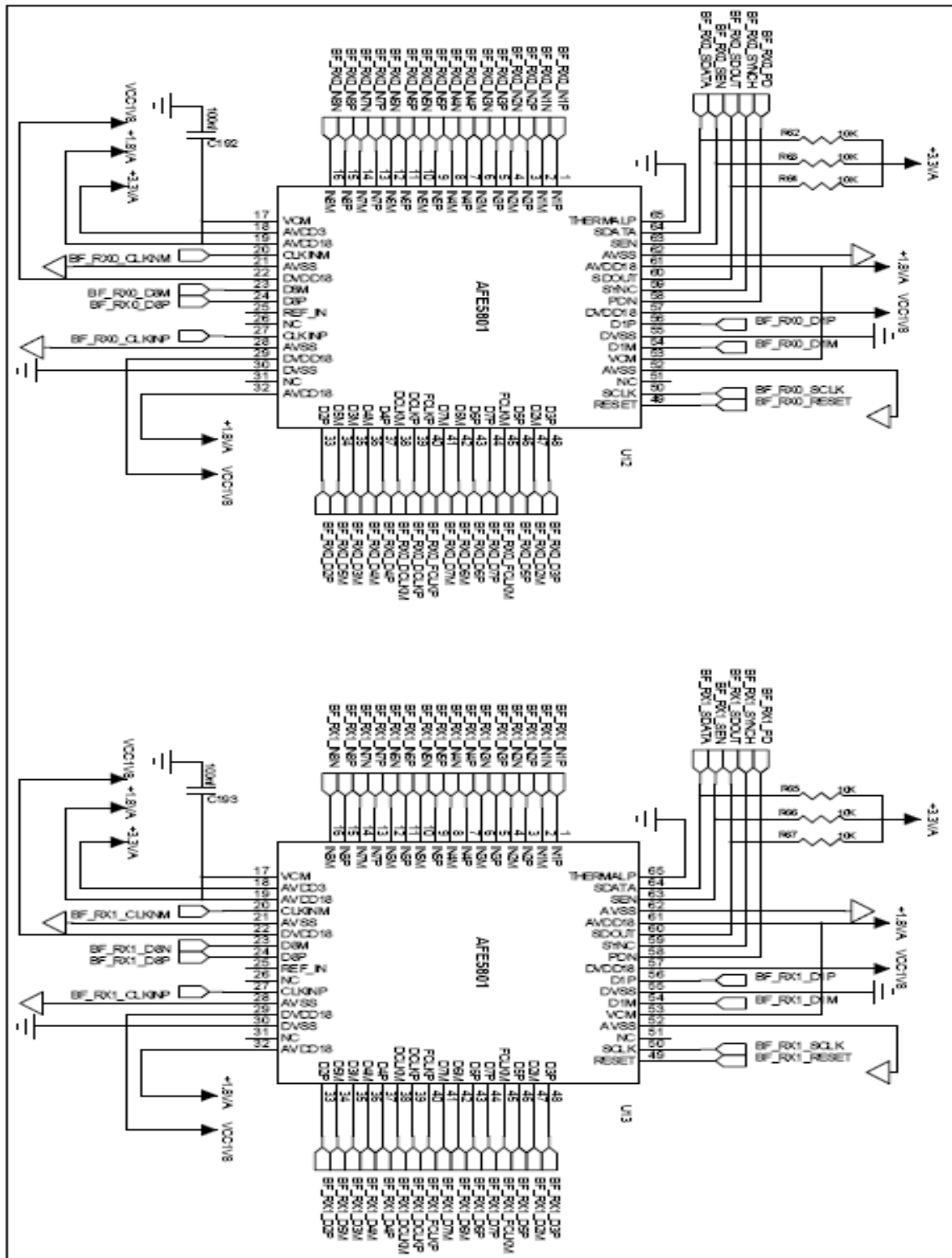
This section is illustrating the ultrasound transmitter section; we will find 2 LM96570 ultrasound transmitters ICs (16 Transmitter) driving 2 ultrasound ICs (16 Pulsers).



FigureA.6-show 2 LM96570 ultrasonic transmitters ICs (16 Transmitter) driving 2 ultrasonic ICs (16 Pulsers).

### G. Ultrasonic Beamformer Receiver

We can see in the next Figure the ultrasound receiver section using Analog front end solution AFE5801 complete receiver IC solution with variable gain controller .Only 2 ICs are acting the whole Beamformer receiver .



FigureA.7-show2 ICs are acting the whole Beamformer receiver.

## H. Ultrasound Beamformer Switching & Isolators

Ultrasound switches being used to switch between the transmitter (High voltage side) and the receivers (Low voltage side). High voltage isolators are used to prevent any voltage

breakdown from the high voltage side to the low voltage side. Figure 7.8 shows the transmitter (High voltage side) and the receivers (Low voltage side).

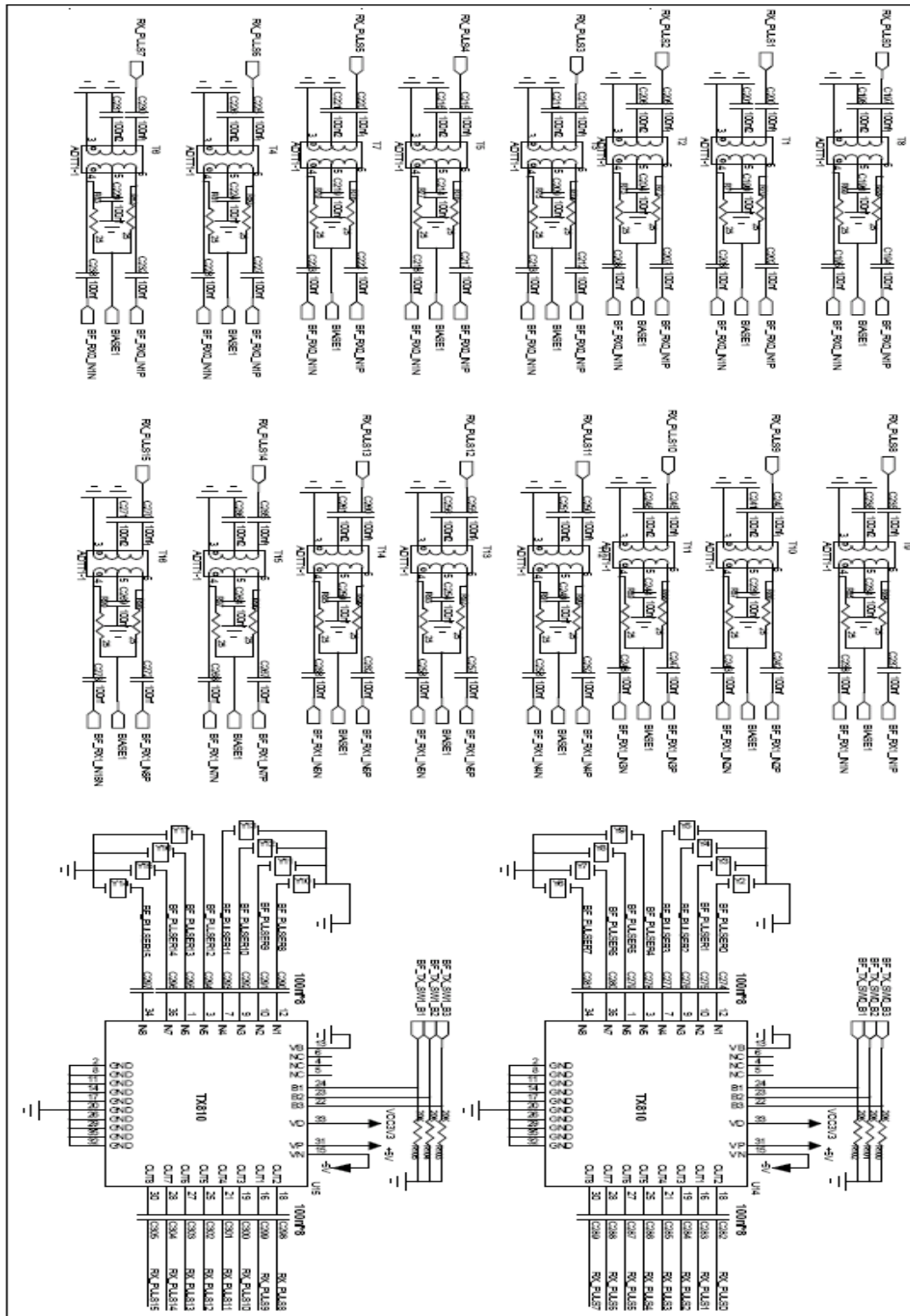


Figure A.8- shows the transmitter (High voltage side) and the receivers (Low voltage side).

## APPENDIX B

## Xilinx Platform Studio

## A. Introduction

From the XPS software, you can design a complete embedded processor system for implementation within a Xilinx FPGA device. The XPS main window is shown in the following figure. Optional Test Drives are provided in this chapter so you can explore the information and tools available in each of the XPS main window areas.

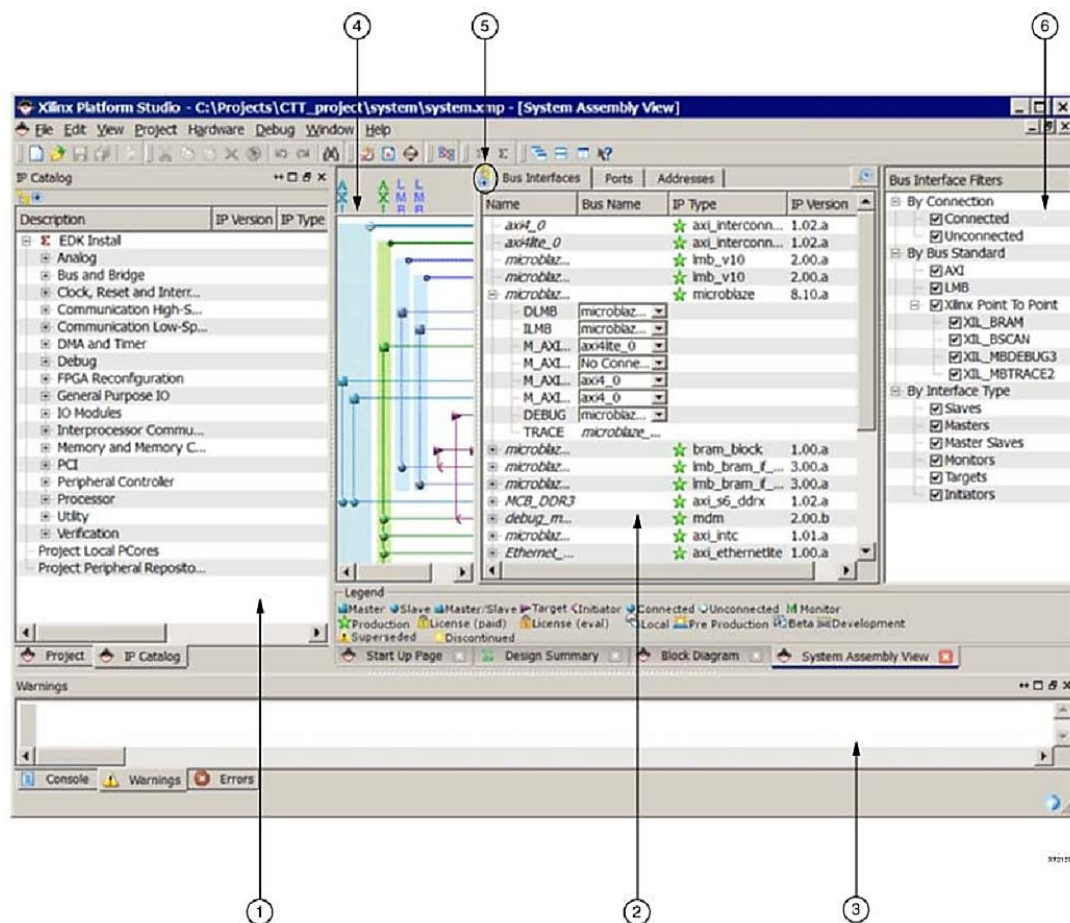


Figure B.1- XPS Project Window.

## B. Using the XPS User Interface

The XPS main window is divided into these three areas:

- Project Information Area (1)
- System Assembly View (2)
- Console Window (3)

The XPS main window also has labels to identify the following areas:

- Connectivity Panel (4)
- View Buttons (5)
- Filters Pane (6)

### **I. Project Information Area**

The Project Information Area offers control of and information about your project. The Project Information Area includes the Project and IP Catalog tabs.

### **II. Project Tab**

The Project Tab, shown in Figure B.2, contains information on the current project, including important project files and implementation settings.

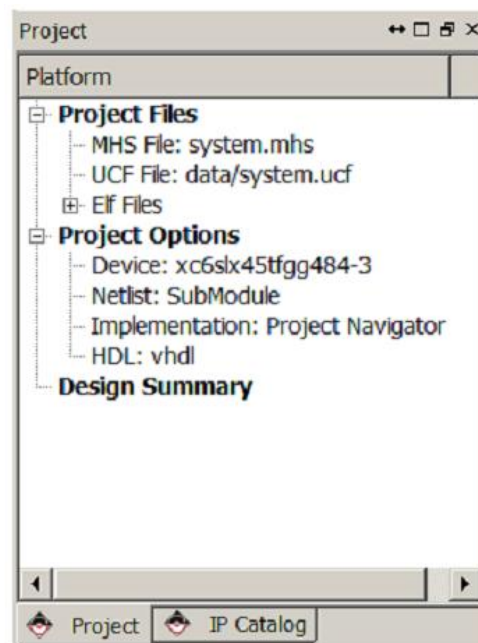


**Figure B.2- Project Information Area, Project Tab.**

### **III. IP Catalog Tab**

The IP catalog tab, lists information about the IP cores, including:

- Core name and licensing status (not licensed, locked, or unlocked)
- Release version and status (active, early access, or deprecated)
- Supported processors
- Classification

Additional details about the IP core, including the version change history, data sheet, and the Microprocessor Peripheral Description (MPD) file, are available when you right-click the IP core in the IP Catalog tab. By default, the IP cores are grouped hierarchically by function.

#### **IV. System Assembly View**

The System Assembly View allows you to view and configure system block elements. If the System Assembly View is not already maximized in the main window, click and open the System Assembly View tab at the bottom of the pane.

#### **V. Bus Interface, Ports, and Addresses Tabs**

The System Assembly View comprises three panes, which you can access by clicking the tabs at the top of the view.

- The Bus Interface tab displays the connectivity in your design. Use this view to modify parameters of peripherals and interconnects.
- The Ports tab displays ports in your design. Use this view to modify the details for each port.
- The Addresses tab displays the address range for each IP instance in your design.

#### **VI. Connectivity Panel**

With the Bus Interfaces tab selected, you'll see the Connectivity Panel, which is a graphical representation of the hardware platform connections. You can hover your mouse over the Connectivity Panel to view available bus connections. AXI interconnect blocks are displayed vertically, and a horizontal line represents an interface to an IP core. If a compatible connection can be made, a connector is displayed at the intersection between the interconnect block and the IP core interface. The lines and connectors are color-coded to show bus compatibility. Differently shaped connection symbols indicate whether IP blocks are masters or slaves. A hollow connector represents a connection that you can make. A filled connector represents an existing connection. Clicking the connector symbol creates or disables a connection.

#### **VII. Filters Pane**

XPS provides filters that you can use to change how you view the Bus Interfaces and Ports in the system assembly view. The filters are listed in the Filters pane when the Bus Interfaces or Ports tabs are selected. Using these filters can unclutter your connectivity panel when creating a design with large number different buses.

## **VIII. View Buttons**

The System Assembly View provides two buttons that change how the data is arranged. With these buttons, you can sort information and revise your design more easily.

## **IX. Console Window**

The Console window provides feedback from the tools invoked during run time. Notice the three tabs: Console, Warnings, and Errors.

## **X. Design Rule Check**

The Design Rule Check (DRC) performs system-level design rule checks in XPS. When this command is performed, the Warnings and Errors tabs in the console are cleared to display the most recent design rule check messages. To check design rules, select Project > Design Rule Checks, or click the Project DRC Button.

## **C. Software Development Kit**

The Xilinx Software Development Kit (SDK) facilitates the development of embedded software application projects. SDK is a complementary program to XPS. You use SDK to develop the software that is used on the embedded platform built in XPS. SDK is based on the Eclipse open source tool suite. SDK examined your hardware specification file (system.xml) and compiled the appropriate libraries corresponding to the components of your hardware platform. You SDK also created the new Board Support Package hello\_world\_bsp\_0. The Project Explorer tab now contains information related to the hardware platform, the software project, and the BSP.

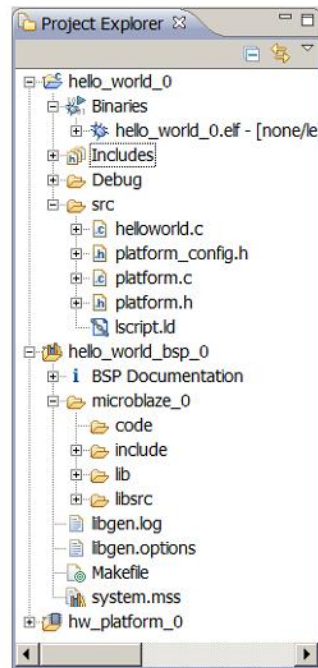


Figure B.3- Project Files Displayed in the Project Explorer Tab.

The hello-world, c file is in the src folder in the C Project called hello\_world\_0. Open hello-world, c and modify it as shown in Figure B.4.

```
19/*
20 * helloworld.c: simple test application
21 */
22
23#include <stdio.h>
24#include "platform.h"
25
26int main()
27{
28    init_platform();
29
30    print("Hello World\n");
31
32    memorytest_main();
33    peripheraltest_main();
34
35    cleanup_platform();
36
37    return 0;
38}
```

Figure B.4- Modified Version of hello-world File.

## D. Creating our Own Intellectual Property

Creating an embedded processor system using Xilinx Platform Studio (XPS) is straightforward because XPS automates most of the design creation. The Base System Builder (BSB) wizard reduces the design effort to a series of selections.

## **I. Using the CIP Wizard**

Though the CIP wizard steps you through the creation of your pcore framework, it is important to understand what is happening and why.

To ensure compliance, you must follow these steps:

1. Determine the interface required by your IP. The bus to which you attach your custom peripheral must be identified. For example, you could select one of the following interfaces:
  - AXI4-Lite: Simpler, non-burst control register style interface. You should use AXI4-Lite for most simple, register based peripherals that only require single beat transfers.
  - AXI4: Burst Capable, high-throughput memory mapped interface. AXI4 provides high performance burst transfers, and you should use it when high speed access to and from memory systems is required.
  - Processor Local Bus (PLB) version 4.6. The PLBv46 provides a high-speed interface between a PowerPC® processor and high-performance peripherals.
  - Fast Simplex Link (FSL). The FSL is a point-to-point FIFO-like interface. It can be used in designs using MicroBlaze™ processors, but generally is not used with PowerPC processor-based systems.
2. Implement and verify your functionality. Remember that you can reuse common functionality available in the EDK peripherals library.
3. Verify your standalone core. Isolating the core ensures easier debugging in the future.
4. Import the IP to EDK. Your peripheral must be copied to an EDK-appropriate repository search path. The Microprocessor Peripheral Definition (MPD) and Peripheral Analyze Order (PAO) files for the Platform Specification Format (PSF) interface must be created, so that the other EDK tools can recognize your peripheral.
5. Add your peripheral to the processor system created in XPS.

## **II. Using the CIP Wizard for Creating Custom IP**

The CIP wizard assists you with the steps required in creating, verifying, and implementing your Custom IP. A common design case is the need to connect your custom logic directly to an AXI interconnect block. With the CIP wizard, you can make that connection even without understanding AXI or AXI-Lite details. Both slave and master connections are available. The CIP wizard helps you implement and verify your design by walking you through IP creation. It sets up a number of templates that you can populate with

your proprietary logic. Besides creating HDL templates, the CIP wizard can create a pcore verification project for Bus Functional Model (BFM) verification. The templates and the BFM project creation are helpful for jump-starting your IP development and ensuring that your IP complies with the system you create. For details of BFM simulation, Next figures shows wizard configuration.

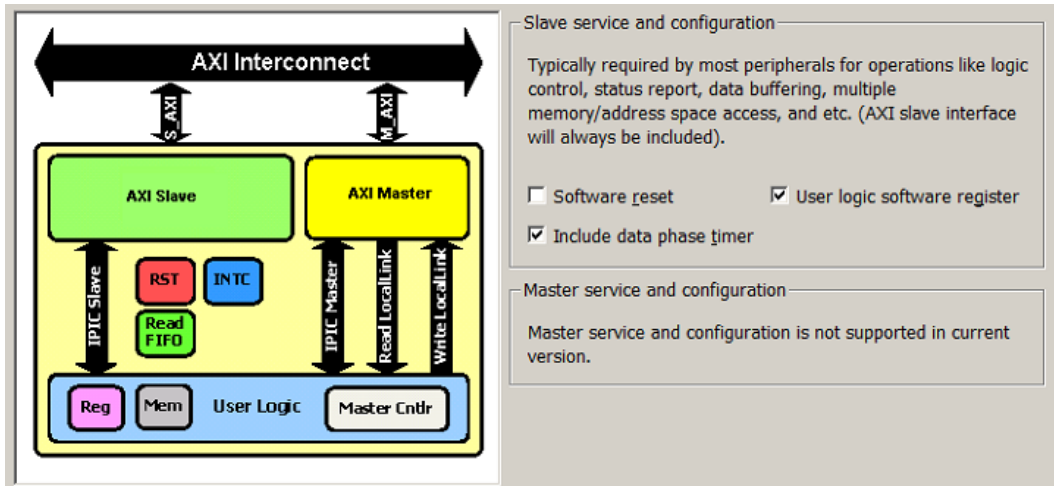


Figure B.5-Slave and master configuration.

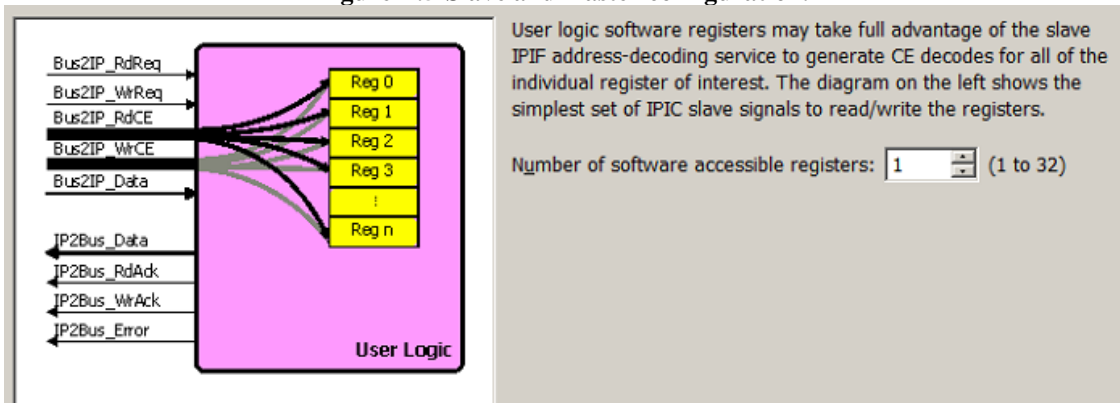


Figure B.6- Show module interface register.

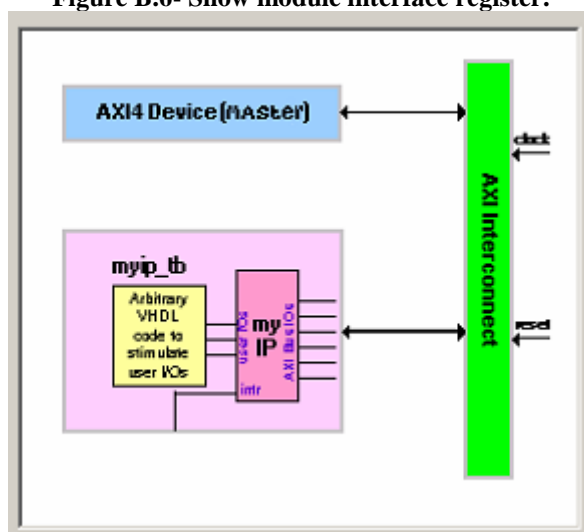


Figure B.7- Shows user module interfacing with other modules.

## APPENDIX C

### Vivado High Level Synthesizer (HLS)

#### A. Introduction

To manage the complexity of the digital design we need to move through new generation which is the high level synthesis, this tool will help us to synthesize our traditional code flow which written into C / C++ into the a complete IP core ready integration and testing as well.

#### B. C- Based Specification

C-based entry is the most popular mechanism to create functional specifications. Currently, ANSI-C (with C99), C++ and System C are standards deployed by many system architects to define the functionality of systems intended to be implemented on an FPGA. High-Level Synthesis provides comprehensive support for C, C++ and System C, the IEEE standard (IEEE-1666) used for modeling and concurrent simulation of hardware. The constructs which cannot be synthesized are those which unbounded at elaboration time and for which a finite sized description cannot be determined. Native C data types live within the classic boundaries of 8-bit, 16-bit, 32-bit and 64-bit words (char, short, int, long, long long). Neither ANSI-C nor C++ has built-in data types to deal with bit-accurate calculations, where the exact bit-width of the data type is used (and which results in optimally sized hardware). High-Level Synthesis provides support for arbitrary precision data types in both C and C++. High-Level Synthesis fully supports the arbitrary precision data types provided by System C.

#### C. Theory of operation

The synthesis of C into RTL employs many advanced transformations working on all aspects of the design area and performance. High-Level Synthesis provides synthesizable support for a large subset of all three input C standards (C, C++ and System C) enabling it to synthesize the C code with minimal modifications. High-Level Synthesis performs two distinct types of synthesis upon the design:

- Algorithm Synthesis takes the content of the functions, and synthesizes the functional statements into RTL statements over a number of clock cycles.

- Interface Synthesis transforms the function arguments (or parameters) into RTL ports with specific timing protocols, allowing the design to communicate with other designs in the system.
  - Interface synthesis can be performed on global variables, top-level function arguments and the return value of the top-level function.
  - The types of available interfaces are:
    - Wire
    - Register
    - One-way & two-way handshakes
    - Bus
    - FIFO
    - RAM
  - In addition, a function level protocol can be synthesized to the top-level function. The function level protocol includes signals which control when the function can start operation and indicate when it has completed.

High-Level Synthesis is executed in multiple steps. The effect of interface synthesis impacts what is achievable in algorithm synthesis and vice versa. Like the numerous decisions made during any manual RTL design, the number of available implementations and optimizations is large and the combinations of how they impact each other is very large. High-Level Synthesis abstracts the user away from these details and allows the user to productively get to the best design in the shortest time.

To better understand how High-Level Synthesis is able to abstract the designer away from the implementation details, it is recommended to review the remainder of this section which explains some of the fundamental concepts of HLS and type of optimizations

High-Level Synthesis provides:

- Control and Datapath Extraction
- Scheduling & Binding
- Arbitrary Precision Data Types
- Optimizations
- Design Constraints

## **I. Control and Datapath Extraction**

The first thing which is performed during HLS is to extract the control and datapath inferred by the code. Figure 6.1 shows a small example on how this is performed. The control

functionality is provided by the loops and conditional branches in the code. Figure 6.1 shows how the control behavior can be extracted from the code. Each time the function requires an entry or exit from a loop, it is equivalent to entering or exiting a state in an RTL Finite State Machine (FSM)<sup>2</sup>. In Figure 6.1 it is assumed that all operations take a single cycle (or state) to complete. In reality, timing delays and the clock frequency may require more cycles to complete the operations, for example state 1 may expand to states 11, 12 and 13, the control logic may be impacted by the IO protocols inferred by interface synthesis and High-Level Synthesis may create a more complex and optimized state machine. The datapath extraction is more straightforward and can be determined by unrolling all the loops and evaluating the conditional statements in the design.

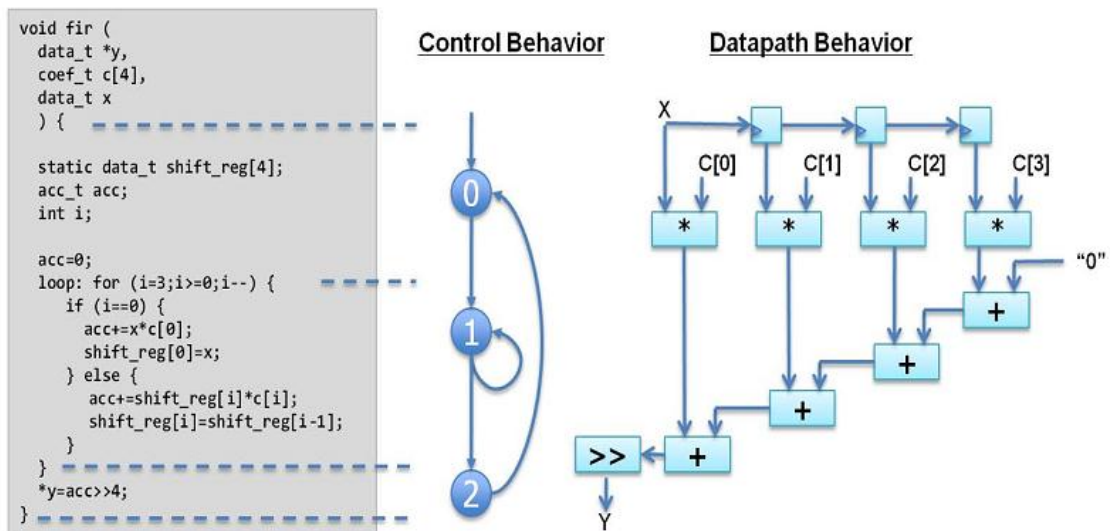


Figure C.1- control and datapath behavior in HLS.

The final datapath implementation in the RTL is unlikely to be as simple as that shown in Figure 6.1: High-Level Synthesis will easily determine that the first adder is not required since the final shift operation is a power of 2 and requires no hardware. More complex optimizations and decisions will be made when the design is scheduled.

## II. Scheduling & Binding

Scheduling and binding are the processes at the heart of high-level synthesis. High-Level Synthesis will determine during the scheduling process in which cycle operations will occur. The decisions made during scheduling take into account, among other things, the clock

frequency and clock uncertainty, timing information from the device technology library, as well as area, latency and throughput directives. For the same example code shown in Figure 6.1, multiple RTL implementations are possible. Figure 6.2 shows just 3 possible implementations.

1. Using 4 clock cycles means a single adder and multiplier can be used, as High-Level Synthesis can share the adder and multiplier across clock cycles: 1 adder, 1 multiplier and 4 clock cycles to complete.
2. If analysis of the target technology timing indicates the adder chain can complete in 1 clock cycle, a design which uses 3 adders and 4 multipliers but which finish in 1 clock cycle can be realized (faster but larger than option 1).
3. Take 2 clock cycles to finish but use only 2 adders and 2 multipliers (smaller than option 2 but faster than option 1).

High-Level Synthesis quickly creates the most optimum implementation based on its own default behavior and the constraints and directives specified by the user. Later chapters explain how to set constraints and directives to quickly arrive at the most ideal solution for the specific requirements.

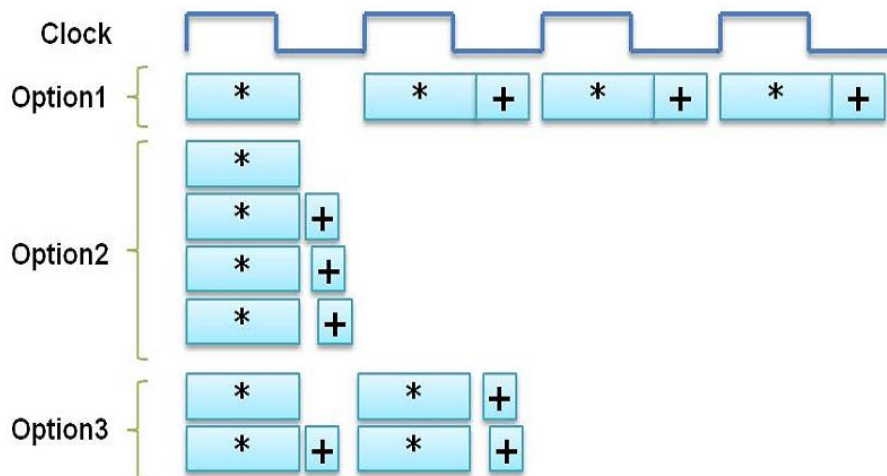


**Figure C.2- options in the synthesize.**

Binding is the process that determines which hardware resource, or core, is used for each schedule operation. For example, High-Level Synthesis will automatically determine if an adder and subtractor will be used or if a single adder-subtractor can be used for both operations. Since the decisions in the binding process can influence the scheduling of operations, for example, using a pipelined multiplier instead of a standard combinational multiplier, binding decisions are considered during scheduling.

### III. Arbitrary Precision Data Types

Native C data types are on 8-bit boundaries (8, 16, 32, 64 bits). RTL operations (corresponding to hardware) support arbitrary widths. HLS needs a mechanism to allow the specification of arbitrary precision bit-widths or the RTL design may use 32-bit multipliers when only 17-bit multipliers are required (not an issue to a C program, but a major issue in an RTL design). These arbitrary types are supported by functions which provide hardware like operations, such as bit-slicing, concatenation and range-selection. Optimizations High-Level Synthesis can perform a number of optimizations on the design to produce high quality RTL satisfying the performance and area goals. This section introduces a few of the optimization techniques to give an overview of the capabilities. Pipelining is an optimization which allows one of the major performance advantages of hardware over software, concurrent or parallel operation, to be automatically implemented in the RTL design. A C program operates in a sequential manner. Given the function "top" shown on the left-hand side of Figure 6.3, every sub-function from "func\_A" to "func\_C" must complete its operation before "func\_A" can once again execute.

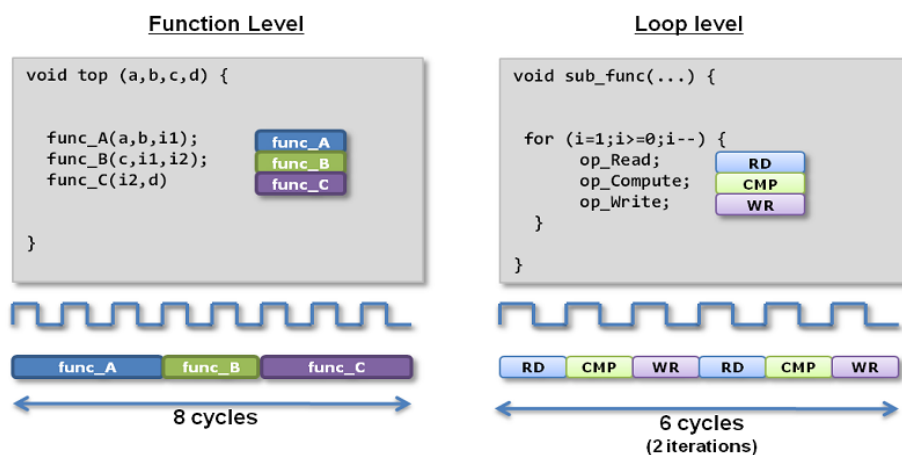


Figure C.3- showing 3 sequence sub-functions in non-pipeline behavior.

Even if "func\_A" is ready to process the next set of operations as soon as it is finished, functions "func\_B" and "func\_C" must complete execution before "func\_A" can once again begin operation. As function "sub\_func" on the right-hand side of Figure 6.3 shows, it is the same at the operator level: the first operation cannot re-execute until the last is complete. The sequential nature of the C language, or another words its lack of concurrency, puts artificial dependencies on operations which must wait their turn for execution. High-Level Synthesis provides the ability to automatically pipeline both functions and loops to ensure the RTL design does not suffer from such limitations. By default, High-Level Synthesis will seek to

execute these operations in parallel and reduce the overall latency of the design. In addition to this, High-Level Synthesis can improve the throughput by pipelining these operations, allowing different executions of the function or different loop iterations to overlap in time. Figure 6.4 shows the result when High-Level Synthesis is used to pipeline the sub-functions and/or operations in a loop.

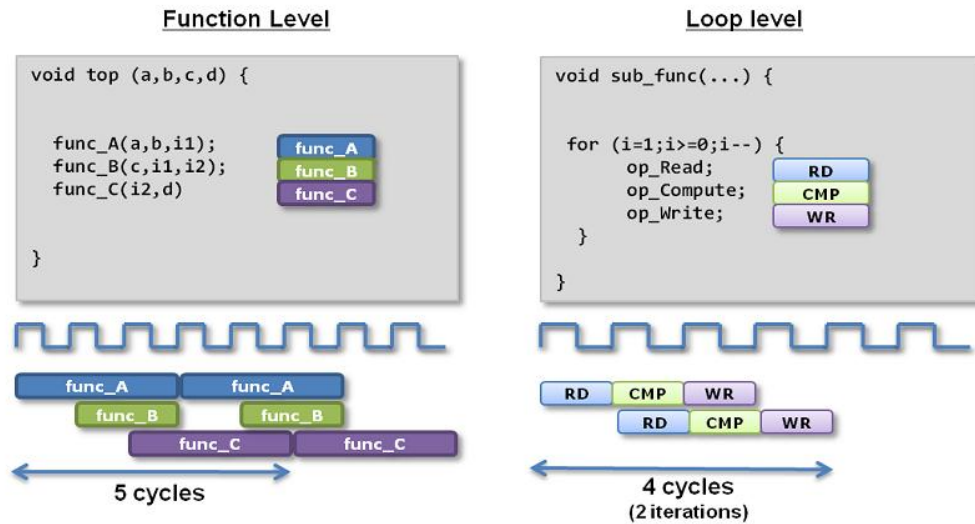


Figure C.4- showing 3 sequence sub-functions in pipelining behavior.

- At the function level, dataflow optimization allows the sub-functions (“func\_A”, “func\_B” and “func\_C” ) to execute as soon as data is available.
  - Function “func\_A” starts its next operation “before func\_C” has completed its first execution.
  - Compared with the previous implementation in Figure C.3, the 8 clock cycles it took to execute the function is now only 5 cycles and “func\_A” starts a new operation every 3 clock cycles instead of every 8.
- Pipelining the loop allows the operations in a loop to execute concurrently.
  - Figure 6.4 shows how loop pipelining can also positively performance compared with Figure C.4: the loop completes in only 4 clock cycles and processes a new input (RD operation) every clock cycle instead of waiting for 3 clock cycles.

Another example of a design optimization which can be automatically implemented by High-Level Synthesis is array partitioning. Within C language descriptions, arrays are used as a convenient way to group similar elements together. When the elements of arrays are synthesized as storage elements (that is, when the value must be maintained across clock

cycles) these array elements can be grouped at the RTL in RAMs or they can be broken into their constituent parts and implemented as individual registers.

- If the elements of an array are accessed one at a time, an efficient implementation in hardware is to keep them grouped together and mapped into a RAM.
- If multiple elements of an array are required simultaneously, it may be more advantageous for performance to implement them as individual registers: allowing parallel access to the data.

Implementing an array of storage elements as individual registers may help performance but this loses the substantial benefits of RAMs: area efficient in all technologies and they are readily available in the device as BRAMs (separate from the LUTs and registers). High-Level Synthesis provides a variety of techniques to ensure arrays are implemented in the most optimal manner:

- Partitioning large arrays into multiple smaller arrays, which can be mapped to different instances of RAM (allowing multiple reads or writes in the same cycle).
- Enabling multiple small arrays to be implemented onto the same RAM resource.

The application of a few simple directives provides for a large number of different implementations, from pipelining to the manipulation of arrays, ensuring that the most optimal implementation for the particular design can be quickly and easily found.

#### **IV. Design Constraints**

Finally, in addition to the clock period and clock uncertainty, High-Level Synthesis offers a number of constraints including the ability to:

- Specify a specific latency across functions, loops and regions.
- Specify a limit on the number of resources used.
- Override the inherent or implied dependencies in the code and permit operations (for example, a memory read before write).

These constraints can be applied using High-Level Synthesis directives to create a design with the desired attributes. Designing with High-Level Synthesis is a HLS flow allows the designer to quickly implement an initial architecture, which will be defined by the dependencies in the code and the default High-Level Synthesis interpretation of C language constructs, and then easily direct the design with directives towards the desired high performance implementation.

**APPENDIX D****DBF Frequency-domain methods**

Frequency-domain beamforming methods often require a different view and approach to that of its temporal counterpart, which at first may seem strange, but the sacrifice in sanity is generally well rewarded with returns of efficiency. The two main techniques currently associated with frequency domain beamforming are the Fourier transform technique and the phase shift beamforming technique. These two techniques will form the basis of discussion within this section, but more emphasis will be placed on the phase-shift beamforming technique as it is the technique of choice for our current project. The Discrete Fourier Transform (DFT) technique, applicable to low-pass and band-pass applications, has the same sampling rate advantage as the phase-shift method where the sampling frequency does not affect the beam steering resolution and only needs to satisfy the Nyquist criterion. This of course translates into decreases in A/D demands and subsequent hardware. The beamforming task can also be implemented with a computationally efficient fast Fourier transform (FFT) algorithm, which is another benefit of the DFT technique. An example of where a FFT algorithm has been implemented is in a 3-dimensional underwater imaging system developed by researchers Murino and Trucco.

Phase-shift beamforming is intended for narrow-band applications where there remains a fixed center frequency. This is due to the inherent properties of a phase-shift process that requires a constant frequency for the reconstructed signal to make sense. Studies have shown that phase-shift beamforming performance degrades rapidly for other than very narrow-band applications. Converting sensor data into complex signals allows the phase-shift process to be carried out using an efficient vector rotation algorithm, namely the CORDIC algorithm. Here signals are represented as complex vectors and are rotated by different amounts based on the current focal angle and transducer location. This rotation in the complex domain or phase-shift is equivalent to a time delay in the time domain. Advantages of this type of implementation are quite significant as all three criteria are used for evaluation within Mucci's paper are met and are at a minimum. This is why the phase shift beamformer was opted for over the remaining techniques as it is one of the easiest to implement, requires a relatively small amount of hardware and still achieves very good results for narrow band applications.

### References

- [1] S. B. Barnett, G. R. Ter Haar, M. C. Ziskin, H. D. Rott, F. A. Duck, and K. Maeda, "International recommendations and guidelines for the safe use of diagnostic ultrasound in medicine," *Ultrasound in Medicine & Biology*, vol. 26, no. 3, pp.355–366, Mar. 2000.
- [2]. Abd-Elmoniem, K. Z., Youssef, A. M., and Kadah, Y. M., Real-Time Speckle Reduction and Coherence Enhancement in Ultrasound Imaging via Nonlinear Anisotropic Diffusion, *IEEE Transactions Biomedical Engineering*, Vol. 49, No. 9, pp. 997-1014, September 2002.
- [3]. Kieran Andrew Wall, a High speed reconfigurable system for ultrasound research, December 2010.
- [4]. Kasai, C., Namekawa, K., Koyano, A., and Omoto, R., Real-Time Two-Dimensional Blood Flow Imaging Using an Autocorrelation Technique, *IEEE Transactions on Sonics and Ultrasonic*, Vol. SU-32, No. 3, pp. 458-464, May 1985.
- [5] M Ali, D Magee, U Dasgupta - Texas Instruments, 2008.
- [6] I. Donald, "Sonar - A new diagnostic echo-sounding technique in obstetrics and gynecology," *Proceedings of the Royal Society of Medicine*, vol. 55, no. 8, pp. 637-6
- [7] S. Levi, "The history of ultrasound in gynecology 1950-1980," *Ultrasound in Medicine & Biology*, vol. 23, no. 4, pp. 481-552, 1997.
- [8] J. J. Wild, "The use of ultrasonic pulses for the measurement of biologic tissues and the detection of tissue density changes," *Surgery*, vol. 27, no. 2, pp. 183-188, Feb. 1950.
- [9] J. J. Wild and J. M. Reid, "Application of echo-ranging techniques to the determination of structure of biological tissues," *Science*, vol. 115, no. 2983, pp.
- [10]. Szabo, T. L., *Diagnostic Ultrasound Imaging: Inside Out*, Elsevier Academic Press: Hartford, Connecticut, 2004.
- [11] G. S. Kino, *Acoustic waves: devices, imaging and analog signal processing*. Englewood Cliffs: Prentice Hall, 1987.
- [12] R. S. Cobbold, *Foundations of biomedical ultrasound*. Oxford University Press, USA, 2007.
- [13] Guy C and ffytyche D. *An Introduction to the Principles of Medical Imaging* Imperial College Press, London. 2000.
- [14] Hussey M. *Basic Physics and Technology of Medical Diagnostic Ultrasound* MacMillan and Sons, London. 1985.
- [15] Hill C R (ed). *Physical Principles of Medical Ultrasonics*. Ellis Horwood, chichester. 1986.
- [16] Webb S (ed). *The Physics of Medical Imaging*. IOP Publishing, Bristol. 1992. pp 319-388.
- [17] A.D. Pierce. *Acoustics: an Introduction to its Physical Principles and Applications*. McGraw-Hill Book Company, Inc., New York, 1981. Also available from the Acoustical Society of America.
- [18] *An Introduction to Acoustics*, S.W. Rienstra & A. Hirschberg, Eindhoven University of Technology, 9 December 2012.
- [19] Jespersen, S. K., Wilhjelm, J. E., and Sillesen, H., "Multi-angle compound imaging", 1998, *Ultrasonic Imaging*, vol. 20, No. 2, pp 82
- [20]. Kim, Y. G., and Park, S. B., "New dynamic focusing scheme for ultrasound scanners", 1987, *Electronic letters* 23, pp 181.
- [21] Sud Vasudevan "Ultrasonic Digital Beamformation : A Comparative Study" September 14, 1998.
- [22] S. O. Hugo, "Variable focus transducer," U.S. Patent US Patent 3,090,030 May-1963.
- [23] F. L. Thurstone, N. I. Kjosnes, and W. M. McKinney, "Ultrasonic scanning of biologic tissue by a new technique," *Science*, vol. 149, no. 3681, pp. 302-303, 1965.

## References

---

- [24] C. B. Burckhardt, P. A. Grand champ, and H. Hoffmann, "Methods for increasing the lateral resolution of B-scan," *Acoustical holography*, p. 391, 1974.
- [25] B. D. Steinberg, *Principles of aperture and array system design: Including random and adaptive arrays*. New York: John Wiley & Sons, 1976.
- [26] F. L. Thurstone and O. T. Von Ramm, "A new ultrasound imaging technique employing two-dimensional electronic beam steering," *Acoustical holography*, vol. 1615, pp. 249–259, 1973.
- [27] O. Von Ramm and F. Thurstone, "Cardiac imaging using a phased-array ultrasound system .1. system-design," *Circulation*, vol. 53, no. 2, pp. 258-262, 1976.
- [28] J. Talman, S. Garverick, and G. Lockwood, "Integrated circuit for high-frequency ultrasound annular array," *Proceedings of the IEEE 2003 Custom Integrated Circuits Conference*, pp. 477-480, 2003.
- [29] R. E. McKeighen and M. P. Buchin, "New techniques for dynamically variable electronic delays for real time ultrasonic imaging," in *Ultrasonic Symposium*, 1977, pp. 250–254, 2005.
- [30] L. Coldren and H. Shaw, "Surface-wave long delay-lines," *Proceedings of the [22]IEEE*, vol. 64, no. 5, pp. 598-609, 1976.
- [31] M. Montrose, E. Li, H. Jin, and W. Yuan, "Analysis of the effectiveness of the 20-H rule for printed-circuit-board layout to reduce edge-radiated coupling," *IEEE Transactions on Electromagnetic Compatibility*, vol. 47, no. 2, pp. 227-233, May. 2005.
- [32]. McKeighan, R. E. and Buchin, M. P., "New techniques for dynamically variable electronic delays for real time ultrasound imaging", 1977, *Ultrasonics Symposium Proceedings*, pp. 250.
- [33] P. R. Gray and R. G. Meyer, *Analysis and design of analog integrated circuits*. Hamilton Printing, 1993.
- [34] A. V. Oppenheim, A. S. Willsky, and S. H. Nawab, *Signals and systems 2nd ed.* New Jersey: Prentice Hall, 1997.
- [35] R. E. Crochiere and L. R. Rabiner, *Multirate digital signal processing*. Englewood Cliffs, NJ: Prentice-Hall, 1983.
- [36] C. Hazard and G. Lockwood, "Developing a high speed beamformer using the TMS320C6201 digital signal processor," *IEEE Ultrasonics Symposium*, pp. 1755-1758, 2000.
- [37] G. E. Trahey, K. Ferrera, J. B. Fowlkes, and others, "Ultrasonic imaging: infrastructure for improved imaging methods," in *Report of the OWH/NCI Sponsored Workshop*, 1999.
- [38]. Walker, J. T. and Meindl, I. D., "A digitally controlled CCD dynamically focused phased array", 1975, *Ultrasonic Symposium Proceedings*, pp. 80.
- [39]. Stonestrom, J. P and Anderson, W. A., "A custom nMOS chip for medical ultrasound", 1982, *VLSI Design*, May, pp. 44.
- [40]. Manes, G. F., Atzeni, C., and Susini, C., "Design of a simplified delay system for ultrasound phased array imaging", 1983, *IEEE Transactions on Sonics and Ultrasonics*, vol. 30, No. 6, pp. 350.
- [41]. Manes, G. F., Atzeni, C., and Susini, C., Somer, J. C., "A new delay technique with application to ultrasound phased-array imaging systems", 1979, *Ultrasonics*, Sept, pp. 225.
- [42]. O'Donnell et. Al, "Real-time phased array imaging using digital beam forming and autonomous channel control", 1990, *Ultrasonics Symposium*, pp. 1499.
- [43] T. Wilson, J. Zagzebski, T. Varghese, Q. Chen, and M. Rao, "The Ultrasonix500RP: A commercial ultrasound research interface," *IEEE Transactions on Ultrasonic, Ferroelectrics and Frequency Control*, vol. 53, no. 10, pp. 1772-1782, Oct. 2006.
- [44] Ultrasonix, "SonixDAQ technical overview," 28-Jun-2010.
- [45] Ultrasonix, "Ultrasound engineered for research."
- [46] Verasonics, "The Verasonics ultrasound engine," 2007.

## References

---

- [47] C. Hu, X. Xu, J. Cannata, J. Yen, and K. Shung, "Development of a real-time, high-frequency ultrasound digital beamformer for high-frequency linear array transducers," *IEEE Transactions on Ultrasonics, Ferroelectrics and Frequency Control*, vol. 53, no. 2, pp. 317-323, Feb. 2006.
- [48] L. Zhang et al., "A high-frequency, high frame rate duplex ultrasound linear array imaging system for small animal imaging," *IEEE Transactions on Ultrasonics, Ferroelectrics and Frequency Control*, vol. 57, no. 7, pp. 1548-1557, 2010.
- [49] K. Satoh, J. Tada, and Y. Tamura, "Three-dimensional ultrasonic imaging operation using FPGA," *IEICE Electronics Express*, vol. 6, no. 2, pp. 84-89, Jan. 2009.
- [50] J. Jensen, M. Hansen, B. Tomov, S. Nikolov, and H. Holten-Lund, "System architecture of an experimental synthetic aperture real-time ultrasound system," *IEEE Ultrasonics Symposium*, pp. 636-640, 2007.
- [51] S. Nikolov, J. Jensen, and B. Tomov, "Fast parametric beamformer for synthetic aperture Imaging," *IEEE Transactions on Ultrasonics, Ferroelectrics and Frequency Control*, vol. 55, no. 8, pp. 1755-1767, Aug. 2008.
- [52] A. Hendy, M. Hassan, R. Eldeeb, D. Kholy, A. Youssef, and Y. Kadah, "PC-based modular digital ultrasound imaging system," *IEEE Ultrasonic Symposium*, pp. 1330-1333, 2009.
- [53] H. W. Johnson and M. Graham, *High speed digital design: a handbook of blackmagic*. Prentice Hall PTR, 1993.
- [54] Texas Instruments Incorporated, "VCA8613 8-channel variable gain amplifier," Oct-2005.
- [55] Xilinx, "Virtex-6 Family Overview," Xilinx, Mar-2010.
- [56] Xilinx, "Spartan-6 family overview," Xilinx, Mar-2010.
- [57] M. Klein, "Power Consumption at 40 and 45 nm," Xilinx, Apr-2009.
- [58] Xilinx, "Spartan-6 FPGA Packaging and Pin outs," Xilinx, Mar-2010.
- [59] M. Brown, *Power supply cookbook*. Newness, 2001.
- [60] Maxim/Dallas Semiconductor, *Maxim/Dallas semiconductor power supply cookbook*. 2007.
- [61] Maxim IC, "Choosing the right power-supply ic for your application," Maxim IC, 164 Mar-2001.
- [62] Digilent, "Atly Board " Reference Manual " , Digilent May 2, 2011.
- [63] M. Defossez, "An interface for Texas Instruments analog-to-digital converters with serial LVDS outputs," Xilinx, Apr-2008.
- [64] Xilinx, "Spartan-6 FPGA SelectIO Resources User Guide," Xilinx, Mar-2010.
- [65] National semiconductor, LM96570 "productbrief" November 30, 2010.
- [66] Xilinx, "SP605 hardware user guide," Xilinx, May-2010.
- [50] R. Seelam, "I/O design flexibility with the FPGA mezzanine card (FMC)," Xilinx, Mar-2010.
- [68] TI, AFE5804 "Reference Manual" SBOS442B, JUNE 2008.
- [69] Xilinx, "Spartan-6 FPGA Clocking Resources," Xilinx, Mar-2010.
- [70] Xilinx, "Spartan-6 FPGA Configuration User Guide," Xilinx, Feb-2010.
- [71] Xilinx, "Spartan-6 FPGA Data Sheet: DC and Switching Characteristics," Xilinx, Feb-2010.
- [72] Dubose, T. J. (1985). "Fetal Biometry: Vertical Calvarial Diameter and Calvarial Volume". *Journal of Diagnostic Medical Sonography*.
- [73] XILINX, UG626 "Synthesis and Simulation Design Guide" January 19, 2012.
- [74] XILINX, "Microblaze Reference Guide" ,UG081 , April , 2012.
- [75] XILINX, "EDK Concepts, Tools, and Techniques", UG683 April 13, 2011.
- [76] XILINX, "VIVADO High-Level Synthesis" UG902 (v2012.2) July 25, 2012.
- [77] XILINX "Application Note: Spartan-6 FPGAs XAPP1064 (v1.1)" June 3, 2010

## References

---

- [78] XILINX, "LogiCORE IP Ethernet Lite MAC", DS787, October 19, 2011.
- [79] XILINX, "Spartan 6 FPGA Memory controller", UG388, August 9, 2012.
- [80] Karaman, M., Bilge, S. H., and O'Donnell, M., "Adaptive multi-element synthetic aperture imaging with motion and phase aberration correction", 1988, IEEE Transactions on Ultrasonics, Ferroelectrics, and Frequency Control, vol. 45, No. 4, pp. 1077.
- [81] S. I. Nikolov, J. A. Jensen, and B. G. Tomov, "Processing in SARUS," Ørsted•DTU, Tech. Univ. Denmark, Tech. Rep., 2006.
- [82] J. A. Jensen, M. Hansen, B. G. Tomov, S. I. Nikolov, and H. Holten-Lund, "System architecture of an experimental synthetic aperture real time ultrasound system," in Proc. IEEE Ultrason. Symp., Oct. 2007, pp. 636–640.
- [83] Svetoslav Ivanov Nikolov, "Fast Parametric Beamformer for Synthetic Aperture Imaging", IEEE Transactions on Ultrasonics, Ferroelectrics, and Frequency Control, vol. 55, no. 8, August 2008.

---

كما نود ان ننوه اننا فى هذه الرسالة راعينا عند التصميم ان نجعل من هذا التصميم اقل تكلفة بكل الوسائل المستطاعة وايضا التوفير فى استهلاك الطاقة وذلك لتوظيف هذا التصميم ايضا فى اجهزة السونار المحمولة ولهذا السبب وجدنا انه بالامكان ان نستخدم SPARTAN 6 ذو البوابات المنطقية الاقل امكانات من VIRTEX6 الاكثر امكانات. فى هذا التصميم لجأنا الى استخدام معظم ادواتنا لبرمجة البوابات المنطقية من شركة XILINX مثل المعالج السوفت MICROBLAZE ونقوم بتطويره من خلال اداه اسمها XILINX Embedded Development Kit EDK اما عند استخدام معالج الاشارات السريعة الرقمية استخدمنا ادوات من شركة TI مثل CODE COMPOSER STUDIO. فى هذه الرسالة سنقوم بعرض خصائص الموجات فوق الصوتيه وكيفية توليدها ايضا سنوضح كيفية القيام بتكوين الصورة من الاشعة المرتردة من الجسم المراد تصويره

## ملخص الرسالة

تعتبر الاشعة الموجات فوق الصوتية واحدة من الاشعة الاكثر انتشارا فى العالم على نطاق واسع فى التصوير الطبى من بين الاشعة الاخرى فهى تستخدم فى التصوير الطبى فى امراض القلب و التوليد وأمراض النساء والتصوير فى البطن . وايضا مما يسهم فى زيادة شعبيتها ان التصوير الطبى بالاشعة الموجات فوق الصوتية يوفر صور عالية الدقة من دون استخدام الاشعاع المؤين للمواد الاخرى ومما تسببه هذه الاشعة من الامراض السرطانية ومشاكلها الكثيرة .التصوير العلاجى باستخدام الموجات فوق الصوتية ينقسم الى ثلاثة اجزاء رئيسية المعالجة الاولية والمعالجة المتوسطة والمرحلة الاخيرة وهى معالجة الصور التى يستخدمها اطباء كتصغير اجزاء وتكبيرها والقيام بالقياس والى ماذلك من المعالجات الظاهرية للمستخدمين . فى هذه الرسالة نقوم بطرح تصميم جديد لمكون الاشعة الموجات فوق الصوتية والذى اشرنا اليه باسم المعالجة الامامية وهو عبارة عن عملية مسح للموجات الصوتية الفوق المرتردة من الجزء المراد تصويره . سوف نطرح تصميم جديد باستخدام المكونات المجمعة داخل IC ومنها TI AFE5801 وهو حل يجمع مراحل مكونات الاستقبال المعالجة الامامية كلها فى IC واحد و ايضا باستخدام LM96570 وهو ايضا حل يجمع مراحل مكونات الارسال للمعالجة الامامية كلها فى IC واحد . هذا الحل مكنا من تجميع مكون للاشعة مكون من ٣٢ قناة باستخدام IC وحيد من البوابات المنطقية القابلة للبرمجة مع اقل عدد من المكونات الالكترونية الفردية كلهم مجمعين فى بوردة صغيرة ولهذه الاسباب نعتقد بان هذا التصميم هو الحل الامثل للحصول على جهاز سونار باقل التكلفة الممكنة واقل استهلاكا للطاقة.

تصميمنا مبنى على اثنين ممن المتحكمين المختلفين الاول وهو برمجة البوابات المنطقية القابلة للبرمجة عن طريق لغة وصف الهاردوير لتحقيق المنطق المطلوب لعمل مكون الاشعة ايضا استخدمنا ادوات تحويل اللغة من لغات برمجة بسيطة الى لغة وصف الهاردوير عن طريق VIVADO HLS هذه الادوات مكنتنا من جعل بوابتنا المنطقية القابلة للبرمجة تعمل بتردد قليل من اداء نفس الوظيفة لمعالج سريع التردد خاص بمعالجة الاشارات الرقمية وهذا هو المتحكم الثانى الذى استخدمناه فى تصميمنا كبديل للحل الاول وايضا كمرجع لنا هذا المعالج C64+ يعمل بتردد يصل الى 1.2 GHZ ومن خلال رساله سوف نرى ما الاختلاف ما بين الحلين وكيف نستطيع ان نصل بحل البوابات المنطقية بامثل الحلول وباقل التكلفة فى القيام بنفس وظيفة المعالج السريع.

تصميم منخفض التكلفة لمكون الاشعة لجهاز الموجات فوق الصوتية باستخدام البوابات  
المنطقية القابلة للبرمجة

اعداد

مهندس / باسم أحمد حسن بركات

قسم الهندسة الحيوية الطبية والمنظومات  
كلية الهندسة جامعة القاهرة

رسالة مقدمة الى كلية الهندسة - جامعة القاهرة  
كجزء من متطلبات الحصول على درجة الماجستير  
في الهندسة الحيوية الطبية و المنظومات

يعتمد من لجنة الممتحنين :

---

الاستاذ الدكتور / ياسر مصطفى قدح المشرف الرئيسى

---

الاستاذ الدكتور / مجدى فكرى

---

الاستاذ الدكتور / محمد ابراهيم العدوى

كلية الهندسة - جامعة القاهرة  
الجيزة - جمهورية مصر العربية  
٢٠١٢ م

تصميم منخفض التكلفة لمكون الاشعة لجهاز الموجات فوق الصوتية باستخدام البوابات  
المنطقية القابلة للبرمجة

اعداد

مهندس / باسم أحمد حسن بركات

قسم الهندسة الحيوية الطبية والمنظومات  
كلية الهندسة جامعة القاهرة

رسالة مقدمة الى كلية الهندسة – جامعة القاهرة

كجزء من متطلبات الحصول على درجة الماجستير

فى

الهندسة الحيوية الطبية و المنظومات

تحت اشراف

أ.د / ياسر مصطفى قـدح

استاذ دكتور الهندسة الحيوية الطبية والمنظومات ورئيس قسم الهندسة الحيوية الطبية والمنظومات – جامعة القاهرة

كلية الهندسة – جامعة القاهرة  
الجيزة – جمهورية مصر العربية  
٢٠١٢ م



جامعة القاهرة



## تصميم منخفض التكلفة لمكون الاشعة لجهاز الموجات فوق الصوتية باستخدام البوابات المنطقية القابلة للبرمجة

اعداد

مهندس / باسم أحمد حسن بركات

قسم الهندسة الحيوية الطبية والمنظومات  
كلية الهندسة جامعة القاهرة

رسالة مقدمة الى كلية الهندسة - جامعة القاهرة  
كجزء من متطلبات الحصول على درجة الماجستير  
في الهندسة الحيوية الطبية و المنظومات

كلية الهندسة - جامعة القاهرة  
الجيزة - جمهورية مصر العربية  
٢٠١٢ م